
Convolutional Learning on Simplicial Complexes

Maosheng Yang¹ Elvin Isufi¹

Abstract

We propose a simplicial complex convolutional neural network (SCCNN) to learn data representations on simplicial complexes. It performs convolutions based on the multi-hop simplicial adjacencies via common faces and cofaces independently and captures the inter-simplicial couplings, generalizing state-of-the-art. Upon studying symmetries of the simplicial domain and the data space, it is shown to be permutation and orientation equivariant, thus, incorporating such inductive biases. Based on the Hodge theory, we perform a spectral analysis to understand how SCCNNs regulate data in different frequencies, showing that the convolutions via faces and cofaces operate in two orthogonal data spaces. Lastly, we study the stability of SCCNNs to domain deformations and examine the effects of various factors. Empirical results show the benefits of higher-order convolutions and inter-simplicial couplings in simplex prediction and trajectory prediction.

1. Introduction

Graphs are commonly used to represent the support of networked data as nodes and capture their pairwise relations as edges. Graph neural networks (GNNs) have emerged as a learning model that leverages this topology information as an inductive bias (Battaglia et al., 2018; Bronstein et al., 2021). However, this bias can be erroneous when the topology structure of data involves with polyadic or higher-order relations, which often arises in real-world problems. For example, in social networks, people often interact in social groups, not just in pairs (Newman et al., 2002). In gene regulatory networks, a collection of molecular regulators interact with each other (Masoomy et al., 2021). In coauthorship networks, collaborations form between several authors rather than just two (Benson et al., 2018; Bick et al., 2021).

¹Department of Intelligent Systems, Delft University of Technology, Delft, The Netherlands. Correspondence to: Maosheng Yang <m.yang-2@tudelft.nl>, Elvin Isufi <e.isufi-1@tudelft.nl>.

Preprint.

Moreover, GNNs are often used to learn representations from data defined on nodes (Kipf & Welling, 2017; Defferrard et al., 2016; Gilmer et al., 2017). However, we also have data defined on higher-order structures in a network. For example, water flows in a water distribution system (Money et al., 2022) and traffic flow in a road network (Jia et al., 2019), such flow-type data are naturally supported on edges of a network. In coauthorship networks, data supported on a multi-set of k nodes can be the frequency or citation of the collaboration between k people (Benson et al., 2018).

Capturing the coupling between the data and these higher-order network structures is key to overcome the limitations of GNNs. As a higher-order network model, simplicial complexes (SCs) support an entity of multiple elements as a simplex and the relations between simplices can be mediated through their common faces and cofaces, referred to as lower and upper (simplicial) adjacencies. In analogy to graph Laplacians, Hodge Laplacians provide an algebraic representation of an SC to encode such adjacencies. This allows for a principled extension of processing and learning techniques from graphs to SCs. For example, Barbarossa & Sardellitti (2020) proposed a spectral signal processing framework in SCs, followed by simplicial convolutional filters (SCFs) (Yang et al., 2021; 2022b). Neural networks on SCs include, among others, Ebli et al. (2020); Roddenberry et al. (2021); Yang et al. (2022a); Bodnar et al. (2021b); Bunch et al. (2020). But they either focus on simplices of the same order, not exploiting the couplings between different orders or apply a message passing scheme based on direct simplicial adjacencies.

With a comprehensive framework to capture both higher-order simplicial adjacencies and inter-simplicial couplings, we conduct a convolution-based study for learning on SCs:

1) *Simplicial complex convolutional neural network*: we propose an SCCNN to propagate information across simplices of the same order via lower and upper adjacencies independently in a multi-hop way while leveraging the inter-simplicial couplings. It generalizes state-of-the-art and admits intra- and extended inter-simplicial localities with a linear computational complexity.

2) *Symmetries*: Based on group theory, we show that there exhibit a permutation symmetry in SCs and an orientation symmetry in the SC data. SCCNNs can be built equivariant

to both symmetries to incorporate such inductive biases.

3) *Spectral analysis*: Based on tools from [Barbarossa & Sardellitti \(2020\)](#); [Yang et al. \(2022b\)](#), we study how each component of the SCCNN regulates the data from the spectral perspective. This analysis generalizes to state-of-the-art.

4) *Stability analysis*: We prove that SCCNNs are stable to domain deformations when the convolutional filters are integral Lipschitz and show how the inter-simplicial couplings propagate the deformations across the SC.

2. Background

We briefly introduce the SC and its algebraic representation, together with the data defined on SCs.

Simplicial Complex. Given a finite set of vertices $\mathcal{V} := \{1, \dots, N_0\}$, a k -simplex s^k is a subset of \mathcal{V} with cardinality $k + 1$. A *face* of s^k is a subset with cardinality k . A *coface* of s^k is a $(k + 1)$ -simplex that has s^k as a face. Nodes, edges and (filled) triangles are geometric realizations of 0-, 1- and 2-simplices. An SC \mathcal{S} of order K is a collection of k -simplices s^k , $k = [K] := 0, \dots, K$, with the inclusion property: $s^{k-1} \in \mathcal{S}$ if $s^{k-1} \subset s^k$ for $s^k \in \mathcal{S}$, e.g., [Figure 1a](#). A graph is also an SC of order one including nodes and edges. We collect the k -simplices in \mathcal{S} in set $\mathcal{S}^k = \{s_i^k | i = 1, \dots, N_k\}$ with $N_k = |\mathcal{S}^k|$, therefore $\mathcal{S} = \bigcup_{k=0}^K \mathcal{S}^k$.

To facilitate computations, an orientation of a simplex is chosen as an ordering of its vertices, which is an equivalence class that two orderings are equivalent if they differ by an even permutation; otherwise anti-aligned ([Munkres, 2018](#); [Lim, 2020](#)). We fix an orientation for a simplex according to the lexicographical ordering of its vertices, $s^k = [1, \dots, k + 1]$, e.g., a triangle $s^2 = \{i, j, k\}$ is oriented as $[i, j, k]$ with $i < j < k$ and a node has a trivial orientation.

Simplicial Adjacency. For s_i^k , we define its *lower (upper) neighborhood* $\mathcal{N}_{i,d}^k$ ($\mathcal{N}_{i,u}^k$) as the set of k -simplices which share a common face (coface) with it. If $s_j^k \in \mathcal{N}_{i,d}^k$ ($\mathcal{N}_{i,u}^k$), we say s_j^k is *lower (upper) adjacent* to s_i^k . In [Figure 1a](#), we have $\mathcal{N}_{1,d}^1 = \{e_2, e_3, e_4, e_5\}$ and $\mathcal{N}_{1,u}^1 = \{e_2, e_4\}$ for e_1 .

Algebraic Representations. We use incidence matrices \mathbf{B}_k , $k = [K]$ to describe the incidence relations in an SC, where \mathbf{B}_1 and \mathbf{B}_2 are the node-to-edge and edge-to-triangle incidence matrices, respectively. Note that \mathbf{B}_0 is not defined. See [Appendix A](#) for those of SC in [Figure 1a](#). By definition, we have $\mathbf{B}_k \mathbf{B}_{k+1} = \mathbf{0}$ ([Lim, 2020](#)).

In an SC of order K , the Hodge Laplacians are defined as

$$\mathbf{L}_k = \mathbf{B}_k^\top \mathbf{B}_k + \mathbf{B}_{k+1} \mathbf{B}_{k+1}^\top, k = [K]$$

with the *lower Laplacian* $\mathbf{L}_{k,d} = \mathbf{B}_k^\top \mathbf{B}_k$ and the *upper Laplacian* $\mathbf{L}_{k,u} = \mathbf{B}_{k+1} \mathbf{B}_{k+1}^\top$, and the graph Laplacian $\mathbf{L}_0 = \mathbf{B}_1 \mathbf{B}_1^\top$ and $\mathbf{L}_K = \mathbf{B}_K^\top \mathbf{B}_K$. Matrices $\mathbf{L}_{k,d}$ and $\mathbf{L}_{k,u}$

encode the lower and upper adjacencies of k -simplices, respectively. In particular, $\mathbf{L}_{1,d}$ and $\mathbf{L}_{1,u}$ encode the edge-to-edge adjacencies through nodes and triangles, respectively.

Simplicial Signals. In an SC, we define k -simplicial signals (or data features) $\mathbf{x}_k = [x_{k,1}, \dots, x_{k,N_k}]^\top$, $k = [K]$ by an alternating map $f_k : \mathcal{S}^k \rightarrow \mathcal{X}^{N_k}$ which assigns a signal $x_{k,i}$ to the i th simplex s_i^k . The alternating map restricts that if the orientation of the simplex is anti-aligned with the reference orientation, denoted by $\bar{s}_i^k = -s_i^k$, then the sign of the signal value will be changed, $f_k(\bar{s}_i^k) = -f_k(s_i^k)$. If the signal value x_i^k is negative, then the signal is anti-aligned with the reference ([Lim, 2020](#); [Schaub et al., 2021](#)). An F -feature simplicial signal $\mathbf{X}_k \in \mathbb{R}^{N_k \times F}$ can be defined.

3. SCCNNs

We introduce the SCCNN to learn from data defined on SCs. Then, we discuss its intra- and inter-simplicial localities, followed by its complexity, and related works.

An L -layer SCCNN defined in an SC \mathcal{S} of order K computes the output \mathbf{x}_k^l at layer l as a nonlinear function of the outputs \mathbf{x}_{k-1}^{l-1} , \mathbf{x}_k^{l-1} and \mathbf{x}_{k+1}^{l-1} at the previous layer $l - 1$

$$\text{SCCNN}_k^l : \{\mathbf{x}_{k-1}^{l-1}, \mathbf{x}_k^{l-1}, \mathbf{x}_{k+1}^{l-1}\} \rightarrow \mathbf{x}_k^l,$$

for $k = [K]$ and $l = 1, \dots, L$, and admits a detailed form

$$\mathbf{x}_k^l = \sigma(\mathbf{H}_{k,d}^l \mathbf{x}_{k,d}^{l-1} + \mathbf{H}_k^l \mathbf{x}_k^{l-1} + \mathbf{H}_{k,u}^l \mathbf{x}_{k,u}^{l-1}) \quad (1)$$

with $\mathbf{x}_{k,d}^{l-1} = \mathbf{B}_k^\top \mathbf{x}_{k-1}^{l-1}$ and $\mathbf{x}_{k,u}^{l-1} = \mathbf{B}_{k+1} \mathbf{x}_{k+1}^{l-1}$, which can be understood as follows:

1) The previous output \mathbf{x}_k^{l-1} is passed through a simplicial convolution filter (SCF) \mathbf{H}_k^l ([Yang et al., 2022b](#)), given by

$$\mathbf{H}_k^l := \mathbf{H}_k^l(\mathbf{L}_{k,d}, \mathbf{L}_{k,u}) = \sum_{t=0}^{T_d} w_{k,d,t}^l \mathbf{L}_{k,d}^t + \sum_{t=0}^{T_u} w_{k,u,t}^l \mathbf{L}_{k,u}^t,$$

which is a sum of two matrix polynomials of $\mathbf{L}_{k,d}$ and $\mathbf{L}_{k,u}$ with trainable filter coefficients $\{w_{k,d,t}^l, w_{k,u,t}^l\}$ and filter orders T_d, T_u . Operator \mathbf{H}_k^l performs simplicial convolutions relying on the lower and upper adjacencies independently.

2) $\mathbf{x}_{k,d}^{l-1}$ and $\mathbf{x}_{k,u}^{l-1}$ are the lower and upper projections from the lower and upper adjacent simplices (i.e., faces and cofaces) to k -simplices via incidence structures \mathbf{B}_k^\top and \mathbf{B}_{k+1} , respectively. $\mathbf{x}_{0,d}^{l-1}$ and $\mathbf{x}_{K,u}^{l-1}$ are not defined.

3) The lower projection $\mathbf{x}_{k,d}^{l-1}$ is passed through another SCF, but it reduces to $\mathbf{H}_{k,d}^l := \sum_{t=0}^{T_d} w_{k,d,t}^l \mathbf{L}_{k,d}^t$ since $\mathbf{L}_{k,u} \mathbf{B}_k^\top = \mathbf{0}$. That is, the lower projection cannot propagate via the upper adjacency. Likewise, the upper projection $\mathbf{x}_{k,u}^{l-1}$ is passed through an upper SCF $\mathbf{H}_{k,u}^l := \sum_{t=0}^{T_u} w_{k,u,t}^l \mathbf{L}_{k,u}^t$, only accounting for the upper adjacency.

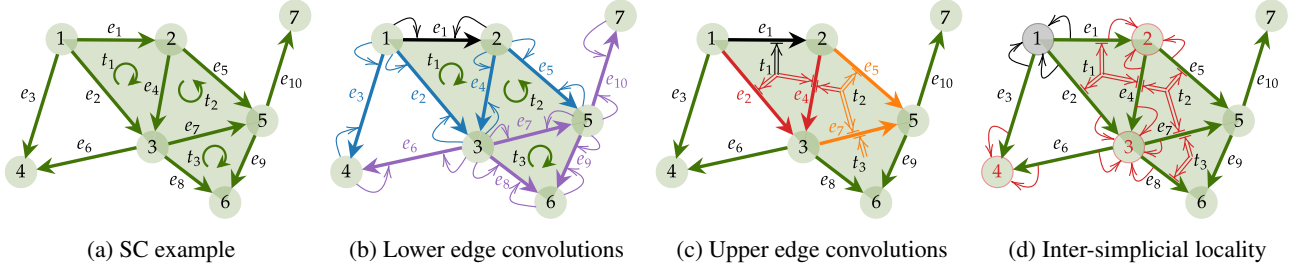


Figure 1. (a) An SC where arrows indicate the reference orientations of edges and triangles. 2-simplices are (filled) triangles shaded in green and open triangle $\{1, 3, 4\}$ is not in the SC. (b) Lower convolution via \mathbf{H}_1 and $\mathbf{H}_{1,d}$ on edge e_1 : SCF \mathbf{H}_1 aggregates the information from its direct lower neighbors (edges in blue) and two-hop lower neighbors (edges in purple) to e_1 (in black) if $T_d = 2$; and lower SCF $\mathbf{H}_{1,d}$ aggregates the projected information from nodes to edges likewise (denoted by the arrows in blue and purple from nodes to edges). (c) Upper convolution via \mathbf{H}_1 and $\mathbf{H}_{1,u}$ on e_1 : \mathbf{H}_1 aggregates the information from direct upper neighbors (edges in red) and two-hop upper neighbors (edges in orange) to e_1 (in black); and upper SCF $\mathbf{H}_{1,u}$ aggregates the projected information from triangles to edges likewise (denoted by double arrows in red and orange from triangle centers to edges). (d) Node 1 (in black) contains information from its neighbors $\{2, 3, 4\}$ (nodes in red), and projected information from edges which contribute to these neighbors (denoted by arrows in red from edges to nodes), and from triangles $\{t_1, t_2, t_3\}$ which contribute to those edges (denoted by double arrows in red from triangle centers to edges). This interaction is the coupling between the intra- and the extended inter-simplicial locality.

4) The sum of the three SCF outputs is passed by an elementwise nonlinearity $\sigma(\cdot)$. A multi-feature variant of SCCNNs can also be defined (see Appendix B.1).

Localities. Consider the output of an SCF on a k -simplicial signal, i.e., $\mathbf{H}_k \mathbf{x}_k$ (with layer index l omitted). We have *simplicial shiftings* $\mathbf{L}_{k,d} \mathbf{x}_k$ and $\mathbf{L}_{k,u} \mathbf{x}_k$ on simplex s_i^k as

$$\begin{aligned} [\mathbf{L}_{k,d} \mathbf{x}_k]_i &= \sum_{j \in \mathcal{N}_{i,d}^k \cup \{i\}} [\mathbf{L}_{k,d}]_{ij} [\mathbf{x}_k]_j, \\ [\mathbf{L}_{k,u} \mathbf{x}_k]_i &= \sum_{j \in \mathcal{N}_{i,u}^k \cup \{i\}} [\mathbf{L}_{k,u}]_{ij} [\mathbf{x}_k]_j, \end{aligned} \quad (2)$$

where s_i^k aggregates signals from its lower and upper neighbors in $\mathcal{N}_{i,d}^k$ and $\mathcal{N}_{i,u}^k$ based on the corresponding adjacencies. We can compute the t -step shifting recursively as $\mathbf{L}_{k,d}^t \mathbf{x}_k = \mathbf{L}_d(\mathbf{L}_{k,d}^{t-1} \mathbf{x}_k)$, a one-step shifting of the $(t-1)$ -shift result; likewise for $\mathbf{L}_{k,u}^t \mathbf{x}_k$. An SCF linearly combines such multi-step simplicial shiftings based on lower and upper adjacencies. Thus, the output $\mathbf{H}_k \mathbf{x}_k$ is localized in T_d -hop lower and T_u -hop upper k -simplicial neighborhoods (Yang et al., 2022b). SCCNNs preserve such *intra-simplicial locality* as the elementwise nonlinearity does not alter the information locality, shown in Figures 1b and 1c.

An SCCNN takes the data on k - and $(k \pm 1)$ -simplices at layer $l-1$ to compute \mathbf{x}_k^l , causing interactions between k -simplices and their (co)faces when all SCFs are identity. In turn, \mathbf{x}_{k-1}^{l-1} contains information on $(k-2)$ -simplices from layer $l-2$. Likewise for \mathbf{x}_{k+1}^{l-1} , thus, \mathbf{x}_k^l also contains information up to $(k \pm 2)$ -simplices if $L \geq 2$, because $\mathbf{B}_k \sigma(\mathbf{B}_{k+1}) \neq \mathbf{0}$ (see Appendix B.3). Accordingly, this *inter-simplicial locality* extends to the whole SC if $L \geq K$, unlike linear filters in an SC where the locality happens up to the adjacent simplices (Isufi & Yang, 2022; Schaub et al., 2021). This locality is further coupled with the intra-locality through three SCFs such that a node not only interacts with

its cofaces (direct edges) and direct triangles including it, but also edges and triangles further hops away which contribute to the neighboring nodes, as shown in Figure 1d.

Complexity. For an SCCNN layer, the parameter complexity is of order $\mathcal{O}(T_d + T_u)$. Denote the maximum of the number of neighbors for k -simplices by $M_k := \max\{|\mathcal{N}_{i,d}^k|, |\mathcal{N}_{i,u}^k|\}_{i=1}^{N_k}$. The computational complexity is of order $\mathcal{O}(k(N_k + N_{k+1}) + N_k M_k (T_d + T_u))$, discussed in Appendix B.2, which is linear to the simplex dimensions.

3.1. Related Works

The related works of this paper concern the following.

Signal Processing on SCs. Recent works on processing SC signals started on edge flows, which intrinsically follow properties like divergence-free, curl-free or harmonic (Jiang et al., 2011; Schaub & Segarra, 2018; Jia et al., 2019). In Barbarossa & Sardellitti (2020); Schaub et al. (2021), a better understanding of simplicial signals was approached via Hodge theory (Lim, 2020). Yang et al. (2021; 2022b) proposed an SCF, providing a spectral analysis of simplicial signals based on the spectrum of Hodge Laplacians. SCF was further extended to a joint filtering of signals on simplices of different orders by Isufi & Yang (2022). These concepts are key to understand the SCCNN spectrally.

NNs on SCs. Roddenberry & Segarra (2019) first used edge-Laplacian $\mathbf{L}_{1,d}$ to build NNs where edge convolution only considers the lower adjacency. Ebli et al. (2020) built an SNN based on a convolution via Hodge Laplacians, jointly relying on the lower and upper adjacencies. Yang et al. (2022a) discussed the limitations of this strategy and proposed separate simplicial convolutions based on the SCF. A one-step simplicial shifting separately by $\mathbf{L}_{k,d}$ and $\mathbf{L}_{k,u}$ was

Table 1. SCCNNs generalize several related works.

Methods	Parameters (n.d. denotes “not defined”)
Ebli et al. (2020)	$w_{k,d,t}^l = w_{k,u,t}^l, \mathbf{H}_{k,d}^l, \mathbf{H}_{k,u}^l$ n.d.
Roddenberry et al. (2021)	$T_d = T_u = 1, \mathbf{H}_{k,d}^l, \mathbf{H}_{k,u}^l$ n.d.
Yang et al. (2022a)	$\mathbf{H}_{k,d}^l, \mathbf{H}_{k,u}^l$ n.d.
Bunch et al. (2020)	$T_d = T_u = 1, \mathbf{H}_{k,d}^l = \mathbf{H}_{k,u}^l = \mathbf{I}$
Bodnar et al. (2021b)	$T_d = T_u = 1, \mathbf{H}_{k,d}^l = \mathbf{H}_{k,u}^l = \mathbf{I}$

proposed by Roddenberry et al. (2021). An attention scheme was applied to the previous two by Giusti et al. (2022); Goh et al. (2022). Information from simplices of adjacent orders was added by Bunch et al. (2020) and Yang et al. (2022c). Instead, Bodnar et al. (2021b) and Hajji et al. (2021) used a message passing scheme to collect such information, in analogy to the graph case (Gilmer et al., 2017). Chen et al. (2022b) combined graph shifting of node features and simplicial shifting of edge features in link predictions. As listed in Table 1 and further discussed in Appendix B.4, most of these solutions can be subsumed into the SCCNNs.

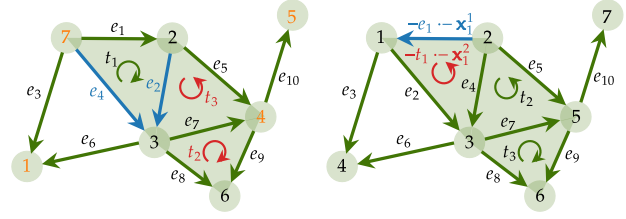
Graph Neural Networks. NNs on SCs return to GNNs when the SC is a graph. Most GNNs vary in terms of the graph convolutions, a shift-and-sum operation via graph shift operators such as graph adjacency and Laplacian matrices, e.g., a one-step graph shifting was performed in Kipf & Welling (2017) in contrast to a general graph convolution in (Defferrard et al., 2016; Gama et al., 2019a; 2020b), which can be obtained as \mathbf{x}_0^l without the upper projection $\mathbf{x}_{0,u}$.

4. Simplicial Complex Symmetry

Machine learning models rely on *symmetries* of the object domain, which are transformations that keep invariant certain object properties. Leveraging such symmetries of the data and the underlying domain imposes inductive biases, allowing the model to learn effective data representations (Bronstein et al., 2021). For example, GNNs leverage the permutation symmetry group to learn from graphs (Hamilton, 2020; Ruiz et al., 2021). Here we study the symmetries of the SC domain and the simplicial signal space, and show that SCCNNs preserve such symmetries, ultimately, extending the approach of Bronstein et al. (2021) to the SCs.

Permutation Symmetry. In an SC \mathcal{S} , the labeling of the k -simplices in $\mathcal{S}^k = \{s_{\mathbf{p}_k(1)}^k, \dots, s_{\mathbf{p}_k(N_k)}^k\}$ is a permutation \mathbf{p}_k of the indices $\{1, \dots, N_k\}$. These permutations form a *permutation group* \mathfrak{P}_k with $N_k!$ elements based on the group axioms (see Appendix C.1): they are associative, every permutation has an identity permutation and an inverse, and every two permutations form another permutation. A permutation $\mathbf{p}_k \in \mathfrak{P}_k$ can be represented by an orthogonal permutation matrix $\mathbf{P}_k \in \{0, 1\}^{N_k \times N_k}$ with entry $[\mathbf{P}_k]_{ij} = 1$ if $i = \mathbf{p}_k(j)$ and $[\mathbf{P}_k]_{ij} = 0$ otherwise.

Thus, the labeling of simplices in \mathcal{S} form a set $\{\mathfrak{P}_k : k =$



(a) Permutation Symmetry

(b) Orientation Symmetry

Figure 2. (a) Simplex relabeling (relabelled nodes, edges and triangles indicated by orange, blue and red) does not alter the SC in Figure 1a. (b) Reorienting simplices (edges in blue, triangles in red) does not alter the chain (simplicial signal) on them.

$[K]\}$ whose elements are permutation groups. This set can be represented by a set of matrices, $\mathbb{P} = \{\mathbb{P}_k : k = [K]\}$ with $\mathbb{P}_k = \{\mathbf{P}_{k,i} \in \{0, 1\}^{N_k \times N_k} : \mathbf{P}_{k,i} \mathbf{1} = \mathbf{1}, \mathbf{P}_{k,i}^\top \mathbf{1} = \mathbf{1}, i = 1, \dots, N_k!\}$ representing the permutation group \mathfrak{P}_k .

We then study how a permutation (labeling) of simplices affects the domain SC and the simplicial signals.

Proposition 4.1 (Permutation Symmetry). *Consider an SC \mathcal{S} with \mathbf{B}_k and \mathbf{L}_k for $k = [K]$. Let $\{\mathbf{P}_k : k = [K]\} \in \mathbb{P}$ represent a sequence of permutations $\{\mathbf{p}_k \in \mathfrak{P}_k : k = [K]\}$. Denote the permuted incidence matrices and Hodge Laplacians by $\bar{\mathbf{B}}_k$ and $\bar{\mathbf{L}}_k$, for $k = [K]$. Then, we have i) $\bar{\mathbf{B}}_k = \mathbf{P}_{k-1} \mathbf{B}_k \mathbf{P}_k^\top$ with entries $[\bar{\mathbf{B}}_k]_{i'j'} = [\mathbf{B}_k]_{ij}$ for $i' = \mathbf{p}_{k-1}(i), j' = \mathbf{p}_k(j)$; ii) $\bar{\mathbf{L}}_k = \mathbf{P}_k \mathbf{L}_k \mathbf{P}_k^\top$ with entries $[\bar{\mathbf{L}}_k]_{i'j'} = [\mathbf{L}_k]_{ij}$ for $i' = \mathbf{p}_k(i), j' = \mathbf{p}_k(j)$; and iii) the spectral property of the SC remains equivariant.*

See proof in Appendix C.2. This states that an SC is unaffected by the labeling of simplices, as well as its simplicial adjacencies, illustrated in Figure 2a. Its algebraic representations remain equivariant to permutations, i.e., they are a rearrangement of the rows and columns of the original ones. The spectral property of algebraic representations remain equivariant as well. Furthermore, the permutation of k -simplices does not affect \mathbf{B}_j for $j \neq k, k+1$, nor \mathbf{L}_j for $j \neq k$. Lastly, a k -simplicial signal \mathbf{x}^k changes into $\bar{\mathbf{x}}_k = \mathbf{P}_k \mathbf{x}_k$ according to the permutation of k -simplices.

Orientation Symmetry. In an oriented SC, the equivalence of an orientation defines that a simplex $s^k = [0, \dots, k]$ and its reoriented version $\bar{s}^k = [\pi(0), \dots, \pi(k)]$ have the same orientation if π is an even permutation of $\{0, \dots, k\}$; and they are anti-aligned $\bar{s}^k = -s^k$, if π is an odd permutation. These two orientations of a k -simplex form an *orientation group* $\mathfrak{O}_k = \{\epsilon, \sigma_-\}$ with two elements. They can be obtained by a group homomorphism which maps all the even permutations of $\{0, \dots, k\}$ to the identity orientation ϵ and all the odd permutations of $[k]$ to the reverse orientation σ_- . Note that $\mathfrak{O}_0 = \{\epsilon\}$ since a node has one trivial orientation and we assume $k \neq 0$ here.

Thus, in an oriented SC \mathcal{S} we have a set whose elements

are orientation groups $\{\mathfrak{D}_{k,i} : k = [K], i = 1, \dots, N_k\}$ with group $\mathfrak{D}_{k,i}$ for the i th k -simplex s_i^k . The subset $\{\mathfrak{D}_{k,i} : i = 1, \dots, N_k\}$ admits a diagonal matrix representation $\mathbf{D}_k \in \{-1, 1\}^{N_k \times N_k}$ with $[\mathbf{D}_k]_{ii} = 1$ if ϵ is applied to s_i^k , and $[\mathbf{D}_k]_{ii} = -1$ if σ_- is applied. Then, we have a set of orientation matrices for \mathcal{S} as $\mathbb{D} = \{\mathbf{D}_k : k = [K]\}$.

A simplicial signal \mathbf{x}_k by definition remains unchanged w.r.t. the underlying simplices after an orientation change. To see this conveniently, we introduce the k -chain space \mathcal{C}_k with a chain $c_k = \sum_{i=1}^{N_k} x_{k,i} s_i^k$ that is a linear combination of k -simplices weighted by the supported signals $x_{k,i}$. With the basis $\{s_i^k : i = 1, \dots, N_k\}$, a k -chain c_k can be represented by the k -simplicial signal vector $\mathbf{x}_k = [x_{k,1}, \dots, x_{k,N_k}]^\top$. By imposing the alternating property to \mathcal{C}_k that if s_i^k is reversed, the weight $x_{k,i}$ changes its sign, a k -chain space \mathcal{C}_k is then isomorphic to the k -simplicial signal space \mathcal{X}_k (Munkres, 2018). Unlike permutation groups, orientation groups do not form a symmetry group in an oriented SC but in the chain space as stated by the following proposition.

Proposition 4.2 (Orientation Symmetry). *Consider an oriented SC \mathcal{S} with \mathbf{B}_k and \mathbf{L}_k for $k = [K]$. Let $\{\mathbf{D}_k : k = [K]\} \in \mathbb{D}$ represent a sequence of orientation changes $\{\mathfrak{D}_i^k : k = [K], i = 1, \dots, N_k\}$ of simplices in \mathcal{S} . In the re-oriented SC, incidence matrices become $\overline{\mathbf{B}}_k = \mathbf{D}_k \mathbf{B}_k \mathbf{D}_{k+1}$ and Hodge Laplacians become $\overline{\mathbf{L}}_k = \mathbf{D}_k \mathbf{L}_k \mathbf{D}_k$. Moreover, a k -simplicial signal \mathbf{x}_k becomes $\overline{\mathbf{x}}_k = \mathbf{D}_k \mathbf{x}_k$ and its underlying k -chain remains unchanged.*

See the proof in Appendix C.3. This states that the incidence relations and the simplicial adjacencies in an oriented SC are altered when the orientations are reversed, whereas the k -chain remains invariant to this transformation and the k -simplicial signal \mathbf{x}_k is equivariant in terms of the basis.

Equivariance of SCCNNs. Upon seeing that permutations form a symmetry group in an SC and orientations form a symmetry group in the simplicial signal space, we show that SCCNNs in (1) are equivariant to the two symmetries.

Proposition 4.3 (Permutation Equivariance). *SCCNN $_k^l$: $\{\mathbf{x}_{k-1}^{l-1}, \mathbf{x}_k^{l-1}, \mathbf{x}_{k+1}^{l-1}\} \rightarrow \mathbf{x}_k^l$ in (1) is equivalent to permutations. In the $\{\mathfrak{P}_k : k = [K]\}$ -permuted SC, it follows*

$$\{\mathbf{P}_{k-1} \mathbf{x}_{k-1}^{l-1}, \mathbf{P}_k \mathbf{x}_k^{l-1}, \mathbf{P}_{k+1} \mathbf{x}_{k+1}^{l-1}\} \rightarrow \mathbf{P}_k \mathbf{x}_k^l,$$

with matrix representation \mathbf{P}_k of \mathfrak{P}_k . Thus, permutations on the SC and the input affect the output in the same way.

Proposition 4.4 (Orientation Equivariance). *SCCNN $_k^l$: $\{\mathbf{x}_{k-1}^{l-1}, \mathbf{x}_k^{l-1}, \mathbf{x}_{k+1}^{l-1}\} \rightarrow \mathbf{x}_k^l$ in (1) with an odd nonlinearity $\sigma(\cdot)$ is equivariant to orientations. In a re-oriented SC by $\{\mathfrak{D}_{k,i} : k = [K], i = 1, \dots, N_k\}$, it follows*

$$\{\mathbf{D}_{k-1} \mathbf{x}_{k-1}^{l-1}, \mathbf{D}_k \mathbf{x}_k^{l-1}, \mathbf{D}_{k+1} \mathbf{x}_{k+1}^{l-1}\} \rightarrow \mathbf{D}_k \mathbf{x}_k^l,$$

with matrix representation \mathbf{D}_k of $\{\mathfrak{D}_{k,i} : i = 1, \dots, N_k\}$, i.e., orientations of the SC affect the output in the same way.

Propositions 4.3 and 4.4 shows that SCCNNs incorporate the inductive biases imposed by the symmetries of the SC and the signal space. If we relabel the SC, the output of an SCCNN on k -simplices will be relabeled according to the labeling of k -simplices and remain unaffected by labeling of j -simplices with $j \neq k$. If the orientation of a simplex is reversed, the output of an SCCNN on this simplex changes its sign. The latter however requires an odd nonlinearity, thus, if ReLU or its alternatives are used, the SCCNN will not leverage the orientation symmetry of the data.

5. Spectral Analysis

We use the spectrum of Hodge Laplacians and the Hodge decomposition (Hodge, 1989) to perform a spectral analysis for the SCCNN, which were also used to analyze SCFs and the NN in Yang et al. (2022a). This analysis also reveals the spectral mechanisms of other NNs in Table 1.

Theorem 5.1 (Hodge Decomposition). *In an SC \mathcal{S} with incidence matrices \mathbf{B}_k and Hodge Laplacians \mathbf{L}_k , we have*

$$\mathcal{X}_k = \text{im}(\mathbf{B}_k^\top) \oplus \ker(\mathbf{L}_k) \oplus \text{im}(\mathbf{B}_{k+1})$$

for $k = [K]$, where \oplus is direct sum operation. Any \mathbf{x}_k can be expressed as a sum of three orthogonal components $\mathbf{x}_k = \mathbf{x}_{k,G} + \mathbf{x}_{k,H} + \mathbf{x}_{k,C}$ with $\mathbf{x}_{k,G} = \mathbf{B}_k^\top \mathbf{x}_{k-1}$ and $\mathbf{x}_{k,C} = \mathbf{B}_{k+1} \mathbf{x}_{k+1}$, for some \mathbf{x}_{k-1} and \mathbf{x}_{k+1} , and $\mathbf{L}_k \mathbf{x}_{k,H} = \mathbf{0}$.

For $k = 1$, $\text{im}(\mathbf{B}_1^\top)$ is the *gradient* space collecting edge flows as the gradient of some node signal; $\text{im}(\mathbf{B}_2)$ is the *curl* space where flows circulate within triangles; and $\ker(\mathbf{L}_1)$ contains *harmonic* flows which are divergence-free (zero netflow at nodes) and curl-free (zero circulation in triangles) (Barbarossa & Sardellitti, 2020; Schaub et al., 2021).

This decomposition implies that \mathbf{x}_k is a sum of $\mathbf{x}_{k,G}$ via lower incident relations from some \mathbf{x}_{k-1} , $\mathbf{x}_{k,C}$ via upper incident relations from some \mathbf{x}_{k+1} , and $\mathbf{x}_{k,H}$ which cannot be diffused to other simplices. This motivates the input \mathbf{x}_{k-1} and \mathbf{x}_{k+1} of an SCCNN layer as they also contain information that contributes to the k -simplicial signal space.

Definition 5.2 (Simplicial Fourier Transform). The SFT of \mathbf{x}_k is $\tilde{\mathbf{x}}_k = \mathbf{U}_k^\top \mathbf{x}_k$ where SFT basis \mathbf{U}_k is the eigenbasis of $\mathbf{L}_k = \mathbf{U}_k \mathbf{\Lambda}_k \mathbf{U}_k^\top$, and the inverse SFT is $\mathbf{x}_k = \mathbf{U}_k \tilde{\mathbf{x}}_k$ (Barbarossa & Sardellitti, 2020).

Proposition 5.3 (Yang et al. (2022b)). *The SFT basis \mathbf{U}_k can be found as $\mathbf{U}_k = [\mathbf{U}_{k,H} \ \mathbf{U}_{k,G} \ \mathbf{U}_{k,C}]$ where*

- 1) $\mathbf{U}_{k,H}$, associated with $N_{k,H}$ zero eigenvalues of \mathbf{L}_k , spans $\ker(\mathbf{L}_k)$, and $\dim(\ker(\mathbf{L}_k)) = N_{k,H}$;
- 2) $\mathbf{U}_{k,G}$, associated with nonzero eigenvalues $\{\lambda_{k,G,i}\}_{i=1}^{N_{k,G}}$ of $\mathbf{L}_{k,d}$, referred to as *gradient frequencies*, spans $\text{im}(\mathbf{B}_k)$, and $\dim(\text{im}(\mathbf{B}_k)) = N_{k,G}$;
- 3) $\mathbf{U}_{k,C}$, associated with nonzero eigenvalues $\{\lambda_{k,C,i}\}_{i=1}^{N_{k,C}}$ of $\mathbf{L}_{k,u}$, referred to as *curl frequencies*, spans $\text{im}(\mathbf{B}_{k+1})$, and $\dim(\text{im}(\mathbf{B}_{k+1})) = N_{k,C}$.

The eigenvalues of \mathbf{L}_k carry two types of simplicial frequencies, which measure the k -simplicial signal variations in terms of faces and cofaces. For $k = 1$, gradient frequencies measure the edge flow ‘‘smoothness’’ in terms of nodal variations, i.e., the total divergence. Curl frequencies measure the smoothness in terms of rotational variations, i.e., the total curl. For $k = 0$, curl frequencies are the graph frequencies in graph signal processing while gradient frequencies do not exist. We refer to [Appendix D.3](#) for more details.

We can now analyze the input of an SCCNN layer in spectral domain. First, the SFT of \mathbf{x}_k is given by

$$\tilde{\mathbf{x}}_k = [\tilde{\mathbf{x}}_{k,H}^\top, \tilde{\mathbf{x}}_{k,G}^\top, \tilde{\mathbf{x}}_{k,C}^\top]^\top \quad (3)$$

with the *harmonic embedding* $\tilde{\mathbf{x}}_{k,H} = \mathbf{U}_{k,H}^\top \mathbf{x}_k = \mathbf{U}_{k,H}^\top \mathbf{x}_{k,H}$ in the zero frequencies, the *gradient embedding* $\tilde{\mathbf{x}}_{k,G} = \mathbf{U}_{k,G}^\top \mathbf{x}_k = \mathbf{U}_{k,G}^\top \mathbf{x}_{k,G}$ in the gradient frequencies, and the *curl embedding* $\tilde{\mathbf{x}}_{k,C} = \mathbf{U}_{k,C}^\top \mathbf{x}_k = \mathbf{U}_{k,C}^\top \mathbf{x}_{k,C}$ in the curl frequencies. Second, the lower projection $\mathbf{x}_{k,d} \in \text{im}(\mathbf{B}_k^\top)$ has only a nonzero gradient embedding $\tilde{\mathbf{x}}_{k,d} = \mathbf{U}_{k,G}^\top \mathbf{x}_{k,d}$. The upper projection $\mathbf{x}_{k,u} \in \text{im}(\mathbf{B}_{k+1})$ contains only a nonzero curl embedding $\tilde{\mathbf{x}}_{k,u} = \mathbf{U}_{k,C}^\top \mathbf{x}_{k,u}$.

Corollary 5.4. $\mathbf{L}_{k,d}$ and $\mathbf{L}_{k,u}$ admit diagonalizations by \mathbf{U}_k . Thus, the simplicial shifting in (2) can be expressed as

$$\begin{aligned} \mathbf{L}_{k,d} \mathbf{x}_k &= \mathbf{U}_{k,G} (\boldsymbol{\lambda}_{k,G} \odot \tilde{\mathbf{x}}_{k,G}) \in \text{im}(\mathbf{B}_k^\top) \\ \mathbf{L}_{k,u} \mathbf{x}_k &= \mathbf{U}_{k,C} (\boldsymbol{\lambda}_{k,C} \odot \tilde{\mathbf{x}}_{k,C}) \in \text{im}(\mathbf{B}_{k+1}) \end{aligned} \quad (4)$$

with the Hadamard product \odot and column vectors $\boldsymbol{\lambda}_{k,G}$ and $\boldsymbol{\lambda}_{k,C}$ collecting gradient and curl frequencies, respectively.

See [Appendix D.4](#) for the proof. (4) implies that a lower shifting of \mathbf{x}_k results a signal living in the gradient space and an upper one results in the curl space. This limits a linear relation between the output and input in terms of the corresponding frequencies as in [Roddenberry et al. \(2021\)](#).

By diagonalizing an SCF \mathbf{H}_k with \mathbf{U}_k , we can further express the simplicial convolution as

$$\mathbf{H}_k \mathbf{x}_k = \mathbf{U}_k \tilde{\mathbf{H}}_k \mathbf{U}_k^\top \mathbf{x}_k = \mathbf{U}_k (\tilde{\mathbf{h}}_k \odot \tilde{\mathbf{x}}_k) \quad (5)$$

where $\tilde{\mathbf{H}}_k = \text{diag}(\tilde{\mathbf{h}}_k)$. Here, $\tilde{\mathbf{h}}_k = [\tilde{\mathbf{h}}_{k,H}^\top, \tilde{\mathbf{h}}_{k,G}^\top, \tilde{\mathbf{h}}_{k,C}^\top]^\top$ is the *filter frequency response*, given by

$$\begin{cases} \text{harmonic response} : \tilde{\mathbf{h}}_{k,H} = (w_{k,d,0} + w_{k,u,0}) \mathbf{1}, \\ \text{gradient response} : \tilde{\mathbf{h}}_{k,G} = \sum_{t=0}^{T_d} w_{k,d,t} \boldsymbol{\lambda}_{k,G}^{\odot t} + w_{k,u,0} \mathbf{1}, \\ \text{curl response} : \tilde{\mathbf{h}}_{k,C} = \sum_{t=0}^{T_u} w_{k,u,t} \boldsymbol{\lambda}_{k,C}^{\odot t} + w_{k,d,0} \mathbf{1}, \end{cases}$$

with $(\cdot)^{\odot t}$ the elementwise t th power of a vector. Furthermore, we can express $\tilde{\mathbf{h}}_k \odot \tilde{\mathbf{x}}_k$ as

$$[(\tilde{\mathbf{h}}_{k,H} \odot \tilde{\mathbf{x}}_{k,H})^\top, (\tilde{\mathbf{h}}_{k,G} \odot \tilde{\mathbf{x}}_{k,G})^\top, (\tilde{\mathbf{h}}_{k,C} \odot \tilde{\mathbf{x}}_{k,C})^\top]^\top. \quad (6)$$

Therefore, the simplicial convolution corresponds to a pointwise multiplication of the SFT of a simplicial signal by the

filter frequency response in the spectral domain. Specifically, the frequency response $\tilde{\mathbf{h}}_{k,H}$ at the zero frequency is determined by the coefficients of the SCF on the identity matrix. The coefficients $\{w_{k,d,t}\}_{t=1}^{T_d}$ on $\mathbf{L}_{k,d}$ and its powers contribute to $\tilde{\mathbf{h}}_{k,G}$, acting in the gradient frequencies and gradient space, while the coefficients $\{w_{k,u,t}\}_{t=1}^{T_u}$ on $\mathbf{L}_{k,u}$ and its powers contribute to $\tilde{\mathbf{h}}_{k,C}$, acting in the curl frequencies and curl space. This is a direct result of [Corollary 5.4](#). Unlike (6), the SCF in [Ebli et al. \(2020\)](#) has the same gradient and curl responses which prohibits different processing in the gradient and curl spaces.

The lower SCF $\mathbf{H}_{k,d}$ has $\tilde{\mathbf{h}}_{k,d} = \sum_{t=0}^{T_d} w'_{k,d,t} \boldsymbol{\lambda}_{k,G}^{\odot t}$ as the frequency response that modulates the gradient embedding of $\mathbf{x}_{k,d}$ and the upper SCF $\mathbf{H}_{k,u}$ has $\tilde{\mathbf{h}}_{k,u} = \sum_{t=0}^{T_u} w'_{k,u,t} \boldsymbol{\lambda}_{k,C}^{\odot t}$ as the frequency response that modulates the curl embedding of $\mathbf{x}_{k,u}$.

Now, consider the output after the linear operation in an SCCNN layer $\mathbf{y}_k = \mathbf{H}_{k,d} \mathbf{x}_{k,d} + \mathbf{H}_k \mathbf{x}_k + \mathbf{H}_{k,u} \mathbf{x}_{k,u}$. Its three spectral embeddings are given by

$$\begin{cases} \tilde{\mathbf{y}}_{k,H} = \tilde{\mathbf{h}}_{k,H} \odot \tilde{\mathbf{x}}_{k,H}, \\ \tilde{\mathbf{y}}_{k,G} = \tilde{\mathbf{h}}_{k,d} \odot \tilde{\mathbf{x}}_{k,d} + \tilde{\mathbf{h}}_{k,G} \odot \tilde{\mathbf{x}}_{k,G}, \\ \tilde{\mathbf{y}}_{k,C} = \tilde{\mathbf{h}}_{k,C} \odot \tilde{\mathbf{x}}_{k,C} + \tilde{\mathbf{h}}_{k,u} \odot \tilde{\mathbf{x}}_{k,u}. \end{cases} \quad (7)$$

This spectral relation shows how SCCNNs regulate the three inputs coming from simplices of different order and enable a flexible processing of inputs in different signal spaces owing to that different coefficients are used in the SCFs.

The nonlinearity induces an information spillage ([Gama et al., 2020a](#)) such that one type of spectral embedding could be spread over other types of frequencies. That is, $\sigma(\tilde{\mathbf{y}}_{k,G})$ could contain information in zero or curl frequencies. For example, a gradient flow projected from a node input could have information spillage in curl frequencies after $\sigma(\cdot)$. This spilled information further contributes to a triangle signal via projection \mathbf{B}_2^\top . Thus, the triangle output of SCCNNs contains information from nodes. This is the spectral perspective of the extended inter-simplicial locality.

6. Stability Analysis

Characterizing the stability of NNs to domain perturbations is key to understand their learning abilities from data ([Bruna & Mallat, 2013](#); [Bronstein et al., 2021](#)). The analysis by [Gama et al. \(2020a\)](#) showed that GNNs could be both stable and selective in contrast to graph convolution filters. We here perform a stability analysis of SCCNNs to understand the effect of various factors on the output of different simplices, with a focus on the roles of lower and upper simplicial adjacencies and inter-simplicial couplings.

Domain perturbations could occur in a weighted SC as a result of misestimated simplicial weights. Denote as \mathbf{M}_k

a weight matrix of k -simplices. A weighted lower Laplacian is defined as $\mathbf{L}_{k,d} = f_{k,d}(\mathbf{B}_k, \mathbf{M}_{k-1}, \mathbf{M}_k)$ a function of incidence matrix \mathbf{B}_k and weights $\mathbf{M}_{k-1}, \mathbf{M}_k$, and likewise for the upper one $\mathbf{L}_{k,u} = f_{k,u}(\mathbf{B}_{k+1}, \mathbf{M}_k, \mathbf{M}_{k+1})$. The projections in SCCNNs are performed by the lower and upper projection matrices in place of \mathbf{B}_k^\top and \mathbf{B}_{k+1} , defined as $\mathbf{R}_{k,d} = f'_{k,d}(\mathbf{B}_k, \mathbf{M}_{k-1}, \mathbf{M}_k)$ and $\mathbf{R}_{k,u} = f'_{k,u}(\mathbf{B}_{k+1}, \mathbf{M}_k, \mathbf{M}_{k+1})$, functions of incidence matrices and weights. See Appendix E.1 for some explicit forms by Grady & Polimeni (2010); Schaub et al. (2020). The misestimations of these weights could be viewed as relative perturbations on Hodge Laplacians and projection matrices.

Definition 6.1 (Relative Perturbation). Consider a weighted SC \mathcal{S} with projection matrices $\mathbf{R}_{k,d}, \mathbf{R}_{k,u}$ and Hodge Laplacians $\mathbf{L}_{k,d}, \mathbf{L}_{k,u}$, $k = [K]$. A relative perturbed SC $\hat{\mathcal{S}}$ has

$$\begin{aligned}\hat{\mathbf{R}}_{k,d} &= \mathbf{R}_{k,d} + \mathbf{J}_{k,d}\mathbf{R}_{k,d}, \quad \hat{\mathbf{R}}_{k,u} = \mathbf{R}_{k,u} + \mathbf{J}_{k,u}\mathbf{R}_{k,u}, \\ \hat{\mathbf{L}}_{k,d} &= \mathbf{L}_{k,d} + \mathbf{E}_{k,d}\mathbf{L}_{k,d} + \mathbf{L}_{k,d}\mathbf{E}_{k,d}, \\ \hat{\mathbf{L}}_{k,u} &= \mathbf{L}_{k,u} + \mathbf{E}_{k,u}\mathbf{L}_{k,u} + \mathbf{L}_{k,u}\mathbf{E}_{k,u}\end{aligned}$$

where small perturbation matrices follow that $\|\mathbf{E}_{k,d}\| \leq \epsilon_{k,d}$ and $\|\mathbf{J}_{k,d}\| \leq \epsilon_{k,d}$, $\|\mathbf{E}_{k,u}\| \leq \epsilon_{k,u}$ and $\|\mathbf{J}_{k,u}\| \leq \epsilon_{k,u}$ with the spectral radius $\|\cdot\|$.

This model generalizes the graph perturbation model in Gama et al. (2019b; 2020a); Parada-Mayorga et al. (2022) and implies that the same degree of perturbations affect differently stronger and weaker simplicial adjacencies. We further describe an SCF by its integral Lipschitz property.

Definition 6.2 (Integral Lipschitz SCF). An SCF \mathbf{H}_k is integral Lipschitz with constants $C_{k,d}$ and $C_{k,u}$ if

$$|\lambda \tilde{h}'_{k,G}(\lambda)| \leq C_{k,d} \text{ and } |\lambda \tilde{h}'_{k,C}(\lambda)| \leq C_{k,u}, \quad (8)$$

with $\tilde{h}'_{k,G}(\lambda)$ and $\tilde{h}'_{k,C}(\lambda)$ the derivatives of the gradient and curl frequency response functions [cf. (5)], respectively.

Integral Lipschitz SCFs can have a large variability in low simplicial frequencies $\lambda \rightarrow 0$, thus, a good selectivity with a low stability, while in large frequencies, they tend to be flat with a better stability at the cost of selectivity. This tradeoff holds independently for the gradient and curl frequencies. See Appendix E.2 for more details. As of the polynomial nature of frequency responses, all SCFs of an SCCNN are integral Lipschitz. We also denote the constant for the lower SCFs $\mathbf{H}_{k,d}$ by $C_{k,d}$ and for the upper SCFs $\mathbf{H}_{k,u}$ by $C_{k,u}$.

Assumption 6.3. The SCFs \mathbf{H}_k of an SCCNN have a normalized bounded frequency response $|\tilde{h}_k(\lambda)| \leq 1$, likewise for $\mathbf{H}_{k,d}$ and $\mathbf{H}_{k,u}$, where we assume one for simplicity.

Assumption 6.4. The lower and upper projections are finite with bounded norms $\|\mathbf{R}_{k,d}\| \leq r_{k,d}$ and $\|\mathbf{R}_{k,u}\| \leq r_{k,u}$.

Assumption 6.5. The initial input \mathbf{x}_k^0 is finite a limited energy $\|\mathbf{x}_k^0\| \leq \beta_k$, $k = [K]$, collected in $\boldsymbol{\beta} = [\beta_0, \dots, \beta_K]^\top$.

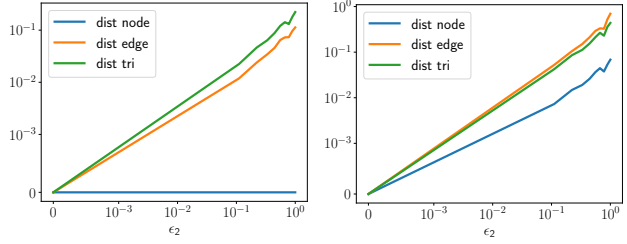


Figure 3. Euclidean distances of node, edge and triangle outputs of an SCCNN with one (Left) and two (Right) layers under perturbations on triangle weights. Edge output is influenced after one layer, while node output is influenced after two layers.

Assumption 6.6. The nonlinearity $\sigma(\cdot)$ is C_σ -Lipschitz, i.e., $|\sigma(b) - \sigma(a)| \leq |b - a|$.

Theorem 6.7 (Stability). Let \mathbf{x}_k^L be the output of an L -layer SCCNN defined on a weighted SC. Let $\hat{\mathbf{x}}_k^L$ be the output of the same SCNN but on a relatively perturbed SC according to Definition 6.1. Under Assumptions 6.3 to 6.6, the Euclidean distance between the two outputs is finite and upper-bounded by $\|\hat{\mathbf{x}}_k^L - \mathbf{x}_k^L\| \leq [\mathbf{d}]_k$ with

$$\mathbf{d} = C_\sigma^L \sum_{l=1}^L \hat{\mathbf{Z}}^{l-1} \mathbf{T} \mathbf{Z}^{L-l} \boldsymbol{\beta}. \quad (9)$$

Here, matrices \mathbf{T} and \mathbf{Z} are tridiagonal, e.g., for $K = 2$,

$$\mathbf{T} = \begin{bmatrix} t_0 & t_{0,u} & \\ t_{1,d} & t_1 & t_{1,u} \\ & t_{2,d} & t_2 \end{bmatrix} \text{ and } \mathbf{Z} = \begin{bmatrix} 1 & r_{0,u} & \\ r_{1,d} & 1 & r_{1,u} \\ & r_{2,d} & 1 \end{bmatrix},$$

with constants $t_{k,d} = r_{k,d}\epsilon_{k,d} + C_{k,d}\Delta_{k,d}\epsilon_{k,d}r_{k,d}$, $t_{k,u} = r_{k,u}\epsilon_{k,u} + C_{k,u}\Delta_{k,u}\epsilon_{k,u}r_{k,u}$ and $t_k = C_{k,d}\Delta_{k,d}\epsilon_{k,d} + C_{k,u}\Delta_{k,u}\epsilon_{k,u}$, where $\Delta_{k,d}$ and $\Delta_{k,u}$ capture the eigenvector misalignment between the respective Hodge Laplacians and their perturbations, scaled by $\sqrt{N_k}$. Matrix $\hat{\mathbf{Z}}$ is defined as \mathbf{Z} but with off-diagonal entries $\hat{r}_{k,d} = r_{k,d}(1 + \epsilon_{k,d})$ and $\hat{r}_{k,u} = r_{k,u}(1 + \epsilon_{k,u})$.

The proof can be found in Appendix E.3. This result shows that SCCNNs are stable to relative domain perturbations, which can be analyzed from two perspectives. First, the stability of k -simplicial output depends on not only factors of k -simplices, but also simplices of other orders due to the inter-simplicial couplings. When $L = 1$, the node output bound d_0 depends on β_0 via t_0 , and β_1 via $t_{0,u}$ where node perturbation $\mathbf{E}_{0,u}$ (described by $\Delta_{0,u}$ and $\epsilon_{0,u}$), node SCFs (by $C_{0,u}$) and projections from edges to nodes (by $r_{0,u}$ and $\epsilon_{0,u}$) play a role. Likewise, d_1 depends on β_0, β_1 and β_2 via factors of perturbations, SCFs and projections in the edge space. When $L = 2$, the bound d_0 is also affected by $t_{1,d}, t_1$ and $t_{1,u}$ containing factors in the edge space. As L increases, factors in the triangle space (and higher-order simplicial space) will appear in d_0 , as illustrated in Figure 3. Thus, while leveraging information from adjacent simplices may be beneficial, it may severely affect the stability when

the SC is perturbed. This can be mitigated by using less layers and higher-order SCFs, imposed by stronger integral Lipschitz properties, to maintain the expressive power.

Second, the integral Lipschitz property $C_{k,d}$ in gradient frequencies plays no role in the stability against upper perturbations, and vice-versa. Thus, if there are only triangle perturbations SCFs in the edge space need not to be strictly integral Lipschitz in gradient frequencies where SCCNNs could be more selective while preserving stability. This is a direct benefit of using different parameter spaces in the gradient and curl spaces unlike in Ebli et al. (2020).

7. Experiments

Simplex Prediction. We consider the task of simplex prediction: *given all the $(k - 1)$ -simplices in a set of $k + 1$ nodes, to predict if this set will be closed to form a k -simplex*, which is an extension of link prediction in graphs (Zhang & Chen, 2018). Our approach is to first learn features of lower-order simplices and then use an MLP to identify if a simplex is closed or open. With coauthorship data in Amar et al. (2018) we built an SC as Ebli et al. (2020) where nodes are authors and collaborations between k -authors are modeled as $(k - 1)$ -simplices. The simplicial signals are the number of citations, e.g., \mathbf{x}_1 and \mathbf{x}_2 are the citations of dyadic and triadic collaborations. Thus, 2-simplex predictions in this SC give rise to predict triadic collaborations given the pairwise collaborations in the triads.

In an SC of order two, for an open triangle, we use an SC-CNN to learn features of nodes and edges. Then, an MLP is used to predict if this triangle shall be closed or not based on its three node or edge features. We also perform a 3-simplex prediction, which amounts to predicting tetradic collaborations. Table 2 reports the AUC results. We include the experiment details and an ablation study in Appendix F.1.

We see that SC solutions achieve better results than using only graphs, validating SCs as an inductive model. SCCNN performs best in both tasks, since it exploits both intra- and extended inter-simplicial localities. First, SCCNN leverages the lower and upper adjacencies individually in a multi-hop fashion to perform convolutions such that it performs better than Bunch. For the same reason, SCNN performs better than SNN and PSNN. Second, SCCNN considers information from adjacent simplices such that it gives better results than methods without the inter-simplicial locality, such as GNN and SCNN, or CF-SC with a limited locality.

Trajectory Prediction. In the trajectory prediction task, a trajectory is represented as an edge flow and the goal is to predict the next node based on this representation (Roddenberry et al., 2021). We consider trajectories in a synthetic SC and ocean drifter trajectories localized around Madagascar (Schaub et al., 2020). The experiment details can

Table 2. Simplex prediction AUC (% , area under the curve) results for ten runs. The *first* and *second* best results are in *red* and *blue*.

Methods	2-Simplex	3-Simplex
Harm. Mean (Benson et al., 2018)	62.8±2.7	63.6±1.6
MLP	68.5±1.6	69.0±2.2
GF (Sandryhaila & Moura, 2013)	78.7±1.2	83.9±2.3
SCF (Yang et al., 2022b)	92.6±1.8	94.9±1.0
CF-SC (Isufi & Yang, 2022)	96.9±0.8	97.9±0.7
GNN (Gama et al., 2020a)	93.9±1.0	96.6±0.5
SNN (Ebli et al., 2020)	92.0±1.8	95.1±1.2
PSNN (Roddenberry et al., 2021)	95.6±1.3	98.1±0.5
SCNN (Yang et al., 2022a)	96.5±1.5	98.3±0.4
Bunch (Bunch et al., 2020)	98.0±0.5	98.5±0.5
SCCNN (ours)	98.4±0.5	99.4±0.3

Table 3. Prediction accuracy of the synthetic data in standard, reverse and generalization tasks, and ocean drifters (Last Column).

Methods	Standard	Reverse	Gen.	Ocean
PSNN	63.1±3.1	58.4±3.9	55.3±2.5	49.0±8.0
SCNN	67.7±1.7	55.3±5.3	61.2±3.2	53.0±7.8
SNN	65.5±2.4	53.6±6.1	59.5±3.7	52.5±6.0
Bunch	62.3±4.0	59.6±6.1	53.9±3.1	46.0±6.2
SCCNN (ours)	65.2±4.1	58.9±4.1	56.8±2.4	54.5±7.9

be found in Appendix F.3. From the results of different methods in Table 3, we see that SCCNN performs better than Bunch due to the use of higher-order convolutions, and likewise, SCNN and SNN give better predictions than PSNN. Also, differentiating the parameter space for lower and upper convolutions improves the performance of SCNN compared to SNN. As zero inputs on nodes and triangles are applied, SCCNN does not perform better than SCNN. Like other NNs, SCCNNs do not deteriorate in the reverse task owing to the orientation equivariance and they show good generalization ability to the unseen data as well.

8. Conclusion

We proposed an SCCNN for learning on SCs, which performs a simplicial convolution with an intra-simplicial locality and multi-hop information from adjacent simplices with an extended inter-simplicial locality. We provide a thorough theoretical study of the proposed architecture from different viewpoints. First, we study the symmetries in an SC and simplicial signal space and show the SCCNN can be built equivariant to permutations and orientations of simplices. We then study its spectral behavior and understand how the learned convolutional filters perform in the different simplicial frequencies, i.e., in different simplicial signal spaces. Finally, we study the stability of the SCCNN, showing that it is stable to domain perturbations and how the inter-simplicial locality affects the performance. We corroborate these results with numerical experiments achieving a comparable performance with state-of-the-art alternatives.

References

- Ammar, W., Groeneveld, D., Bhagavatula, C., Beltagy, I., Crawford, M., Downey, D., Dunkelberger, J., Elgohary, A., Feldman, S., Ha, V., et al. Construction of the literature graph in semantic scholar. *arXiv preprint arXiv:1805.02262*, 2018.
- Barbarossa, S. and Sardellitti, S. Topological signal processing over simplicial complexes. *IEEE Transactions on Signal Processing*, 68:2992–3007, 2020.
- Battaglia, P. W., Hamrick, J. B., Bapst, V., Sanchez-Gonzalez, A., Zambaldi, V., Malinowski, M., Tacchetti, A., Raposo, D., Santoro, A., Faulkner, R., et al. Relational inductive biases, deep learning, and graph networks. *arXiv preprint arXiv:1806.01261*, 2018.
- Benson, A. R., Abebe, R., Schaub, M. T., Jadbabaie, A., and Kleinberg, J. Simplicial closure and higher-order link prediction. *Proceedings of the National Academy of Sciences*, 115(48):E11221–E11230, 2018.
- Bick, C., Gross, E., Harrington, H. A., and Schaub, M. T. What are higher-order networks? *arXiv preprint arXiv:2104.11329*, 2021.
- Bodnar, C., Frasca, F., Otter, N., Wang, Y. G., Liò, P., Montufar, G. F., and Bronstein, M. Weisfeiler and lehman go cellular: Cw networks. *Advances in Neural Information Processing Systems*, 34, 2021a.
- Bodnar, C., Frasca, F., Wang, Y., Otter, N., Montufar, G. F., Lio, P., and Bronstein, M. Weisfeiler and lehman go topological: Message passing simplicial networks. In *International Conference on Machine Learning*, pp. 1026–1037. PMLR, 2021b.
- Bronstein, M. M., Bruna, J., Cohen, T., and Velicković, P. Geometric deep learning: Grids, groups, graphs, geodesics, and gauges. *arXiv preprint arXiv:2104.13478*, 2021.
- Bruna, J. and Mallat, S. Invariant scattering convolution networks. *IEEE transactions on pattern analysis and machine intelligence*, 35(8):1872–1886, 2013.
- Bunch, E., You, Q., Fung, G., and Singh, V. Simplicial 2-complex convolutional neural networks. In *TDA & Beyond*, 2020. URL <https://openreview.net/forum?id=TLbnsKrt6J->.
- Candogan, O., Menache, I., Ozdaglar, A., and Parrilo, P. A. Flows and decompositions of games: Harmonic and potential games. *Mathematics of Operations Research*, 36(3):474–503, 2011.
- Chen, Y., Gel, Y., and Poor, H. V. Time-conditioned dances with simplicial complexes: Zigzag filtration curve based supra-hodge convolution networks for time-series forecasting. In *Advances in Neural Information Processing Systems*, 2022a.
- Chen, Y., Gel, Y. R., and Poor, H. V. Bscnets: Block simplicial complex neural networks. *Proceedings of the AAAI Conference on Artificial Intelligence*, 36(6):6333–6341, 2022b. doi: 10.1609/aaai.v36i6.20583. URL <https://ojs.aaai.org/index.php/AAAI/article/view/20583>.
- Cordonnier, J.-B. and Loukas, A. Extrapolating paths with graph neural networks. In *Proceedings of the Twenty-Eighth International Joint Conference on Artificial Intelligence, IJCAI-19*, pp. 2187–2194. International Joint Conferences on Artificial Intelligence Organization, 7 2019. doi: 10.24963/ijcai.2019/303. URL <https://doi.org/10.24963/ijcai.2019/303>.
- De Longueville, M. *A course in topological combinatorics*. Springer Science & Business Media, 2012.
- Defferrard, M., Bresson, X., and Vandergheynst, P. Convolutional neural networks on graphs with fast localized spectral filtering. In Lee, D., Sugiyama, M., Luxburg, U., Guyon, I., and Garnett, R. (eds.), *Advances in Neural Information Processing Systems*, volume 29. Curran Associates, Inc., 2016. URL <https://proceedings.neurips.cc/paper/2016/file/04df4d434d481c5bb723be1b6df1ee65-Paper.pdf>.
- Ebli, S., Defferrard, M., and Spreemann, G. Simplicial neural networks. In *NeurIPS 2020 Workshop on Topological Data Analysis and Beyond*, 2020.
- Gama, F., Marques, A. G., Leus, G., and Ribeiro, A. Convolutional graph neural networks. In *2019 53rd Asilomar Conference on Signals, Systems, and Computers*, pp. 452–456. IEEE, 2019a.
- Gama, F., Ribeiro, A., and Bruna, J. Stability of graph scattering transforms. *Advances in Neural Information Processing Systems*, 32, 2019b.
- Gama, F., Bruna, J., and Ribeiro, A. Stability properties of graph neural networks. *IEEE Transactions on Signal Processing*, 68:5680–5695, 2020a.
- Gama, F., Isufi, E., Leus, G., and Ribeiro, A. Graphs, convolutions, and neural networks: From graph filters to graph neural networks. *IEEE Signal Processing Magazine*, 37(6):128–138, 2020b.

- Ghosh, A., Rozemberczki, B., Ramamoorthy, S., and Sarkar, R. Topological signatures for fast mobility analysis. In *Proceedings of the 26th ACM SIGSPATIAL International Conference on Advances in Geographic Information Systems*, pp. 159–168, 2018.
- Gilmer, J., Schoenholz, S. S., Riley, P. F., Vinyals, O., and Dahl, G. E. Neural message passing for quantum chemistry. In *International conference on machine learning*, pp. 1263–1272. PMLR, 2017.
- Giusti, L., Battiloro, C., Di Lorenzo, P., Sardellitti, S., and Barbarossa, S. Simplicial attention networks. *arXiv preprint arXiv:2203.07485*, 2022.
- Goh, C. W. J., Bodnar, C., and Lio, P. Simplicial attention networks. In *ICLR 2022 Workshop on Geometrical and Topological Representation Learning*, 2022.
- Grady, L. J. and Polimeni, J. R. *Discrete calculus: Applied analysis on graphs for computational science*, volume 3. Springer, 2010.
- Hajij, M., Istvan, K., and Zamzmi, G. Cell complex neural networks. In *NeurIPS 2020 Workshop on Topological Data Analysis and Beyond*, 2020.
- Hajij, M., Zamzmi, G., Papamarkou, T., Maroulas, V., and Cai, X. Simplicial complex representation learning. *arXiv preprint arXiv:2103.04046*, 2021.
- Hajij, M., Zamzmi, G., Papamarkou, T., Miolane, N., Guzmán-Sáenz, A., and Ramamurthy, K. N. Higher-order attention networks. *arXiv preprint arXiv:2206.00606*, 2022.
- Hamilton, W. L. *Graph representation learning*. Morgan & Claypool Publishers, 2020.
- Hansen, J. and Ghrist, R. Toward a spectral theory of cellular sheaves. *Journal of Applied and Computational Topology*, 3(4):315–358, 2019.
- Hodge, W. V. D. *The theory and applications of harmonic integrals*. CUP Archive, 1989.
- Horak, D. and Jost, J. Spectra of combinatorial laplace operators on simplicial complexes. *Advances in Mathematics*, 244:303–336, 2013.
- Isufi, E. and Yang, M. Convolutional filtering in simplicial complexes. In *ICASSP 2022 - 2022 IEEE International Conference on Acoustics, Speech and Signal Processing (ICASSP)*, pp. 5578–5582, 2022. doi: 10.1109/ICASSP43922.2022.9746349.
- Jia, J., Schaub, M. T., Segarra, S., and Benson, A. R. Graph-based semi-supervised & active learning for edge flows. In *Proceedings of the 25th ACM SIGKDD International Conference on Knowledge Discovery & Data Mining*, pp. 761–771, 2019.
- Jiang, X., Lim, L.-H., Yao, Y., and Ye, Y. Statistical ranking and combinatorial hodge theory. *Mathematical Programming*, 127(1):203–244, 2011.
- Keros, A. D., Nanda, V., and Subr, K. Dist2cycle: A simplicial neural network for homology localization. *Proceedings of the AAAI Conference on Artificial Intelligence*, 36(7):7133–7142, 2022. doi: 10.1609/aaai.v36i7.20673. URL <https://ojs.aaai.org/index.php/AAAI/article/view/20673>.
- Kipf, T. N. and Welling, M. Variational graph auto-encoders. *arXiv preprint arXiv:1611.07308*, 2016.
- Kipf, T. N. and Welling, M. Semi-supervised classification with graph convolutional networks. In *International Conference on Learning Representations (ICLR)*, 2017.
- Lim, L.-H. Hodge laplacians on graphs. *SIAM Review*, 62(3):685–715, 2020.
- Masoomy, H., Askari, B., Tajik, S., Rizi, A. K., and Jafari, G. R. Topological analysis of interaction patterns in cancer-specific gene regulatory network: persistent homology approach. *Scientific Reports*, 11(1):1–11, 2021.
- Money, R., Krishnan, J., Beferull-Lozano, B., and Isufi, E. Online edge flow imputation on networks. *IEEE Signal Processing Letters*, 2022.
- Munkres, J. R. *Elements of algebraic topology*. CRC press, 2018.
- Newman, M. E., Watts, D. J., and Strogatz, S. H. Random graph models of social networks. *Proceedings of the national academy of sciences*, 99(suppl.1):2566–2572, 2002.
- Nikhil, N. and Tran Morris, B. Convolutional neural network for trajectory prediction. In *Proceedings of the European Conference on Computer Vision (ECCV) Workshops*, pp. 0–0, 2018.
- Parada-Mayorga, A., Wang, Z., Gama, F., and Ribeiro, A. Stability of aggregation graph neural networks. *arXiv preprint arXiv:2207.03678*, 2022.
- Roddenberry, T. M. and Segarra, S. Hodgenet: Graph neural networks for edge data. In *2019 53rd Asilomar Conference on Signals, Systems, and Computers*, pp. 220–224. IEEE, 2019.
- Roddenberry, T. M., Glaze, N., and Segarra, S. Principled simplicial neural networks for trajectory prediction. In *International Conference on Machine Learning*, pp. 9020–9029. PMLR, 2021.

- Roddenberry, T. M., Schaub, M. T., and Hajij, M. Signal processing on cell complexes. In *ICASSP 2022-2022 IEEE International Conference on Acoustics, Speech and Signal Processing (ICASSP)*, pp. 8852–8856. IEEE, 2022.
- Rudenko, A., Palmieri, L., Herman, M., Kitani, K. M., Gavrila, D. M., and Arras, K. O. Human motion trajectory prediction: A survey. *The International Journal of Robotics Research*, 39(8):895–935, 2020.
- Ruiz, L., Gama, F., and Ribeiro, A. Graph neural networks: architectures, stability, and transferability. *Proceedings of the IEEE*, 109(5):660–682, 2021.
- Sandryhaila, A. and Moura, J. M. Discrete signal processing on graphs. *IEEE Transactions on Signal Processing*, 61(7):1644–1656, 2013.
- Sandryhaila, A. and Moura, J. M. Discrete signal processing on graphs: Frequency analysis. *IEEE Transactions on Signal Processing*, 62(12):3042–3054, 2014.
- Sardellitti, S., Barbarossa, S., and Testa, L. Topological signal processing over cell complexes. In *2021 55th Asilomar Conference on Signals, Systems, and Computers*, pp. 1558–1562. IEEE, 2021.
- Schaub, M. T. and Segarra, S. Flow smoothing and denoising: Graph signal processing in the edge-space. In *2018 IEEE Global Conference on Signal and Information Processing (GlobalSIP)*, pp. 735–739. IEEE, 2018.
- Schaub, M. T., Benson, A. R., Horn, P., Lippner, G., and Jadbabaie, A. Random walks on simplicial complexes and the normalized hodge 1-laplacian. *SIAM Review*, 62(2):353–391, 2020.
- Schaub, M. T., Zhu, Y., Seby, J.-B., Roddenberry, T. M., and Segarra, S. Signal processing on higher-order networks: Livin’ on the edge... and beyond. *Signal Processing*, 187:108149, 2021.
- Shuman, D. I., Narang, S. K., Frossard, P., Ortega, A., and Vandergheynst, P. The emerging field of signal processing on graphs: Extending high-dimensional data analysis to networks and other irregular domains. *IEEE Signal Processing Magazine*, 30(3):83–98, 2013.
- Sleijpen, G. L. and Van der Vorst, H. A. A jacobi–davidson iteration method for linear eigenvalue problems. *SIAM review*, 42(2):267–293, 2000.
- Watkins, D. S. *The matrix eigenvalue problem: GR and Krylov subspace methods*. SIAM, 2007.
- Wu, F., Souza, A., Zhang, T., Fifty, C., Yu, T., and Weinberger, K. Simplifying graph convolutional networks. In *International conference on machine learning*, pp. 6861–6871. PMLR, 2019.
- Wu, H., Chen, Z., Sun, W., Zheng, B., and Wang, W. Modeling trajectories with recurrent neural networks. In *Proceedings of the Twenty-Sixth International Joint Conference on Artificial Intelligence, IJCAI-17*, pp. 3083–3090, 2017. doi: 10.24963/ijcai.2017/430. URL <https://doi.org/10.24963/ijcai.2017/430>.
- Yang, M., Isufi, E., Schaub, M. T., and Leus, G. Finite Impulse Response Filters for Simplicial Complexes. In *2021 29th European Signal Processing Conference (EUSIPCO)*, pp. 2005–2009, August 2021. doi: 10.23919/EUSIPCO54536.2021.9616185. ISSN: 2076-1465.
- Yang, M., Isufi, E., and Leus, G. Simplicial convolutional neural networks. In *ICASSP 2022 - 2022 IEEE International Conference on Acoustics, Speech and Signal Processing (ICASSP)*, pp. 8847–8851, 2022a. doi: 10.1109/ICASSP43922.2022.9746017.
- Yang, M., Isufi, E., Schaub, M. T., and Leus, G. Simplicial convolutional filters. *IEEE Transactions on Signal Processing*, 70:4633–4648, 2022b. doi: 10.1109/TSP.2022.3207045.
- Yang, R., Sala, F., and Bogdan, P. Efficient representation learning for higher-order data with simplicial complexes. In *The First Learning on Graphs Conference*, 2022c. URL <https://openreview.net/forum?id=nGqJY4DODN>.
- Zhang, M. and Chen, Y. Link prediction based on graph neural networks. *Advances in neural information processing systems*, 31, 2018.

Supplementary Material

In this supplement, we discuss necessary materials to aid the exposition of this paper. We organize them according to the corresponding sections.

A. Background

In [Section 2](#) we give the definition of an abstract SC and think of it in terms of a geometric realization, i.e., nodes, edges, triangle faces and so on. While this is helpful to understand, it might not be trivial. Thus, we discuss the geometric SC and show that every abstract SC has a geometric realization.

A.1. Abstract Simplicial Complex and its Geometric Realizations

If $\mathbf{v}_0, \dots, \mathbf{v}_k \in \mathbb{R}^m$ are affinely independent, then *the (affine) simplex* s^k spanned by $\mathbf{v}_0, \dots, \mathbf{v}_k$ is defined to be their convex hull

$$s_g^k = \text{conv}(\mathbf{v}_0, \dots, \mathbf{v}_k) = \left\{ \sum_{i=0}^k \lambda_i \mathbf{v}_i : \lambda_i \geq 0, \sum_{i=0}^k \lambda_i = 1 \right\}.$$

[Figure A.1](#) illustrates some simplices. The prototype of a k -dimensional simplex is given by the *standard k -simplex* s^k defined by the standard basis vectors $e_1, \dots, e_{k+1} \in \mathbb{R}^{k+1}$: $s_g^k = \text{conv}(e_1, \dots, e_{k+1}) \subseteq \mathbb{R}^{k+1}$.

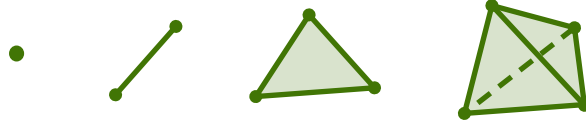


[Figure A.1](#). A 0-simplex is a node (point), a 1-simplex is a line segment (edge), a 2-simplex is a (filled) triangle and a 3-simplex is a (filled) tetrahedron

Definition A.1. A (finite geometric) simplicial complex \mathcal{S}_g is a finite set of (affine) simplices in \mathbb{R}^m such that 1) $s \in \mathcal{S}_g$ and $t \subset s$ implies $t \in \mathcal{S}_g$ (inclusion property); and 2) if $s_1, s_2 \in \mathcal{S}_g$, then $s_1 \cap s_2$ is a face of s_1 and a face of s_2 .

Any geometric SC \mathcal{S}_g gives rise to an associated abstract SC. Recall the definition of an abstract SC in [Section 2](#).

Definition A.2. A *simplicial map* of abstract simplicial complexes \mathcal{S}_1 and \mathcal{S}_2 is defined to be a map between their vertex sets $f : \mathcal{S}_1^0 \rightarrow \mathcal{S}_2^0$ preserving simplices, i.e., $f(s) \in \mathcal{S}_2$ for each $s \in \mathcal{S}_1$.

Definition A.3. A geometric simplicial complex \mathcal{S}_g is a *geometric realization* of an abstract simplicial complex \mathcal{S} if there exists a bijection $\varphi : \mathcal{S}^0 \rightarrow \mathcal{S}_g^0$ such that for any set $\mathbf{v}_0, \dots, \mathbf{v}_k \in \mathcal{S}^0$ of vertices of \mathcal{S} ,

$$\{\mathbf{v}_0, \dots, \mathbf{v}_k\} \in \mathcal{S} \iff \text{conv}(\varphi(\mathbf{v}_0), \dots, \varphi(\mathbf{v}_k)) \in \mathcal{S}_g.$$

In other words, \mathcal{S}_g is a geometric realization of \mathcal{S} if and only if its associated abstract SC is simplicially isomorphic to \mathcal{S} .

Proposition A.4. Any abstract simplicial complex \mathcal{S} of dimension K admits a geometric realization in \mathbb{R}^{2K+1} .

Proposition A.5. Any two geometric simplicial complexes are simplicially homeomorphic if and only if the associated abstract simplicial complexes are simplicially isomorphic.

The proofs can be found in [De Longueville \(2012, P. 177-178\)](#) and [Munkres \(2018\)](#). They imply that a geometric realization of an abstract SC is unique up to simplicial homeomorphisms.

A.2. Algebraic Representations of an SC

Given an oriented SC \mathcal{S} with vertex set $\mathcal{V} = \{1, \dots, N_0\}$, the entries of $\mathbf{B}_1 \in \mathbb{R}^{N_0 \times N_1}$ and $\mathbf{B}_2 \in \mathbb{R}^{N_1 \times N_2}$ are given by

$$[\mathbf{B}_1]_{ie} = \begin{cases} -1, & \text{for } e = [i, \cdot] \\ 1, & \text{for } e = [\cdot, i] \\ 0, & \text{otherwise.} \end{cases} \quad [\mathbf{B}_2]_{et} = \begin{cases} 1, & \text{for } e = [i, j], t = [i, j, k] \\ -1, & \text{for } e = [i, k], t = [i, j, k] \\ 1, & \text{for } e = [j, k], t = [i, j, k] \\ 0, & \text{otherwise.} \end{cases} \quad (\text{A.1})$$

In the following, we show the two incidence matrices of the SC in Figure 1a.

$$\mathbf{B}_1 = \begin{matrix} & e_1 & e_2 & e_3 & e_4 & e_5 & e_6 & e_7 & e_8 & e_9 & e_{10} \\ \begin{matrix} 1 \\ 2 \\ 3 \\ 4 \\ 5 \\ 6 \\ 7 \end{matrix} & \begin{pmatrix} -1 & -1 & -1 & 0 & 0 & 0 & 0 & 0 & 0 & 0 & 0 \\ 1 & 0 & 0 & -1 & -1 & 0 & 0 & 0 & 0 & 0 & 0 \\ 0 & 1 & 0 & 1 & 0 & -1 & -1 & -1 & 0 & 0 & 0 \\ 0 & 0 & 1 & 0 & 0 & 1 & 0 & 0 & 0 & 0 & 0 \\ 0 & 0 & 0 & 0 & 1 & 0 & 1 & 0 & -1 & -1 & 0 \\ 0 & 0 & 0 & 0 & 0 & 0 & 0 & 1 & 1 & 0 & 0 \\ 0 & 0 & 0 & 0 & 0 & 0 & 0 & 0 & 0 & 0 & 1 \end{pmatrix} \end{matrix}, \quad \mathbf{B}_2 = \begin{matrix} & t_1 & t_2 & t_3 \\ \begin{matrix} e_1 \\ e_2 \\ e_3 \\ e_4 \\ e_5 \\ e_6 \\ e_7 \\ e_8 \\ e_9 \\ e_{10} \end{matrix} & \begin{pmatrix} 1 & 0 & 0 \\ -1 & 0 & 0 \\ 0 & 0 & 0 \\ 1 & 1 & 0 \\ 0 & -1 & 0 \\ 0 & 0 & 0 \\ 0 & 1 & 1 \\ 0 & 0 & -1 \\ 0 & 0 & 1 \\ 0 & 0 & 0 \end{pmatrix} \end{matrix} \quad (\text{A.2})$$

B. Simplicial Complex Convolutional Neural Networks

B.1. Multi-Feature SCCNN

A multi-feature SCCNN at layer l takes $\{\mathbf{X}_{k-1}^{l-1}, \mathbf{X}_k^{l-1}, \mathbf{X}_{k+1}^{l-1}\}$ as inputs, each of which has F_{l-1} features, and generates an output \mathbf{X}_k^l with F_l features as

$$\mathbf{X}_k^l = \sigma \left(\sum_{t=0}^{T_d} \mathbf{L}_{k,d}^t \mathbf{B}_k^\top \mathbf{X}_{k-1}^{l-1} \mathbf{W}_{k,d,t}^l + \sum_{t=0}^{T_d} \mathbf{L}_{k,d}^t \mathbf{X}_k^{l-1} \mathbf{W}_{k,d,t}^l + \sum_{t=0}^{T_u} \mathbf{L}_{k,u}^t \mathbf{X}_k^{l-1} \mathbf{W}_{k,u,t}^l + \sum_{t=0}^{T_u} \mathbf{L}_{k,u}^t \mathbf{B}_{k+1} \mathbf{X}_{k+1}^{l-1} \mathbf{W}_{k,u,t}^l \right) \quad (\text{B.1})$$

where \mathbf{L}^t indicates the matrix t -power of \mathbf{L} , while superscript l indicates the layer index.

B.2. Complexity

In an SCCNN layer for computing \mathbf{x}_k^l , there are $2 + T_d + T_u$ filter coefficients for the SCF \mathbf{H}_k^l , and $1 + T_d$ and $1 + T_u$ for $\mathbf{H}_{k,d}^l$ and $\mathbf{H}_{k,u}^l$, respectively, which gives the parameter complexity of order $\mathcal{O}(T_d + T_u)$. This complexity will increase by $F_l F_{l-1}$ fold for the multi-feature case, and likewise for the computational complexity. Given the inputs $\{\mathbf{x}_{k-1}^{l-1}, \mathbf{x}_k^{l-1}, \mathbf{x}_{k+1}^{l-1}\}$, we discuss the computation complexity of \mathbf{x}_k^l in (1).

First, consider the SCF operation $\mathbf{H}_k^l \mathbf{x}_k^{l-1}$. As discussed in the localities, it is a composition of T_d -step lower and T_u -step upper simplicial shiftings. Each simplicial shifting has a computational complexity of order $\mathcal{O}(N_k M_k)$ dependent on the number of neighbors. Thus, this operation has a complexity of order $\mathcal{O}(N_k M_k (T_d + T_u))$.

Second, consider the lower SCF operation $\mathbf{H}_{k,d}^l \mathbf{B}_k^\top \mathbf{x}_{k-1}^{l-1}$. As incidence matrix \mathbf{B}_k is sparse, it has $N_k(k+1)$ nonzero entries as each k -simplex has $k+1$ faces. This leads to a complexity of order $\mathcal{O}(N_k k)$ for operation $\mathbf{B}_k^\top \mathbf{x}_{k-1}^{l-1}$. Followed by a lower SCF operation, i.e., a T_d -step lower simplicial shifting, thus, a complexity of order $\mathcal{O}(k N_k + N_k M_k T_d)$ is needed.

Third, consider the upper SCF operation $\mathbf{H}_{k,u}^l \mathbf{B}_{k+1} \mathbf{x}_{k+1}^{l-1}$. Likewise, incidence matrix \mathbf{B}_{k+1} has $N_{k+1}(k+2)$ nonzero entries. This leads to a complexity of order $\mathcal{O}(N_{k+1} k)$ for the projection operation $\mathbf{B}_{k+1} \mathbf{x}_{k+1}^{l-1}$. Followed by an upper SCF operation, i.e., a T_u -step upper simplicial shifting, thus, a complexity of order $\mathcal{O}(k N_{k+1} + N_k M_k T_u)$ is needed.

Finally, we have a computational complexity of order $\mathcal{O}(k(N_k + N_{k+1}) + N_k M_k (T_d + T_u))$ in total.

Remark B.1. The lower SCF operation $\mathbf{H}_{k,d}^l \mathbf{B}_k^\top \mathbf{x}_{k-1}^{l-1}$ can be further reduced if $N_{k-1} \ll N_k$. Note that we have

$$\mathbf{H}_{k,d}^l \mathbf{B}_k^\top \mathbf{x}_{k-1}^{l-1} = \sum_{t=0}^{T_d} w_{k,d,t}^l \mathbf{L}_{k,d}^t \mathbf{B}_k^\top \mathbf{x}_{k-1}^{l-1} = \mathbf{B}_k^\top \sum_{t=0}^{T_d} w_{k,d,t}^l \mathbf{L}_{k-1,u}^t \mathbf{x}_{k-1}^{l-1}, \quad (\text{B.2})$$

where the second equality comes from that $\mathbf{L}_{k,d} \mathbf{B}_k^\top = \mathbf{B}_k^\top \mathbf{B}_k \mathbf{B}_k^\top = \mathbf{B}_k^\top \mathbf{L}_{k-1,u}$, $\mathbf{L}_{k,d}^2 \mathbf{B}_k^\top = (\mathbf{B}_k^\top \mathbf{B}_k)(\mathbf{B}_k^\top \mathbf{B}_k) \mathbf{B}_k^\top = \mathbf{B}_k^\top (\mathbf{B}_k \mathbf{B}_k^\top)(\mathbf{B}_k \mathbf{B}_k^\top) = \mathbf{B}_k^\top \mathbf{L}_{k-1,u}$ and likewise for general t . Using the RHS of (B.2) where the simplicial shifting is performed in the $(k-1)$ -simplicial space, we have a complexity of order $\mathcal{O}(k N_k + N_{k-1} M_{k-1} T_d)$. Similarly, we have

$$\mathbf{H}_{k,u}^l \mathbf{B}_{k+1} \mathbf{x}_{k+1}^{l-1} = \sum_{t=0}^{T_u} w_{k,u,t}^l \mathbf{L}_{k,u}^t \mathbf{B}_{k+1} \mathbf{x}_{k+1}^{l-1} = \mathbf{B}_{k+1} \sum_{t=0}^{T_u} w_{k,u,t}^l \mathbf{L}_{k+1,d}^t \mathbf{x}_{k+1}^{l-1} \quad (\text{B.3})$$

where the simplicial shifting is performed in the $(k+1)$ -simplicial space. If it follows that $N_{k+1} \ll N_k$, we have a smaller complexity of $\mathcal{O}(kN_{k+1} + N_{k+1}M_{k+1}T_u)$ by using the RHS of (B.3).

B.3. Extended Simplicial Locality for SCCNN of order $K = 2$

We use an SCCNN of order $K = 2$ to illustrate the extended simplicial locality in detail. At layer l , we have

$$\begin{aligned} \mathbf{x}_0^l &= \sigma(\mathbf{H}_0^l \mathbf{x}_0^{l-1} + \mathbf{H}_{0,u}^l \mathbf{B}_1 \mathbf{x}_1^{l-1}) \\ \mathbf{x}_1^l &= \sigma(\mathbf{H}_{1,d}^l \mathbf{B}_1^\top \mathbf{x}_0^{l-1} + \mathbf{H}_1^l \mathbf{x}_1^{l-1} + \mathbf{H}_{1,u}^l \mathbf{B}_2 \mathbf{x}_2^{l-1}) \\ \mathbf{x}_2^l &= \sigma(\mathbf{H}_{2,d}^l \mathbf{B}_2^\top \mathbf{x}_1^{l-1} + \mathbf{H}_2^l \mathbf{x}_2^{l-1}) \end{aligned} \quad (\text{B.4})$$

from which we can see the inter-simplicial locality that each k -simplicial signal contain information from its adjacent $(k \pm 1)$ -simplices and itself. To see the extended inter-simplicial locality, we focus on the node output, which admits the following expression

$$\mathbf{x}_0^l = \sigma(\mathbf{H}_0 \mathbf{x}_0^{l-1} + \mathbf{H}_{0,u} \mathbf{B}_1 \sigma(\mathbf{H}_{1,d}^{l-1} \mathbf{B}_1^\top \mathbf{x}_0^{l-2} + \mathbf{H}_1^{l-1} \mathbf{x}_1^{l-2} + \mathbf{H}_{1,u}^{l-1} \mathbf{B}_2 \mathbf{x}_2^{l-2})) \quad (\text{B.5})$$

where the contribution from triangle output \mathbf{x}_2^{l-2} at layer $(l-2)$ is contained in \mathbf{x}_0^l , owing to the fact that $\mathbf{B}_1 \sigma(\mathbf{H}_{1,u}^{l-1} \mathbf{B}_2) \neq \mathbf{0}$. This is also illustrated in Figure 1d where node 1 contains information not only from its neighbors including nodes $\{2, 3, 4\}$ and edges (cofaces) $\{e_1, e_2, e_3\}$ that contribute to those neighbors, but also from direct triangle t_1 and triangles $\{t_2, t_3\}$ further away, which project information to those edges.

B.4. Related Works in Detail

We describe how the SCCNN in (B.1) generalize other NNs on graphs and SCs in Table 1. For simplicity, we use \mathbf{Y} and \mathbf{X} to denote the output and input, respectively, without the index l . Note that for GNNs, $\mathbf{L}_{0,d}$ is not defined.

Gama et al. (2020a) proposed to build a GNN layer with the form

$$\mathbf{Y}_0 = \sigma \left(\sum_{t=0}^{T_u} \mathbf{L}_0^t \mathbf{X}_0 \mathbf{W}_{0,u,t} \right) \quad (\text{B.6})$$

where the convolution step is performed via a graph filter (Sandryhaila & Moura, 2013; 2014; Gama et al., 2019a; 2020b). This GNN can be easily built as a special SCCNN without contributions from edges. Furthermore, Defferrard et al. (2016) considered a fast implementation of this GNN via a Chebyshev polynomial, while Wu et al. (2019) simplified this by setting $\mathbf{W}_{0,t,u}$ as zeros for $t < T_u$. Kipf & Welling (2017) further simplified this by setting $T_u = 1$, namely, GCN.

Yang et al. (2022a) proposed a simplicial convolutional neural network (SCNN) to learn from k -simplicial signals

$$\mathbf{Y}_k = \sigma \left(\sum_{t=0}^{T_d} \mathbf{L}_{k,d}^t \mathbf{X}_k \mathbf{W}_{k,d,t} + \sum_{t=0}^{T_u} \mathbf{L}_{k,u}^t \mathbf{X}_k \mathbf{W}_{k,u,t} \right) \quad (\text{B.7})$$

where the linear operation is also defined as a simplicial convolution filter in Yang et al. (2022b). This is a special SCCNN with a focus on one simplex level without taking into the lower and upper contributions consideration. The simplicial neural network (SNN) of Ebli et al. (2020) did not differentiate the lower and the upper convolutions with a form of $\mathbf{Y}_k = \sigma(\sum_{t=0}^T \mathbf{L}_k^t \mathbf{X}_k \mathbf{W}_{k,t})$, which leads to a joint processing in the gradient and curl subspaces as analyzed in Section 5.

While Roddenberry et al. (2021) proposed an architecture (referred to as PSNN) of a particular form of (B.7) with $T_d = T_u = 1$, performing only a one-step simplicial shifting (2). Keros et al. (2022) also performs a one-step simplicial shifting but with an inverted Hodge Laplacian to localize the homology group in an SC. An attention mechanism was added to both SCNNs and PSNNs by Giusti et al. (2022) and Goh et al. (2022), respectively.

To account for the information from adjacent simplices, Bunch et al. (2020) proposed a simplicial 2-complex CNN (S2CCNN)

$$\begin{aligned} \mathbf{Y}_0 &= \sigma(\mathbf{L}_0 \mathbf{X}_0 \mathbf{W}_{0,u,1} + \mathbf{B}_1 \mathbf{X}_1 \mathbf{W}'_{0,u,0}) \\ \mathbf{Y}_1 &= \sigma(\mathbf{B}_1^\top \mathbf{X}_0 \mathbf{W}_{1,d,0} + \mathbf{L}_1 \mathbf{X}_1 \mathbf{W}_{1,1} + \mathbf{B}_2 \mathbf{X}_2 \mathbf{W}'_{1,u,0}) \\ \mathbf{Y}_2 &= \sigma(\mathbf{B}_2^\top \mathbf{X}_1 \mathbf{W}_{2,d,0} + \mathbf{L}_{2,u} \mathbf{X}_2 \mathbf{W}_{2,u,1}) \end{aligned} \quad (\text{B.8})$$

which is limited to SCs of order two. Note that instead of Hodge Laplacians, simplicial adjacency matrices with self-loops are used in [Bunch et al. \(2020\)](#), which encode equivalent information as setting all filter orders in SCCNNs as one. It is a particular form of the SCCNN where the SCF is a one-step simplicial shifting operation without differentiating the lower and upper shifting, and the lower and upper contributions are simply added, not convolved or shifted by lower and upper SCFs. That is, [Bunch et al. \(2020\)](#) can be obtained from (1) by setting lower and upper SCFs as identity, $\mathbf{H}_{k,d} = \mathbf{H}_{k,u} = \mathbf{I}$, and setting $w_{k,d,t} = w_{k,u,t}$ and $T_d = T_u = 1$ for the SCF \mathbf{H}_k .

The convolution in [Yang et al. \(2022c, eq. 3\)](#) is the same as [Bunch et al. \(2020\)](#) though it was performed in a block matrix fashion. The combination of graph shifting and edge shifting in [Chen et al. \(2022b\)](#) can be again seen as a special S2CCNN, where the implementation was performed in a block matrix fashion. [Bodnar et al. \(2021b\)](#) proposed a message passing scheme which collects information from one-hop simplicial neighbors and direct faces and cofaces as [Bunch et al. \(2020\)](#) and [Yang et al. \(2022c\)](#), but replacing the one-step shifting and projections from (co)faces by some learnable functions. The same message passing was applied for simplicial representation learning by [Hajij et al. \(2021\)](#).

Lastly, there are works on signal processing and NNs on cell complexes. For example, [Sardellitti et al. \(2021\)](#); [Roddenberry et al. \(2022\)](#) generalized the signal processing techniques from SCs to cell complexes, [Bodnar et al. \(2021a\)](#); [Hajij et al. \(2020\)](#) performed message passing on cell complexes as in SCs and [Hajij et al. \(2022\)](#) added the attention mechanism. Cell complexes are a more general model compared to SCs, where k -cells compared to k -simplices contain any shapes homeomorphic to a k -dimensional closed balls in Euclidean space, e.g., a filled polygon is a 2-cell while only triangles are 2-simplices. We refer to [Hansen & Ghrist \(2019\)](#) for a more formal definition of cell complexes. Despite cell complexes are more powerful to model real-world higher-order structures, SCCNNs can be easily generalized to cell complexes by considering any k -cells instead of only k -simplices in the algebraic representations, and the theoretical analysis in this paper can be adapted to cell complexes as well.

C. Simplicial Complex Symmetries

C.1. Background on Groups

In the following, we briefly introduce some definitions in group theory, following from [Bronstein et al. \(2021\)](#).

Definition C.1 (Groups). A group is a set \mathcal{G} along with a binary operation $\circ : \mathcal{G} \times \mathcal{G} \rightarrow \mathcal{G}$ called *composition*, e.g., addition and multiplication of numbers or matrices, or union and intersection of sets, satisfying the following axioms:

- 1) Associativity: $(\mathfrak{g} \circ \mathfrak{h}) \circ \mathfrak{k} = \mathfrak{g} \circ (\mathfrak{h} \circ \mathfrak{k})$ for all $\mathfrak{g}, \mathfrak{h}, \mathfrak{k} \in \mathfrak{P}$.
- 2) Identity: there exists a unique identity $\epsilon \in \mathfrak{P}$ satisfying $\epsilon \circ \mathfrak{g} = \mathfrak{g} \circ \epsilon = \mathfrak{g}$ for all $\mathfrak{g} \in \mathfrak{P}_k$.
- 3) Inverse: for each $\mathfrak{g} \in \mathfrak{P}$ there is a unique inverse $\mathfrak{g}^{-1} \in \mathfrak{P}_k$ such that $\mathfrak{g} \circ \mathfrak{g}^{-1} = \mathfrak{g}^{-1} \circ \mathfrak{g} = \epsilon$.
- 4) Closure: the group is closed under composition, i.e., for every $\mathfrak{g}, \mathfrak{h} \in \mathfrak{P}$, we have $\mathfrak{g} \circ \mathfrak{h} \in \mathfrak{P}$.

Consider a signal space $\mathcal{X}(\Omega)$ supported on some underlying domain Ω . A *group action* of \mathcal{G} on set Ω is defined as a mapping $(\mathfrak{g}, u) \mapsto \mathfrak{g}.u$ associating a group element $\mathfrak{g} \in \mathcal{G}$ and a point $u \in \Omega$ with some other point $\mathfrak{g}.u$ on Ω . Group actions admit associativity. Moreover, if we have a group \mathcal{G} acting on Ω , we also obtain an action of \mathcal{G} on the signal space $\mathcal{X}(\Omega)$: $(\mathfrak{g}.x)(u) = x(\mathfrak{g}^{-1}.u)$ respecting associativity as well. This group action is linear, which can be described by inducing a map $\rho : \mathcal{G} \rightarrow \mathbb{R}^{n \times n}$ that assigns each group element \mathfrak{g} an (invertible) matrix $\rho(\mathfrak{g})$, satisfying the condition $\rho(\mathfrak{g}\mathfrak{h}) = \rho(\mathfrak{g})\rho(\mathfrak{h})$ for all $\mathfrak{g}, \mathfrak{h} \in \mathcal{G}$. A representation is called unitary or orthogonal if the matrix $\rho(\mathfrak{g})$ is unitary or orthogonal for all $\mathfrak{g} \in \mathcal{G}$.

Definition C.2 (Equivariant Functions). A function $f : \mathcal{X}(\Omega) \rightarrow \mathcal{Y}$ is \mathcal{G} -equivariant if $f(\rho(\mathfrak{g})x) = \rho(\mathfrak{g})f(x)$ for all $\mathfrak{g} \in \mathcal{G}$ and $x \in \mathcal{X}(\Omega)$, i.e., group action on the input affects the output in the same way.

Definition C.3 (Invariant Functions). We say f is \mathcal{G} -invariant if $f(\rho(\mathfrak{g})x) = f(x)$ for all $\mathfrak{g} \in \mathcal{G}$ and $x \in \mathcal{X}(\Omega)$, i.e., its output is unaffected by the group action on the input.

Definition C.4 (Permutation Equivalence and Similarity). Let $\mathbf{A}, \mathbf{B} \in \mathbb{R}^{m \times n}$ be two matrices of dimension $m \times n$. If $\mathbf{A} = \mathbf{S}\mathbf{B}\mathbf{T}$ with square and nonsingular matrices \mathbf{S} and \mathbf{T} , we say that \mathbf{A} is equivalent to \mathbf{B} . When \mathbf{S} and \mathbf{T} are unitary, we say \mathbf{A} and \mathbf{B} are unitarily equivalent. If \mathbf{S} and \mathbf{T} are two permutation matrices, we say \mathbf{A} and \mathbf{B} are permutation equivalent. When $m = n$ and $\mathbf{B} = \mathbf{S}^{-1}\mathbf{A}\mathbf{S}$ with a nonsingular $\mathbf{S} \in \mathbb{R}^{n \times n}$, we say \mathbf{B} is similar to \mathbf{A} . When \mathbf{S} is unitary (or real orthogonal), we say \mathbf{B} is unitarily (or real orthogonally) similar to \mathbf{A} . We say \mathbf{B} is permutation similar to \mathbf{A} if there is a permutation matrix \mathbf{P} such that $\mathbf{B} = \mathbf{P}\mathbf{A}\mathbf{P}^\top$.

C.2. Proof of Proposition 4.1

Proof. The permuted incidence matrices and Hodge Laplacians can be found by the definition of the permutations \mathfrak{p}_k and $\mathfrak{p}_{k\pm 1}$, given by $\bar{\mathbf{B}}_k = \mathbf{P}_k \mathbf{B}_k \mathbf{P}_{k+1}^\top$ and $\bar{\mathbf{L}}_k = \mathbf{P}_k \mathbf{L}_k \mathbf{P}_k^\top$. We mainly show that the algebraic property encoded in \mathbf{B}_k and \mathbf{L}_k of the SC is preserved after this sequence of permutations.

Based on Definition C.4, the permuted incidence matrix $\bar{\mathbf{B}}_k$ is permutation equivalent to \mathbf{B}_k , since all permutation matrices \mathbf{P}_k are real orthogonal. Consider an SVD of $\mathbf{B}_k = \mathbf{U}_k \Sigma_k \mathbf{V}_k^*$ with unitary matrices \mathbf{U}_k and \mathbf{V}_k of dimensions $N_k \times N_k$ and $N_{k+1} \times N_{k+1}$. We have then $\bar{\mathbf{B}}_k = \mathbf{P}_{k-1} \mathbf{U}_k \Sigma_k \mathbf{V}_k^* \mathbf{P}_k^\top$ which is an SVD of $\bar{\mathbf{B}}_k$ with unitary matrices $\mathbf{P}_{k-1} \mathbf{U}_k$ and $\mathbf{P}_k \mathbf{V}_k$ collecting the left and the right singular vectors. Note that $\mathbf{P}_{k-1} \mathbf{U}_k$ and $\mathbf{P}_k \mathbf{V}_k$ are row-permuted versions of \mathbf{U}_k and \mathbf{V}_k according to the permutations of $k-1$ - and k -simplices. That is, the singular vectors and singular values of the incidence matrices of the SC remain equivariant before and after permutations.

We then consider the permuted Hodge Laplacian $\bar{\mathbf{L}}_k$. Matrix $\bar{\mathbf{L}}_k$ has same eigenvalues as \mathbf{L}_k , as they are permutation similar to each other. Consider an eigen-decomposition $\mathbf{L}_k = \mathbf{W}_k \Lambda_k \mathbf{W}_k^\top$. We have then $\bar{\mathbf{L}}_k = \mathbf{P}_k \mathbf{W}_k \Lambda_k \mathbf{W}_k^\top \mathbf{P}_k^\top$ where matrix $\mathbf{P}_k \mathbf{W}_k$ collects the eigenvectors in the permuted SC with the same eigenvalues. These eigenvectors are row-permuted versions of \mathbf{W}_k according to the permutations of k -simplices. That is, the eigenvectors and eigenvalues of the Hodge Laplacians of the SC remain equivariant before and after permutations. Thus, the spectral properties of the SC remain. \square

C.3. Proof of Proposition 4.4

Proof. Given the representation of the reoriented incidence matrix $\bar{\mathbf{B}}_k$ and the reoriented Hodge Laplacian $\bar{\mathbf{L}}_k$, we can easily see that they differ from the original ones, as reversing the orientation of s_i^k results in multiplying the i th row of \mathbf{B}_k and the i th column of \mathbf{B}_{k-1} by -1 , as well as the i th row and column of \mathbf{L}_k by -1 . Likewise, the corresponding simplicial signal $x_{k,i}$ becomes $-x_{k,i}$. However, the underlying k -chain remains unchanged. That is, we have $\bar{c}_k = c_k = \sum_{i=1}^{N_k} x_{k,i} s_{k,i}$ because for each $\bar{s}_i^k = -s_i^k$, we have $\bar{x}_{k,i} = -x_{k,i}$. This can be understood as the simplicial signal remains unchanged in terms of the underlying simplices. \square

C.4. Proof of Proposition 4.3

Proof. Prior to the permutations by $\{\mathfrak{P}_k : k = [K]\}$, we have the output of an SCCNN layer on k -simplices as

$$\mathbf{x}_k^l = \sigma(\mathbf{H}_{k,d}^l \mathbf{B}_k^\top \mathbf{x}_{k-1}^{l-1} + \mathbf{H}_k^l \mathbf{x}_k^{l-1} + \mathbf{H}_{k,u}^l \mathbf{B}_{k+1} \mathbf{x}_{k+1}^{l-1}) \quad (\text{C.1})$$

with $\mathbf{H}_k^l := \sum_{t=0}^{T_d} w_{k,d,t}^l (\mathbf{L}_{k,d})^t + \sum_{t=0}^{T_u} w_{k,u,t}^l (\mathbf{L}_{k,u})^t$, $\mathbf{H}_{k,d}^l := \sum_{t=0}^{T_d} w_{k,d,t}^l (\mathbf{L}_{k,d})^t$ and $\mathbf{H}_{k,u}^l := \sum_{t=0}^{T_u} w_{k,u,t}^l (\mathbf{L}_{k,u})^t$.

When applying $\{\mathfrak{P}_k : k = [K]\}$ to the SC, we have the input tuple $\{\mathbf{P}_{k-1} \mathbf{x}_{k-1}^{l-1}, \mathbf{P}_k \mathbf{x}_k^{l-1}, \mathbf{P}_{k+1} \mathbf{x}_{k+1}^{l-1}\}$. The incidence matrices become $\bar{\mathbf{B}}_k = \mathbf{P}_{k-1} \mathbf{B}_k \mathbf{P}_k^\top$ and the Hodge Laplacians become $\bar{\mathbf{L}}_k = \mathbf{P}_k \mathbf{L}_k \mathbf{P}_k^\top$ for all k , likewise for their lower and upper counterparts. The SCF $\bar{\mathbf{H}}_{k,d}^l$ is given by

$$\begin{aligned} \bar{\mathbf{H}}_{k,d}^l &= \sum_{t=0}^{T_d} w_{k,d,t}^l (\mathbf{P}_k \mathbf{L}_{k,d} \mathbf{P}_k^\top)^t + \sum_{t=0}^{T_u} w_{k,u,t}^l (\mathbf{P}_k \mathbf{L}_{k,u} \mathbf{P}_k^\top)^t \\ &= \sum_{t=0}^{T_d} w_{k,d,t}^l \mathbf{P}_k (\mathbf{L}_{k,d})^t \mathbf{P}_k^\top + \sum_{t=0}^{T_u} w_{k,u,t}^l \mathbf{P}_k (\mathbf{L}_{k,u})^t \mathbf{P}_k^\top = \mathbf{P}_k \mathbf{H}_{k,d}^l \mathbf{P}_k^\top \end{aligned} \quad (\text{C.2})$$

owing to fact that \mathbf{P}_k is orthogonal. Following the same procedure, we have $\bar{\mathbf{H}}_{k,d}^l = \mathbf{P}_k \mathbf{H}_{k,d}^l \mathbf{P}_k^\top$ and $\bar{\mathbf{H}}_{k,u}^l = \mathbf{P}_k \mathbf{H}_{k,u}^l \mathbf{P}_k^\top$. We can now express the output on the permuted SC as

$$\begin{aligned} \bar{\mathbf{x}}_k^l &= \sigma(\bar{\mathbf{H}}_{k,d}^l \bar{\mathbf{B}}_k^\top \mathbf{P}_{k-1} \mathbf{x}_{k-1}^{l-1} + \bar{\mathbf{H}}_k^l \mathbf{P}_k \mathbf{x}_k^{l-1} + \bar{\mathbf{H}}_{k,u}^l \bar{\mathbf{B}}_{k+1} \mathbf{P}_{k+1} \mathbf{x}_{k+1}^{l-1}) \\ &= \sigma(\mathbf{P}_k \mathbf{H}_{k,d}^l \mathbf{P}_k^\top \mathbf{P}_k \mathbf{B}_k^\top \mathbf{P}_{k-1} \mathbf{x}_{k-1}^{l-1} + \mathbf{P}_k \mathbf{H}_k^l \mathbf{P}_k^\top \mathbf{P}_k \mathbf{x}_k^{l-1} + \mathbf{P}_k \mathbf{H}_{k,u}^l \mathbf{P}_k^\top \mathbf{P}_k \mathbf{B}_{k+1} \mathbf{P}_{k+1}^\top \mathbf{P}_{k+1} \mathbf{x}_{k+1}^{l-1}) \\ &= \sigma(\mathbf{P}_k \mathbf{H}_{k,d}^l \mathbf{B}_k^\top \mathbf{x}_{k-1}^{l-1} + \mathbf{P}_k \mathbf{H}_k^l \mathbf{x}_k^{l-1} + \mathbf{P}_k \mathbf{H}_{k,u}^l \mathbf{B}_{k+1} \mathbf{x}_{k+1}^{l-1}) \\ &= \mathbf{P}_k \sigma(\mathbf{H}_{k,d}^l \mathbf{B}_k^\top \mathbf{x}_{k-1}^{l-1} + \mathbf{H}_k^l \mathbf{x}_k^{l-1} + \mathbf{H}_{k,u}^l \mathbf{B}_{k+1} \mathbf{x}_{k+1}^{l-1}) = \mathbf{P}_k \mathbf{x}_k^l, \end{aligned} \quad (\text{C.3})$$

where we use the fact \mathbf{P}_k for all k are orthogonal and the elementwise nonlinearity does not affect permutations. \square

C.5. Proof of Proposition 4.4

Proof. In an oriented SC, the output of an SCCNN layer on k -simplices is given in (C.1). If the underlying simplices change their orientations according to $\{\mathcal{D}_{k,i} : k = [K], i = 1, \dots, N_k\}$, then we have the input tuple become $\{\mathbf{D}_{k-1}\mathbf{x}_{k-1}^{l-1}, \mathbf{D}_k\mathbf{x}_k^{l-1}, \mathbf{D}_{k+1}\mathbf{x}_{k+1}^{l-1}\}$. The incidence matrices become $\bar{\mathbf{B}}_k = \mathbf{D}_{k-1}\mathbf{B}_k\mathbf{D}_k^\top$ and the Hodge Laplacians become $\bar{\mathbf{L}}_k = \mathbf{D}_k\mathbf{L}_k\mathbf{D}_k^\top$ for all k , likewise for their lower and upper counterparts. Since \mathbf{D}_k is diagonal and orthogonal, we can follow the similar procedure in (C.3). Thus, we have $\bar{\mathbf{H}}_{k,d}^l = \mathbf{D}_k\mathbf{H}_{k,d}^l\mathbf{D}_k^\top$ and $\bar{\mathbf{H}}_{k,u}^l = \mathbf{D}_k\mathbf{H}_{k,u}^l\mathbf{D}_k^\top$. We can now express the output on the reoriented SC as

$$\begin{aligned} \bar{\mathbf{x}}_k^l &= \sigma(\bar{\mathbf{H}}_{k,d}^l \bar{\mathbf{B}}_k^\top \mathbf{D}_{k-1} \mathbf{x}_{k-1}^{l-1} + \bar{\mathbf{H}}_k^l \mathbf{D}_k \mathbf{x}_k^{l-1} + \bar{\mathbf{H}}_{k,u}^l \bar{\mathbf{B}}_{k+1} \mathbf{D}_{k+1} \mathbf{x}_{k+1}^{l-1}) \\ &= \sigma(\mathbf{D}_k \mathbf{H}_{k,d}^l \mathbf{B}_k^\top \mathbf{x}_{k-1}^{l-1} + \mathbf{D}_k \mathbf{H}_k^l \mathbf{x}_k^{l-1} + \mathbf{D}_k \mathbf{H}_{k,u}^l \mathbf{B}_{k+1} \mathbf{x}_{k+1}^{l-1}) \\ &= \mathbf{D}_k \sigma(\mathbf{H}_{k,d}^l \mathbf{B}_k^\top \mathbf{x}_{k-1}^{l-1} + \mathbf{H}_k^l \mathbf{x}_k^{l-1} + \mathbf{H}_{k,u}^l \mathbf{B}_{k+1} \mathbf{x}_{k+1}^{l-1}) = \mathbf{D}_k \mathbf{x}_k^l, \end{aligned} \quad (\text{C.4})$$

where we use the fact that \mathbf{D}_k for all k are diagonal and orthogonal for all k and that $\sigma(\cdot)$ is an odd function, $\sigma(-\mathbf{x}) = -(\sigma(\mathbf{x}))$, such that $\sigma(\mathbf{D}_k \mathbf{x}_k^l) = \mathbf{D}_k \sigma(\mathbf{x}_k^l)$. \square

D. Spectral Analysis

As tools from simplicial signal processing based on Hodge theory are rather unfamiliar, which have been used to analyze simplicial signals by Barbarossa & Sardellitti (2020) and SCFs by Yang et al. (2022b), Thus, we append the necessary background to assist the exposition of Section 5, together with some illustrations.

D.1. Divergence, Gradient, and Curl Operations on SCs

We first show how incidence matrices \mathbf{B}_1 and \mathbf{B}_2 relate to the physical divergence and curl operations (Barbarossa & Sardellitti, 2020). Consider an edge flow \mathbf{x}_1 . By applying \mathbf{B}_1 to \mathbf{x}_1 , we obtain a node signal whose i th entry on node i can be expressed as

$$[\mathbf{B}_1 \mathbf{x}_1]_i = \sum_{j < i} [\mathbf{x}_1]_{[j,i]} - \sum_{i < k} [\mathbf{x}_1]_{[i,k]}, \quad (\text{D.1})$$

which is the total inflow minus the total outflow at node i , i.e., the netflow at node i . This operation $\mathbf{B}_1 \mathbf{x}_1$ is also known as the *divergence* operation, reflecting the *irrotational* property of the edge flow.

Consider the adjoint \mathbf{B}_1^\top applied to a node signal \mathbf{x}_0 . We can obtain an edge flow which is the difference between two adjacent node signals, and specifically, on edge $e = [i, j]$ we have

$$[\mathbf{B}_1^\top \mathbf{x}_0]_{[i,j]} = [\mathbf{x}_0]_j - [\mathbf{x}_0]_i. \quad (\text{D.2})$$

This is the *gradient* operation and it also explains that $\text{im}(\mathbf{B}_1^\top)$ is named as gradient space since it contains edge flows which can be expressed as a gradient of some node signal.

Likewise, by applying \mathbf{B}_2^\top to an edge flow \mathbf{x}_1 , we compute a resulting triangle signal which circulates around triangles. Specifically, at triangle $t = [i, j, k]$, we have

$$[\mathbf{B}_2^\top \mathbf{x}_1]_{[i,j,k]} = [\mathbf{x}_1]_{[i,j]} + [\mathbf{x}_1]_{[j,k]} - [\mathbf{x}_1]_{[i,k]}, \quad (\text{D.3})$$

which is the *curl* operation, reflecting the *solenoidal* property of the edge flow.

Lastly, by applying \mathbf{B}_2 to a triangle signal \mathbf{x}_2 , we obtain an edge flow $\mathbf{B}_2 \mathbf{x}_2$, which is in the curl space $\text{im}(\mathbf{B}_2)$.

The above operations hold for general k -simplicial signal space by using \mathbf{B}_k and \mathbf{B}_{k+1} . Although the physical interpretations like divergence and curl do not generalize, the operation $\mathbf{B}_k \mathbf{x}_k$ can be used to measure how a k -simplicial signal varies in terms of the lower adjacent simplices (faces), and the operation $\mathbf{B}_{k+1}^\top \mathbf{x}_k$ reflects how a k -simplicial signal varies in terms of the upper adjacent simplices (cofaces). For $k = 0$, we only have $\mathbf{B}_1^\top \mathbf{x}_0$, which measures how a graph signal varies along the edges (Sandryhaila & Moura, 2013; 2014; Shuman et al., 2013).

D.2. Decomposition of an Edge Flow

Given an edge flow \mathbf{x}_1 , the Hodge decomposition in [Theorem 5.1](#) gives

$$\mathbf{x}_1 = \mathbf{x}_{1,G} + \mathbf{x}_{1,C} + \mathbf{x}_{1,H} \quad (\text{D.4})$$

with $\mathbf{x}_{1,G} = \mathbf{B}_1^\top \mathbf{x}_0$ for some node signal \mathbf{x}_0 and $\mathbf{x}_{1,C} = \mathbf{B}_2 \mathbf{x}_2$ for some triangle signal \mathbf{x}_2 . Some examples of physical edge flows can be electric currents, electromagnetic waves, or water flows. We also refer to [Jiang et al. \(2011\)](#); [Candogan et al. \(2011\)](#); [Jia et al. \(2019\)](#) for some edge flows generated from real-world problems.

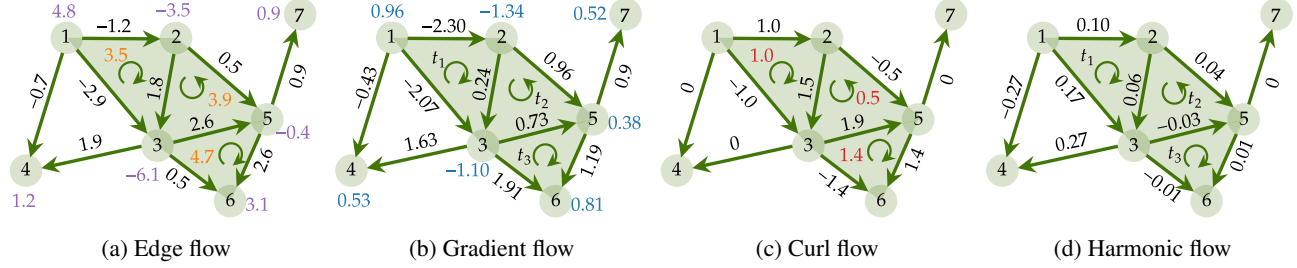


Figure D.1. Hodge decomposition of an edge flow. (b)-(d) are the Hodge decomposition of the example edge flow in (a) (we denote its divergence and curl in purple and orange, respectively). The gradient flow is the gradient of some node signal (in blue) and is curl-free. The curl flow can be obtained from some triangle flow (in red), and is divergence-free. The harmonic flow has zero divergence and zero curl, which is circulating around the hole $\{1, 3, 4\}$. Note that in this figure and [Figure D.2](#), the flow numbers are rounded up to two decimal places. Thus, at some nodes or triangles with zero-divergence or zero-curl, the divergence or curl might not be exactly zero.

D.3. SFT and Simplicial Frequency

Proof of Proposition 5.3. The proof can be found in [Yang et al. \(2022b\)](#). □

Here we show how the eigenvalues of \mathbf{L}_k carry the notion of simplicial frequency. To ease composition, we consider the case of $k = 1$. The three sets of eigenvalues follow that:

- *Gradient Frequency:* the nonzero eigenvalues associated with the eigenvectors $\mathbf{U}_{1,G}$ of $\mathbf{L}_{1,d}$, which span the gradient space $\text{im}(\mathbf{B}_1^\top)$, admit $\mathbf{L}_{1,d} \mathbf{u}_{1,G} = \lambda_{1,G} \mathbf{u}_{1,G}$ for any eigenpair $\mathbf{u}_{1,G}$ and $\lambda_{1,G}$. From the definition of $\mathbf{L}_{1,d}$, we have $\mathbf{B}_1^\top \mathbf{B}_1 \mathbf{u}_{1,G} = \lambda_{1,G} \mathbf{u}_{1,G}$, which translates to $\lambda_{1,G} = \mathbf{u}_{1,G}^\top \mathbf{B}_1^\top \mathbf{B}_1 \mathbf{u}_{1,G} = \|\mathbf{B}_1 \mathbf{u}_{1,G}\|_2^2$. This is an Euclidean norm of the divergence, i.e., the total nodal variation of $\mathbf{u}_{1,G}$. If an eigenvector has a larger eigenvalue, it has a larger total divergence. For the SFT of an edge flow, if the gradient embedding $\tilde{\mathbf{x}}_{1,G}$ has a large weight on such an eigenvector, it contains components with a large divergence, and we say it has a large gradient frequency. Thus, we call such eigenvalues associated with $\mathbf{U}_{1,G}$ gradient frequencies, measuring the extent of the total divergence of an edge flow.
- *Curl Frequency:* the nonzero eigenvalues associated with the eigenvectors $\mathbf{U}_{1,C}$ of $\mathbf{L}_{1,u}$, which span the curl space $\text{im}(\mathbf{B}_2)$, admit $\mathbf{L}_{1,u} \mathbf{u}_{1,C} = \lambda_{1,C} \mathbf{u}_{1,C}$ for any eigenpair $\mathbf{u}_{1,C}$ and $\lambda_{1,C}$. From the definition of $\mathbf{L}_{1,u}$, we have $\mathbf{B}_2 \mathbf{B}_2^\top \mathbf{u}_{1,C} = \lambda_{1,C} \mathbf{u}_{1,C}$ which translates to $\lambda_{1,C} = \mathbf{u}_{1,C}^\top \mathbf{B}_2 \mathbf{B}_2^\top \mathbf{u}_{1,C} = \|\mathbf{B}_2^\top \mathbf{u}_{1,C}\|_2^2$. Eigenvalue $\lambda_{1,C}$ then is an Euclidean norm of the curl, i.e., the total rotational variation, of the eigenvector $\mathbf{u}_{1,C}$. If an eigenvector has a larger eigenvalue, it has a larger total curl. For the SFT of an edge flow, if the curl embedding $\tilde{\mathbf{x}}_{1,C}$ has a large weight on such an eigenvector, it contains components with a large curl, and we say it has a large curl frequency. Thus, we call such eigenvalues associated with $\mathbf{U}_{1,C}$ curl frequencies, measuring the extent of the total curl of an edge flow.
- *Harmonic Frequency:* the zero eigenvalues associated with the eigenvectors $\mathbf{U}_{1,H}$, which span the harmonic space $\text{ker}(\mathbf{L}_1)$, admit $\mathbf{L}_1 \mathbf{u}_{1,H} = \mathbf{0}$ for any eigenpair $\mathbf{u}_{1,H}$ and $\lambda_{1,H} = 0$. From the definition of \mathbf{L}_1 , we have $\mathbf{B}_1 \mathbf{u}_{1,H} = \mathbf{B}_2^\top \mathbf{u}_{1,H} = \mathbf{0}$. That is, the eigenvector $\mathbf{u}_{1,H}$ has a zero-divergence and a zero-curl, or equivalently, divergence- and curl-free. We also say such an eigenvector has zero signal variation in terms of the nodes and triangles. This resembles the constant graph signal in the node space. We call such zero eigenvalues as harmonic frequencies.

[Figure D.2](#) shows the simplicial Fourier basis and the corresponding simplicial frequencies of the SC in [Figure 1a](#), from which we see how the eigenvalues of \mathbf{L}_1 can be interpreted as the simplicial frequencies.

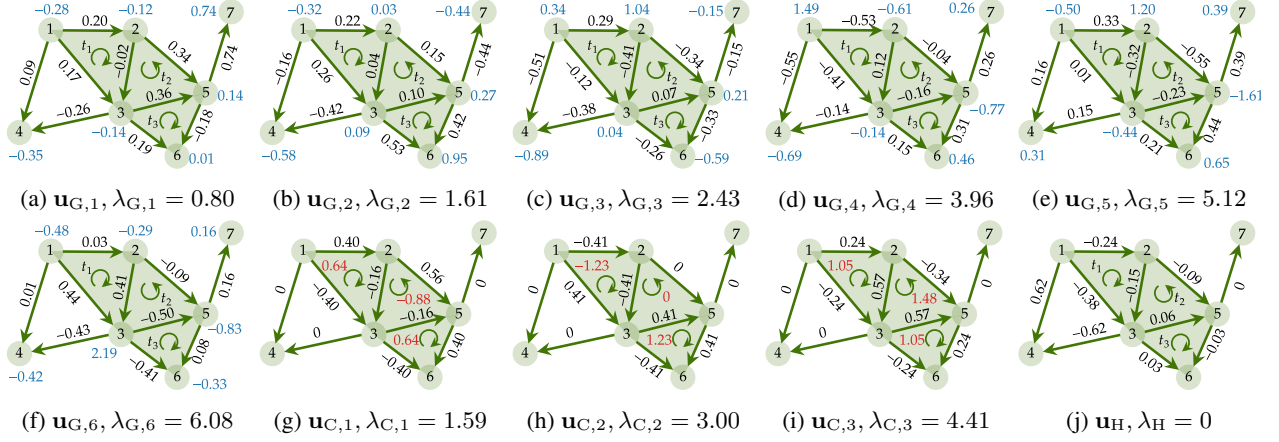


Figure D.2. Eigenvalues of L_1 carry the notion of simplicial frequency. (a)-(f) Six gradient frequencies and the corresponding Fourier basis. We also annotate their divergences, and we see that these eigenvectors with a small eigenvalue have a small magnitude of total divergence, i.e., the edge flow variation in terms of the nodes. Gradient frequencies reflect the nodal variations. (g)-(i) Three curl frequencies and the corresponding Fourier basis. We annotate their curls and we see that these eigenvectors with a small eigenvalue have a small magnitude of total curl, i.e., the edge flow variation in terms of the triangles. Curl frequencies reflect the rotational variations. (j) Harmonic basis with a zero frequency, which has a zero nodal and zero rotational variation.

For $k = 0$, the eigenvalues of L_0 carry the notion of graph frequency, which measures the graph (node) signal smoothness w.r.t. the upper adjacent simplices, i.e., edges. Thus, the curl frequency of $k = 0$ coincides with the graph frequency and a constant graph signal has only harmonic frequency component, and there is no divergence frequency. For a more general k , there exist these three types of simplicial frequencies, which measure the k -simplicial signal total variations in terms of faces and cofaces.

D.4. Proof of Corollary 5.4

Proof. Diagonalizing the lower and upper Hodge Laplacians by $U_k = [U_{k,H} \ U_{k,G} \ U_{k,C}]$, we have

$$L_{k,d} = U_k \text{diag}([0 \ \lambda_{k,G}^\top \ 0]^\top) U_k^\top, \quad L_{k,u} = U_k \text{diag}([0 \ 0 \ \lambda_{k,C}^\top]^\top) U_k^\top \quad (D.5)$$

where $\text{diag}(\cdot)$ is a diagonal matrix operator of a column vector, $\lambda_{k,G}$ and $\lambda_{k,C}$ are column vectors collecting the gradient and curl frequencies, i.e., the nonzero eigenvalues, and $\mathbf{0}$ is all-zero vector of appropriate dimension. We can then express the lower and upper simplicial shifting as

$$\begin{aligned} L_{k,d} \mathbf{x}_k &= U_k \text{diag}([0 \ \lambda_{k,G}^\top \ 0]^\top) U_k^\top \mathbf{x}_k = U_k \text{diag}([0 \ \lambda_{k,G}^\top \ 0]^\top) \tilde{\mathbf{x}}_k, \\ L_{k,u} \mathbf{x}_k &= U_k \text{diag}([0 \ 0 \ \lambda_{k,C}^\top]^\top) U_k^\top \mathbf{x}_k = U_k \text{diag}([0 \ 0 \ \lambda_{k,C}^\top]^\top) \tilde{\mathbf{x}}_k. \end{aligned}$$

By substituting the spectral embedding $\tilde{\mathbf{x}}_k = [\tilde{\mathbf{x}}_{k,H}^\top, \tilde{\mathbf{x}}_{k,G}^\top, \tilde{\mathbf{x}}_{k,C}^\top]^\top$, we have

$$\begin{aligned} L_{k,d} \mathbf{x}_k &= U_k \text{diag}([0 \ \lambda_{k,G}^\top \ 0]^\top) [\tilde{\mathbf{x}}_{k,H}^\top, \tilde{\mathbf{x}}_{k,G}^\top, \tilde{\mathbf{x}}_{k,C}^\top]^\top = U_k \text{diag}(\lambda_{k,G}) \tilde{\mathbf{x}}_{k,G} = U_{k,G} (\lambda_{k,G} \odot \tilde{\mathbf{x}}_{k,G}), \\ L_{k,u} \mathbf{x}_k &= U_k \text{diag}([0 \ 0 \ \lambda_{k,C}^\top]^\top) [\tilde{\mathbf{x}}_{k,H}^\top, \tilde{\mathbf{x}}_{k,G}^\top, \tilde{\mathbf{x}}_{k,C}^\top]^\top = U_k \text{diag}(\lambda_{k,C}) \tilde{\mathbf{x}}_{k,C} = U_{k,C} (\lambda_{k,C} \odot \tilde{\mathbf{x}}_{k,C}), \end{aligned}$$

where \odot is the Hadamard (elementwise) product. Combined with Proposition 5.3, the proof is completed. \square

D.5. Effect of Nonlinearity

We use a simple example to illustrate the information spillage effect of a nonlinearity $\sigma(\cdot)$. Figure D.3 shows the SFT embeddings of a gradient flow in Figure D.1b which contains only nonzero gradient embedding $\tilde{\mathbf{x}}_G$ at the gradient frequencies shown in Figure D.2, and harmonic and curl embeddings are zeros at zero and curl frequencies. We pass this flow through a nonlinearity $\tanh(\cdot)$. We then see that at both zero and curl frequencies contain nonzero embeddings, i.e., the information spillage effect. This allows the information projected to an edge flow from nodes (contained in the gradient embedding) to be propagated to triangles, which is the spectral perspective of the extended inter-simplicial locality.

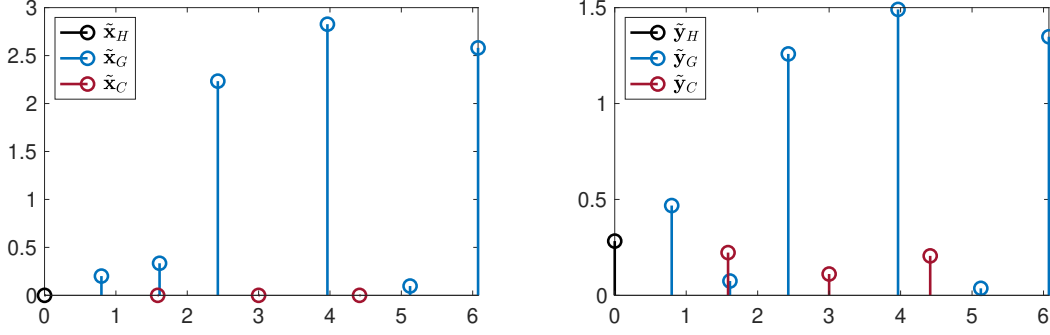


Figure D.3. The information spillage effect of a nonlinearity $\sigma(\cdot)$. (Left): the SFT embeddings of the gradient flow \mathbf{x}_G in Figure D.1b. (Right): the SFT embeddings of $\mathbf{y} = \tanh(\mathbf{x}_G)$. We see that information in a gradient flow after passed by a nonlinearity contains information in the harmonic and curl frequencies.

E. Stability Analysis

In this section, we discuss the details in Section 6 to serve the stability of SCCNNs in Theorem 6.7.

E.1. SCCNNs in Weighted SCs

A weighted SC can be defined through specifying the weights of simplices. We give the definition of a commonly used weighted SC with weighted Hodge Laplacians in Grady & Polimeni (2010); Horak & Jost (2013).

Definition E.1 (Weighted SC and Hodge Laplacians). In an oriented and weighted SC, we have diagonal weighting matrices \mathbf{M}_k with $[\mathbf{M}]_{ii}$ measuring the weight of i th k -simplex. A weighted k th Hodge Laplacian is given by

$$\mathbf{L}_k = \mathbf{L}_{k,d} + \mathbf{L}_{k,u} = \mathbf{M}_k \mathbf{B}_k^\top \mathbf{M}_{k-1}^{-1} \mathbf{B}_k + \mathbf{B}_{k+1} \mathbf{M}_{k+1} \mathbf{B}_{k+1}^\top \mathbf{M}_k^{-1}. \quad (\text{E.1})$$

where $\mathbf{L}_{k,d}$ and $\mathbf{L}_{k,u}$ are the weighted lower and upper Laplacians. A symmetric version follows $\mathbf{L}_k^s = \mathbf{M}_k^{-1/2} \mathbf{L}_k \mathbf{M}_k^{1/2}$, and likewise, we have $\mathbf{L}_{k,d}^s = \mathbf{M}_k^{1/2} \mathbf{B}_k^\top \mathbf{M}_{k-1}^{-1} \mathbf{B}_k \mathbf{M}_k^{1/2}$ and $\mathbf{L}_{k,u}^s = \mathbf{M}_k^{-1/2} \mathbf{B}_{k+1} \mathbf{M}_{k+1} \mathbf{B}_{k+1}^\top \mathbf{M}_k^{-1/2}$.

SCCNNs in weighted SC. The SCCNN layer defined in a weighted SC is of form

$$\mathbf{x}_k^l = \sigma(\mathbf{H}_{k,d}^l \mathbf{R}_{k,d} \mathbf{x}_{k-1}^{l-1} + \mathbf{H}_k^l \mathbf{x}_k^{l-1} + \mathbf{H}_{k,u}^l \mathbf{R}_{k,u} \mathbf{x}_{k+1}^{l-1}) \quad (\text{E.2})$$

where the three SCFs are defined based on the weighted Laplacians (E.1), and the lower and upper contributions $\mathbf{x}_{k,d}^l$ and $\mathbf{x}_{k,u}^l$ are obtained via projection matrices $\mathbf{R}_{k,d} \in \mathbb{R}^{N_k \times N_{k-1}}$ and $\mathbf{R}_{k,u} \in \mathbb{R}^{N_k \times N_{k+1}}$, instead of \mathbf{B}_k^\top and \mathbf{B}_{k+1} . Projection operator $\mathbf{R}_{k,d}$ can be defined via the incidence matrix \mathbf{B}_k^\top and weight matrices \mathbf{M}_{k-1} and \mathbf{M}_k . For example, Bunch et al. (2020) considered $\mathbf{R}_{1,d} = \mathbf{M}_1 \mathbf{B}_1^\top \mathbf{M}_0^{-1}$ and $\mathbf{R}_{1,u} = \mathbf{B}_2 \mathbf{M}_2$.

Although we focus on the unweighted SC to emphasize the mechanism of the SCCNN, the discussions on localities [cf. Section 3] and symmetries [cf. Section 4] can be extended to a weighted SC, as well as the spectral analysis [cf. Section 5] based on a weighted Hodge decomposition

$$\mathcal{X}_k = \text{im}(\mathbf{M}_k^{1/2} \mathbf{B}_k^\top) \oplus \ker(\mathbf{L}_k^s) \oplus \text{im}(\mathbf{M}_k^{-1/2} \mathbf{B}_{k+1}). \quad (\text{E.3})$$

We refer to Schaub et al. (2020) details. Moreover, the SFT can be likewise defined with the basis given by the eigenvectors of \mathbf{L}_k^s . Proposition 5.3 can be generalized based on the weighted Hodge decomposition and the eigenspace of \mathbf{L}_k^s . Lastly, the eigenvalues of \mathbf{L}_k^s carry the meaning of simplicial frequency, which are the same as those of \mathbf{L}_k since they admit a similarity transformation.

E.2. Integral Lipschitz SCFs

Definition E.2 (Equivalent Definition of Integral Lipschitz SCF). The integral Lipschitz SCF in Definition 6.2 is equivalent to that there exist constants $C_{k,d}, C_{k,u} > 0$ such that, for $\lambda_1, \lambda_2 \geq 0$

$$|\tilde{h}_{k,G}(\lambda_2) - \tilde{h}_{k,G}(\lambda_1)| \leq C_{k,d} 2|\lambda_2 - \lambda_1|/|\lambda_2 + \lambda_1|, \quad |\tilde{h}_{k,C}(\lambda_2) - \tilde{h}_{k,C}(\lambda_1)| \leq C_{k,u} 2|\lambda_2 - \lambda_1|/|\lambda_2 + \lambda_1|. \quad (\text{E.4})$$

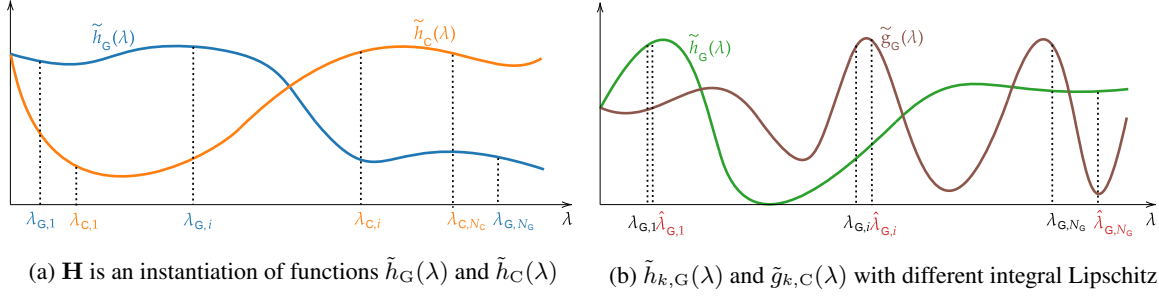


Figure E.1. (a) Given the continuous functions $\tilde{h}_G(\lambda)$ and $\tilde{h}_C(\lambda)$, the gradient frequency response $\tilde{\mathbf{h}}_G(\boldsymbol{\lambda})$ of \mathbf{H}_k is an instantiation of $\tilde{h}_G(\lambda)$ at the discrete gradient frequencies $\boldsymbol{\lambda} = [\lambda_{G,1}, \dots, \lambda_{G,N_G}]$ given by the SC, and likewise for the curl frequency response $\tilde{\mathbf{h}}_C(\boldsymbol{\lambda})$. (b) Gradient frequency response $\tilde{h}_G(\lambda)$ has a better integral Lipschitz property than $\tilde{g}_G(\lambda)$ since the former has a smaller integral Lipschitz constant such that it has smaller variability at larger simplicial frequencies. This results in a better stability of $\tilde{h}_G(\lambda)$ since $\tilde{h}_G(\lambda)$ is closer to $\tilde{h}_G(\hat{\lambda})$ for a relatively perturbed SC.

Figure E.1a shows that an SCF \mathbf{H}_k is an instantiation of the continuous gradient and curl frequency response functions $\tilde{h}_{k,G}(\lambda)$ and $\tilde{h}_{k,C}(\lambda)$ where the frequency responses of \mathbf{H}_k are instantiated at the discrete simplicial frequencies determined by the SC. Figure E.1b shows two gradient frequency response functions with different integral Lipschitz properties, where $\hat{\lambda}_{G,i} = \lambda_{G,i}(1 + \epsilon)$ with an error ϵ . For a fixed ϵ , small eigenvalues are less perturbed than large eigenvalues. For an SCF defined by $\tilde{h}_G(\lambda)$, its frequency response at both small and large eigenvalues does not vary much when eigenvalues are relatively shifted by a small ϵ . However, for an SCF defined by $\tilde{g}_G(\lambda)$, its frequency response at large eigenvalues changes substantially from $\tilde{g}_G(\lambda_{G,N_G})$ to $\tilde{g}_G(\hat{\lambda}_{G,N_G})$ as it has a weaker integral Lipschitz property.

E.3. Proof of Stability of SCCNNs in Theorem 6.7

For an SCCNN in (E.2) in a weighted SC \mathcal{S} , we consider its perturbed version in a perturbed SC $\hat{\mathcal{S}}$ at layer l , given by

$$\hat{\mathbf{x}}_k^l = \sigma(\hat{\mathbf{H}}_{k,d}^l \hat{\mathbf{R}}_{k,d} \hat{\mathbf{x}}_{k-1}^{l-1} + \hat{\mathbf{H}}_k^l \hat{\mathbf{x}}_k^{l-1} + \hat{\mathbf{H}}_{k,u}^l \hat{\mathbf{R}}_{k,u} \hat{\mathbf{x}}_{k+1}^{l-1}) \quad (\text{E.5})$$

which is defined based on perturbed Laplacians with the same set of filter coefficients, and the perturbed projection operators following Definition 6.1. Given the initial input \mathbf{x}_k^0 for $k = [K]$, our goal is to upper bound the Euclidean distance between the outputs \mathbf{x}_k^l and $\hat{\mathbf{x}}_k^l$ for $l = 1, \dots, L$,

$$\|\hat{\mathbf{x}}_k^l - \mathbf{x}_k^l\|_2 = \|\sigma(\hat{\mathbf{H}}_{k,d}^l \hat{\mathbf{R}}_{k,d} \hat{\mathbf{x}}_{k-1}^{l-1} - \mathbf{H}_{k,d}^l \mathbf{R}_{k,d} \mathbf{x}_{k-1}^{l-1} + \hat{\mathbf{H}}_k^l \hat{\mathbf{x}}_k^{l-1} - \mathbf{H}_k^l \mathbf{x}_k^{l-1} + \hat{\mathbf{H}}_{k,u}^l \hat{\mathbf{R}}_{k,u} \hat{\mathbf{x}}_{k+1}^{l-1} - \mathbf{H}_{k,u}^l \mathbf{R}_{k,u} \mathbf{x}_{k+1}^{l-1})\|_2. \quad (\text{E.6})$$

We proceed the proof in two steps: first, we analyze the operator norm $\|\hat{\mathbf{H}}_k^l - \mathbf{H}_k^l\|_2$ of an SCF \mathbf{H}_k^l and its perturbed version $\hat{\mathbf{H}}_k^l$; then we look for the bound of the output distance for a general L -layer SCCNN. To ease notations, we omit the subscript such that $\|\mathbf{A}\| = \max_{\|\mathbf{x}\|_2=1} \|\mathbf{A}\mathbf{x}\|_2$ is the operator norm (spectral radius) of a matrix \mathbf{A} , and $\|\mathbf{x}\|$ is the Euclidean norm of a vector \mathbf{x} .

In the first step we omit the indices k and l for simplicity since they hold for general k and l . We first give a useful lemma.

Lemma E.3. Given the i th eigenvector \mathbf{u}_i of $\mathbf{L} = \mathbf{U}\mathbf{A}\mathbf{U}^\top$, for lower and upper perturbations \mathbf{E}_d and \mathbf{E}_u in Definition 6.1, we have

$$\mathbf{E}_d \mathbf{u}_i = q_{di} \mathbf{u}_i + \mathbf{E}_1 \mathbf{u}_i, \quad \mathbf{E}_u \mathbf{u}_i = q_{ui} \mathbf{u}_i + \mathbf{E}_2 \mathbf{u}_i \quad (\text{E.7})$$

with eigendecompositions $\mathbf{E}_d = \mathbf{V}_d \mathbf{Q}_d \mathbf{V}_d^\top$ and $\mathbf{E}_u = \mathbf{V}_u \mathbf{Q}_u \mathbf{V}_u^\top$ where $\mathbf{V}_d, \mathbf{V}_u$ collect the eigenvectors and $\mathbf{Q}_d, \mathbf{Q}_u$ the eigenvalues. It holds that $\|\mathbf{E}_1\| \leq \epsilon_d \delta_d$ and $\|\mathbf{E}_2\| \leq \epsilon_u \delta_u$, with $\delta_d = (\|\mathbf{V}_d - \mathbf{U}\| + 1)^2 - 1$ and $\delta_u = (\|\mathbf{V}_u - \mathbf{U}\| + 1)^2 - 1$ measuring the eigenvector misalignments.

Proof. We first prove that $\mathbf{E}_d \mathbf{u}_i = q_{di} \mathbf{u}_i + \mathbf{E}_1 \mathbf{u}_i$. The perturbation matrix on the lower Laplacian can be written as $\mathbf{E}_d = \mathbf{E}'_d + \mathbf{E}_1$ with $\mathbf{E}'_d = \mathbf{U} \mathbf{Q}_d \mathbf{U}^\top$ and $\mathbf{E}_1 = (\mathbf{V}_d - \mathbf{U}) \mathbf{Q}_d (\mathbf{V}_d - \mathbf{U})^\top + \mathbf{U} \mathbf{Q}_d (\mathbf{V}_d - \mathbf{U})^\top + (\mathbf{V}_d - \mathbf{U}) \mathbf{Q}_d \mathbf{U}^\top$. For the i th eigenvector \mathbf{u}_i , we have that

$$\mathbf{E}_d \mathbf{u}_i = \mathbf{E}'_d \mathbf{u}_i + \mathbf{E}_1 \mathbf{u}_i = q_{di} \mathbf{u}_i + \mathbf{E}_1 \mathbf{u}_i \quad (\text{E.8})$$

where the second equality follows from $\mathbf{E}'_d \mathbf{u}_i = q_{di} \mathbf{u}_i$. Since $\|\mathbf{E}_d\| \leq \epsilon_d$, it follows that $\|\mathbf{Q}_d\| \leq \epsilon_d$. Then, applying the triangle inequality, we have that

$$\begin{aligned} \|\mathbf{E}_1\| &\leq \|(\mathbf{V}_d - \mathbf{U})\mathbf{Q}_d(\mathbf{V}_d - \mathbf{U})^\top\| + \|\mathbf{U}\mathbf{Q}_d(\mathbf{V}_d - \mathbf{U})^\top\| + \|(\mathbf{V}_d - \mathbf{U})\mathbf{Q}_d\mathbf{U}\| \\ &\leq \|\mathbf{V}_d - \mathbf{U}\|^2 \|\mathbf{Q}_d\| + 2\|\mathbf{V}_d - \mathbf{U}\| \|\mathbf{Q}_d\| \|\mathbf{U}\| \leq \epsilon_d \|\mathbf{V}_d - \mathbf{U}\|^2 + 2\epsilon_d \|\mathbf{V}_d - \mathbf{U}\| \\ &= \epsilon_d (\|\mathbf{V}_d - \mathbf{U}\| + 1)^2 - 1 = \epsilon_d \delta_d, \end{aligned} \quad (\text{E.9})$$

which completes the proof for the lower perturbation matrix. Likewise, we can prove for $\mathbf{E}_u \mathbf{u}_i$. \square

E.3.1. STEP I: STABILITY OF THE SCF \mathbf{H}_k^t

Proof. 1. Low-order approximation of $\widehat{\mathbf{H}} - \mathbf{H}$. Given an SCF $\mathbf{H} = \sum_{t=0}^{T_d} w_{d,t} \mathbf{L}_d^t + \sum_{t=0}^{T_u} w_{u,t} \mathbf{L}_u^t$, we denote its perturbed version by $\widehat{\mathbf{H}} = \sum_{t=0}^{T_d} w_{d,t} \widehat{\mathbf{L}}_d^t + \sum_{t=0}^{T_u} w_{u,t} \widehat{\mathbf{L}}_u^t$, where the filter coefficients are the same. The difference between \mathbf{H} and $\widehat{\mathbf{H}}$ can be expressed as

$$\widehat{\mathbf{H}} - \mathbf{H} = \sum_{t=0}^{T_d} w_{d,t} (\widehat{\mathbf{L}}_d^t - \mathbf{L}_d^t) + \sum_{t=0}^{T_u} w_{u,t} (\widehat{\mathbf{L}}_u^t - \mathbf{L}_u^t), \quad (\text{E.10})$$

in which we can compute the first-order Taylor expansion of $\widehat{\mathbf{L}}_d^t$ as

$$\widehat{\mathbf{L}}_d^t = (\mathbf{L}_d + \mathbf{E}_d \mathbf{L}_d + \mathbf{L}_d \mathbf{E}_d)^t = \mathbf{L}_d^t + \mathbf{D}_{d,t} + \mathbf{C}_d \quad (\text{E.11})$$

with $\mathbf{D}_{d,t} := \sum_{r=0}^{t-1} (\mathbf{L}_d^r \mathbf{E}_d \mathbf{L}_d^{t-r} + \mathbf{L}_d^{r+1} \mathbf{E}_d \mathbf{L}_d^{t-r-1})$ parameterized by t and \mathbf{C}_d following $\|\mathbf{C}_d\| \leq \sum_{r=2}^t \binom{t}{r} \|\mathbf{E}_d \mathbf{L}_d + \mathbf{L}_d \mathbf{E}_d\|^r \|\mathbf{L}_d\|^{t-r}$. Likewise, we can expand $\widehat{\mathbf{L}}_u^t$ as

$$\widehat{\mathbf{L}}_u^t = (\mathbf{L}_u + \mathbf{E}_u \mathbf{L}_u + \mathbf{L}_u \mathbf{E}_u)^t = \mathbf{L}_u^t + \mathbf{D}_{u,t} + \mathbf{C}_u \quad (\text{E.12})$$

with $\mathbf{D}_{u,t} := \sum_{r=0}^{t-1} (\mathbf{L}_u^r \mathbf{E}_u \mathbf{L}_u^{t-r} + \mathbf{L}_u^{r+1} \mathbf{E}_u \mathbf{L}_u^{t-r-1})$ parameterized by t and \mathbf{C}_u following $\|\mathbf{C}_u\| \leq \sum_{r=2}^t \binom{t}{r} \|\mathbf{E}_u \mathbf{L}_u + \mathbf{L}_u \mathbf{E}_u\|^r \|\mathbf{L}_u\|^{t-r}$. Then, by substituting (E.11) and (E.12) into (E.10), we have

$$\widehat{\mathbf{H}} - \mathbf{H} = \sum_{t=0}^{T_d} w_{d,t} \mathbf{D}_{d,t} + \sum_{t=0}^{T_u} w_{u,t} \mathbf{D}_{u,t} + \mathbf{F}_d + \mathbf{F}_u \quad (\text{E.13})$$

with negligible terms $\|\mathbf{F}_d\| = \mathcal{O}(\|\mathbf{E}_d\|^2)$ and $\|\mathbf{F}_u\| = \mathcal{O}(\|\mathbf{E}_u\|^2)$ because perturbations are small and the coefficients of higher-order power terms are the derivatives of analytic functions $\tilde{h}_G(\lambda)$ and $\tilde{h}_C(\lambda)$, which are bounded [cf. Definition 6.2].

2. Spectrum of $(\widehat{\mathbf{H}} - \mathbf{H})\mathbf{x}$. Consider a simplicial signal \mathbf{x} with an SFT $\tilde{\mathbf{x}} = \mathbf{U}^\top \mathbf{x} = [\tilde{x}_1, \dots, \tilde{x}_N]$, thus, $\mathbf{x} = \sum_{i=1}^N \tilde{x}_i \mathbf{u}_i$. Then, we study the effect of the difference of the SCFs on a simplicial signal from the spectral perspective via

$$(\widehat{\mathbf{H}} - \mathbf{H})\mathbf{x} = \sum_{i=1}^N \tilde{x}_i \sum_{t=0}^{T_d} w_{d,t} \mathbf{D}_{d,t}^t \mathbf{u}_i + \sum_{i=1}^N \tilde{x}_i \sum_{t=0}^{T_u} w_{u,t} \mathbf{D}_{u,t}^t \mathbf{u}_i + \mathbf{F}_d \mathbf{x} + \mathbf{F}_u \mathbf{x} \quad (\text{E.14})$$

where we have

$$\mathbf{D}_{d,t}^t \mathbf{u}_i = \sum_{r=0}^{t-1} (\mathbf{L}_d^r \mathbf{E}_d \mathbf{L}_d^{t-r} + \mathbf{L}_d^{r+1} \mathbf{E}_d \mathbf{L}_d^{t-r-1}) \mathbf{u}_i, \text{ and } \mathbf{D}_{u,t}^t \mathbf{u}_i = \sum_{r=0}^{t-1} (\mathbf{L}_u^r \mathbf{E}_u \mathbf{L}_u^{t-r} + \mathbf{L}_u^{r+1} \mathbf{E}_u \mathbf{L}_u^{t-r-1}) \mathbf{u}_i. \quad (\text{E.15})$$

Since the lower and upper Laplacians admit the eigendecompositions [cf. (D.5)]

$$\mathbf{L}_d \mathbf{u}_i = \lambda_{di} \mathbf{u}_i, \quad \mathbf{L}_u \mathbf{u}_i = \lambda_{ui} \mathbf{u}_i, \quad (\text{E.16})$$

we can express the terms in (E.14) as

$$\mathbf{L}_d^r \mathbf{E}_d \mathbf{L}_d^{t-r} \mathbf{u}_i = \mathbf{L}_d^r \mathbf{E}_d \lambda_{di}^{t-r} \mathbf{u}_i = \lambda_{di}^{t-r} \mathbf{L}_d^r (q_{di} \mathbf{u}_i + \mathbf{E}_1 \mathbf{u}_i) = q_{di} \lambda_{di}^t \mathbf{u}_i + \lambda_{di}^{t-r} \mathbf{L}_d^r \mathbf{E}_1 \mathbf{u}_i, \quad (\text{E.17})$$

where the second equality holds from Lemma E.3. Thus, we have

$$\mathbf{L}_d^{r+1} \mathbf{E}_d \mathbf{L}_d^{t-r-1} \mathbf{u}_i = q_{di} \lambda_{di}^t \mathbf{u}_i + \lambda_{di}^{t-r-1} \mathbf{L}_d^{r+1} \mathbf{E}_1 \mathbf{u}_i. \quad (\text{E.18})$$

With the results in (E.17) and (E.18), we can write the first term in (E.14) as

$$\sum_{i=1}^N \tilde{x}_i \sum_{t=0}^{T_d} w_{d,t} \mathbf{D}_{d,t}^t \mathbf{u}_i = \underbrace{\sum_{i=1}^N \tilde{x}_i \sum_{t=0}^{T_d} w_{d,t} \sum_{r=0}^{t-1} 2q_{di} \lambda_{di}^t \mathbf{u}_i}_{\text{term 1}} + \underbrace{\sum_{i=1}^N \tilde{x}_i \sum_{t=0}^{T_d} w_{d,t} \sum_{r=0}^{t-1} (\lambda_{di}^{t-r} \mathbf{L}_d^r \mathbf{E}_1 \mathbf{u}_i + \lambda_{di}^{t-r-1} \mathbf{L}_d^{r+1} \mathbf{E}_1 \mathbf{u}_i)}_{\text{term 2}}. \quad (\text{E.19})$$

Term 1 can be further expanded as

$$\text{term 1} = 2 \sum_{i=1}^N \tilde{x}_i q_{di} \sum_{t=0}^{T_d} t w_{d,t} \lambda_{di}^t \mathbf{u}_i = 2 \sum_{i=1}^N \tilde{x}_i q_{di} \lambda_{di} \tilde{h}'_G(\lambda_{di}) \mathbf{u}_i \quad (\text{E.20})$$

where we used the fact that $\sum_{t=0}^{T_d} t w_{d,t} \lambda_{di}^t = \lambda_{di} \tilde{h}'_G(\lambda_{di})$. Using $\mathbf{L}_d = \mathbf{U} \mathbf{\Lambda}_d \mathbf{U}^\top$ we can write term 2 in (E.19) as

$$\text{term 2} = \sum_{i=1}^N \tilde{x}_i \mathbf{U} \text{diag}(\mathbf{g}_{di}) \mathbf{U}^\top \mathbf{E}_1 \mathbf{u}_i \quad (\text{E.21})$$

where $\mathbf{g}_{di} \in \mathbb{R}^N$ has the j th entry

$$[\mathbf{g}_{di}]_j = \sum_{t=0}^{T_d} w_{d,t} \sum_{r=0}^{t-1} \left(\lambda_{di}^{t-r} [\mathbf{\Lambda}_d]_j^r + \lambda_{di}^{t-r-1} [\mathbf{\Lambda}_d]_j^{r+1} \right) = \begin{cases} 2\lambda_{di} \tilde{h}'_G(\lambda_{di}) & \text{for } j = i, \\ \frac{\lambda_{di} + \lambda_{dj}}{\lambda_{di} - \lambda_{dj}} (\tilde{h}_G(\lambda_{di}) - \tilde{h}_G(\lambda_{dj})) & \text{for } j \neq i. \end{cases} \quad (\text{E.22})$$

Now, substituting (E.20) and (E.21) into (E.19), we have

$$\sum_{i=1}^N \tilde{x}_i \sum_{t=0}^{T_d} w_{d,t} \mathbf{D}_{d,t}^t \mathbf{u}_i = 2 \sum_{i=1}^N \tilde{x}_i q_{di} \lambda_{di} \tilde{h}'_G(\lambda_{di}) \mathbf{u}_i + \sum_{i=1}^N \tilde{x}_i \mathbf{U} \text{diag}(\mathbf{g}_{di}) \mathbf{U}^\top \mathbf{E}_1 \mathbf{u}_i. \quad (\text{E.23})$$

By following the same steps as in (E.19)-(E.22), we can express also the second term in (E.14) as

$$\sum_{i=1}^N \tilde{x}_i \sum_{t=0}^{T_d} w_{u,t} \mathbf{D}_{u,t}^t \mathbf{u}_i = 2 \sum_{i=1}^N \tilde{x}_i q_{ui} \lambda_{ui} \tilde{h}'_G(\lambda_{ui}) \mathbf{u}_i + \sum_{i=1}^N \tilde{x}_i \mathbf{U} \text{diag}(\mathbf{g}_{ui}) \mathbf{U}^\top \mathbf{E}_2 \mathbf{u}_i \quad (\text{E.24})$$

where $\mathbf{g}_{ui} \in \mathbb{R}^N$ is defined as

$$[\mathbf{g}_{ui}]_j = \sum_{t=0}^{T_d} w_{u,t} \sum_{r=0}^{t-1} \left(\lambda_{ui}^{t-r} [\mathbf{\Lambda}_u]_j^r + \lambda_{ui}^{t-r-1} [\mathbf{\Lambda}_u]_j^{r+1} \right) = \begin{cases} 2\lambda_{ui} \tilde{h}'_G(\lambda_{ui}) & \text{for } j = i, \\ \frac{\lambda_{ui} + \lambda_{uj}}{\lambda_{ui} - \lambda_{uj}} (\tilde{h}_G(\lambda_{ui}) - \tilde{h}_G(\lambda_{uj})) & \text{for } j \neq i. \end{cases} \quad (\text{E.25})$$

3. Bound of $\|(\widehat{\mathbf{H}} - \mathbf{H})\mathbf{x}\|$. Now we are ready to bound $\|(\widehat{\mathbf{H}} - \mathbf{H})\mathbf{x}\|$ based on triangle inequality. First, given the small perturbations $\|\mathbf{E}_d\| \leq \epsilon_d$ and $\|\mathbf{E}_u\| \leq \epsilon_u$, we have for the last two terms in (E.14)

$$\|\mathbf{F}_d \mathbf{x}\| \leq \mathcal{O}(\epsilon_d^2) \|\mathbf{x}\|, \text{ and } \|\mathbf{F}_u \mathbf{x}\| \leq \mathcal{O}(\epsilon_u^2) \|\mathbf{x}\|. \quad (\text{E.26})$$

Second, for the first term $\|\sum_{i=1}^N \tilde{x}_i \sum_{t=0}^{T_d} w_{d,t} \mathbf{D}_{d,t}^t \mathbf{u}_i\|$ in (E.14), we can bound its two terms in (E.20) and (E.21) as

$$\left\| \sum_{i=1}^N \tilde{x}_i \sum_{t=0}^{T_d} w_{d,t} \mathbf{D}_{d,t}^t \mathbf{u}_i \right\| \leq \left\| 2 \sum_{i=1}^N \tilde{x}_i q_{di} \lambda_{di} \tilde{h}'_G(\lambda_{di}) \mathbf{u}_i \right\| + \left\| \sum_{i=1}^N \tilde{x}_i \mathbf{U} \text{diag}(\mathbf{g}_{di}) \mathbf{U}^\top \mathbf{E}_1 \mathbf{u}_i \right\|. \quad (\text{E.27})$$

For the first term on the RHS of (E.27), we can write

$$\left\| 2 \sum_{i=1}^N \tilde{x}_i q_{di} \lambda_{di} \tilde{h}'_G(\lambda_{di}) \mathbf{u}_i \right\|^2 \leq 4 \sum_{i=1}^N |\tilde{x}_i|^2 |q_{di}|^2 |\lambda_{di} \tilde{h}'_G(\lambda_{di})|^2 \leq 4\epsilon_d^2 C_d^2 \|\mathbf{x}\|^2, \quad (\text{E.28})$$

which results from, first, $|q_{di}| \leq \epsilon_d = \|\mathbf{E}_d\|$ since q_{di} is an eigenvalue of \mathbf{E}_d ; second, the integral Lipschitz property of the SCF $|\lambda \tilde{h}'_G(\lambda)| \leq C_d$; and lastly, the fact that $\sum_{i=1}^N |\tilde{x}_i|^2 = \|\tilde{\mathbf{x}}\|^2 = \|\mathbf{x}\|^2$ and $\|\mathbf{u}_i\|^2 = 1$. We then have

$$\left\| 2 \sum_{i=1}^N \tilde{x}_i q_{di} \lambda_{di} \tilde{h}'_G(\lambda_{di}) \mathbf{u}_i \right\| \leq 2\epsilon_d C_d \|\mathbf{x}\|. \quad (\text{E.29})$$

For the second term in RHS of (E.27), we have

$$\left\| \sum_{i=1}^N \tilde{x}_i \mathbf{U} \text{diag}(\mathbf{g}_{di}) \mathbf{U}^\top \mathbf{E}_1 \mathbf{u}_i \right\| \leq \sum_{i=1}^N |\tilde{x}_i| \|\mathbf{U} \text{diag}(\mathbf{g}_{di}) \mathbf{U}^\top\| \|\mathbf{E}_1\| \|\mathbf{u}_i\|, \quad (\text{E.30})$$

which stems from the triangle inequality. We further have $\|\mathbf{U} \text{diag}(\mathbf{g}_{di}) \mathbf{U}^\top\| = \|\text{diag}(\mathbf{g}_{di})\| \leq 2C_d$ resulting from $\|\mathbf{U}\| = 1$ and the C_d -integral Lipschitz of $\tilde{h}_G(\lambda)$ [cf. Definition 6.2]. Moreover, it follows that $\|\mathbf{E}_1\| \leq \epsilon_d \delta_d$ from Lemma E.3, which results in

$$\left\| \sum_{i=1}^N \tilde{x}_i \mathbf{U} \text{diag}(\mathbf{g}_{di}) \mathbf{U}^\top \mathbf{E}_1 \mathbf{u}_i \right\| \leq 2C_d \epsilon_d \delta_d \sqrt{N} \|\mathbf{x}\| \quad (\text{E.31})$$

where we use that $\sum_{i=1}^N |\tilde{x}_i| = \|\tilde{\mathbf{x}}\|_1 \leq \sqrt{N} \|\tilde{\mathbf{x}}\| = \sqrt{N} \|\mathbf{x}\|$. By combining (E.28) and (E.31), we have

$$\left\| \sum_{i=1}^N \tilde{x}_i \sum_{t=0}^{T_d} w_{d,t} \mathbf{D}_{d,t}^t \mathbf{u}_i \right\| \leq 2\epsilon_d C_d \|\mathbf{x}\| + 2C_d \epsilon_d \delta_d \sqrt{N} \|\mathbf{x}\|. \quad (\text{E.32})$$

Analogously, we can show that

$$\left\| \sum_{i=1}^N \tilde{x}_i \sum_{t=0}^{T_u} w_{u,t} \mathbf{D}_{u,t}^t \mathbf{u}_i \right\| \leq 2\epsilon_u C_u \|\mathbf{x}\| + 2C_u \epsilon_u \delta_u \sqrt{N} \|\mathbf{x}\|. \quad (\text{E.33})$$

Now by combining (E.26), (E.32) and (E.33), we can bound $\|(\hat{\mathbf{H}} - \mathbf{H})\mathbf{x}\|$ as

$$\|(\hat{\mathbf{H}} - \mathbf{H})\mathbf{x}\| \leq 2\epsilon_d C_d \|\mathbf{x}\| + 2C_d \epsilon_d \delta_d \sqrt{N} \|\mathbf{x}\| + \mathcal{O}(\epsilon_d^2) \|\mathbf{x}\| + 2\epsilon_u C_u \|\mathbf{x}\| + 2C_u \epsilon_u \delta_u \sqrt{N} \|\mathbf{x}\| + \mathcal{O}(\epsilon_u^2) \|\mathbf{x}\|. \quad (\text{E.34})$$

By defining $\Delta_d = 2(1 + \delta_d \sqrt{N})$ and $\Delta_u = 2(1 + \delta_u \sqrt{N})$, we can obtain that

$$\|\hat{\mathbf{H}} - \mathbf{H}\| \leq C_d \Delta_d \epsilon_d + C_u \Delta_u \epsilon_u + \mathcal{O}(\epsilon_d^2) + \mathcal{O}(\epsilon_u^2). \quad (\text{E.35})$$

Thus, we have $\|\mathbf{H}_k^l - \hat{\mathbf{H}}_k^l\| \leq C_{k,d} \Delta_{k,d} \epsilon_{k,d} + C_{k,u} \Delta_{k,u} \epsilon_{k,u}$ with $\Delta_{k,d} = 2(1 + \delta_{k,d} \sqrt{N_k})$ and $\Delta_{k,u} = 2(1 + \delta_{k,u} \sqrt{N_k})$ where we ignore the second and higher order terms on $\epsilon_{k,d}$ and $\epsilon_{k,u}$. Likewise, we have $\|\mathbf{H}_{k,d}^l - \hat{\mathbf{H}}_{k,d}^l\| \leq C_{k,d} \Delta_{k,d} \epsilon_{k,d}$ for the lower SCF and $\|\mathbf{H}_{k,u}^l - \hat{\mathbf{H}}_{k,u}^l\| \leq C_{k,u} \Delta_{k,u} \epsilon_{k,u}$ for the upper SCF. \square

E.3.2. STEP II: STABILITY OF SCCNNs

Proof. Given the initial input \mathbf{x}_k^0 , the Euclidean distance between \mathbf{x}_k^l and $\hat{\mathbf{x}}_k^l$ at layer l can be bounded by using triangle inequality and the C_σ -Lipschitz property of $\sigma(\cdot)$ [cf. assumption 6.6] as

$$\|\hat{\mathbf{x}}_k^l - \mathbf{x}_k^l\|_2 \leq C_\sigma (\phi_{k,d}^l + \phi_k^l + \phi_{k,u}^l), \quad (\text{E.36})$$

with

$$\begin{aligned} \phi_{k,d}^l &:= \|\hat{\mathbf{H}}_{k,d}^l \hat{\mathbf{R}}_{k,d} \hat{\mathbf{x}}_{k-1}^{l-1} - \mathbf{H}_{k,d}^l \mathbf{R}_{k,d} \mathbf{x}_{k-1}^{l-1}\|, \\ \phi_k^l &:= \|\hat{\mathbf{H}}_k^l \hat{\mathbf{x}}_k^{l-1} - \mathbf{H}_k^l \mathbf{x}_k^{l-1}\|, \\ \phi_{k,u}^l &:= \|\hat{\mathbf{H}}_{k,u}^l \hat{\mathbf{R}}_{k,u} \hat{\mathbf{x}}_{k+1}^{l-1} - \mathbf{H}_{k,u}^l \mathbf{R}_{k,u} \mathbf{x}_{k+1}^{l-1}\|. \end{aligned} \quad (\text{E.37})$$

We now focus on upper bounding each of the terms.

1. Term ϕ_k^l . By subtracting and adding $\widehat{\mathbf{H}}_k^l \mathbf{x}_k^{l-1}$ within the norm, and using the triangle inequality, we obtain

$$\begin{aligned} \phi_k^l &\leq \|\widehat{\mathbf{H}}_k^l(\hat{\mathbf{x}}_k^{l-1} - \mathbf{x}_k^{l-1})\| + \|(\widehat{\mathbf{H}}_k^l - \mathbf{H}_k^l)\mathbf{x}_k^{l-1}\| \leq \|\hat{\mathbf{x}}_k^{l-1} - \mathbf{x}_k^{l-1}\| + \|\widehat{\mathbf{H}}_k^l - \mathbf{H}_k^l\| \|\mathbf{x}_k^{l-1}\| \\ &\leq \|\hat{\mathbf{x}}_k^{l-1} - \mathbf{x}_k^{l-1}\| + (C_{k,d}\Delta_{k,d}\epsilon_{k,d} + C_{k,u}\Delta_{k,u}\epsilon_{k,u}) \|\mathbf{x}_k^{l-1}\| \end{aligned} \quad (\text{E.38})$$

where we used the SCF stability in (E.35) and that all SCFs have a normalized bounded frequency response in assumption 6.3. Note that $\widehat{\mathbf{H}}_k^l$ is also characterized by $\tilde{h}_G(\lambda)$ with the same set of filter coefficients as \mathbf{H}_k^l .

2. Term $\phi_{k,d}^l$ and $\phi_{k,u}^l$. By subtracting and adding a term $\widehat{\mathbf{H}}_{k,d}^l \widehat{\mathbf{R}}_{k,d} \mathbf{x}_{k-1}^{l-1}$ within the norm, we have

$$\begin{aligned} \phi_{k,d}^l &\leq \|\widehat{\mathbf{H}}_{k,d}^l \widehat{\mathbf{R}}_{k,d}(\hat{\mathbf{x}}_{k-1}^{l-1} - \mathbf{x}_{k-1}^{l-1})\| + \|(\widehat{\mathbf{H}}_{k,d}^l \widehat{\mathbf{R}}_{k,d} - \mathbf{H}_{k,d}^l \mathbf{R}_{k,d})\mathbf{x}_{k-1}^{l-1}\| \\ &\leq \|\widehat{\mathbf{R}}_{k,d}\| \|\hat{\mathbf{x}}_{k-1}^{l-1} - \mathbf{x}_{k-1}^{l-1}\| + \|\widehat{\mathbf{H}}_{k,d}^l \widehat{\mathbf{R}}_{k,d} - \mathbf{H}_{k,d}^l \mathbf{R}_{k,d}\| \|\mathbf{x}_{k-1}^{l-1}\|, \end{aligned} \quad (\text{E.39})$$

where we used again triangle inequality and $\|\widehat{\mathbf{H}}_{k,d}^l\| \leq 1$ from assumption 6.3. For the term $\|\widehat{\mathbf{R}}_{k,d}\|$, we have $\|\widehat{\mathbf{R}}_{k,d}\| \leq \|\mathbf{R}_{k,d}^l\| + \|\mathbf{J}_{k,d}\| \|\mathbf{R}_{k,d}^l\| \leq r_{k,d}(1 + \varepsilon_{k,d})$ where we used $\|\mathbf{R}_{k,d}^l\| \leq r_{k,d}$ in assumption 6.4 and $\|\mathbf{J}_{k,d}\| \leq \varepsilon_{k,d}$. For the second term of RHS in (E.39), by adding and subtracting $\widehat{\mathbf{H}}_{k,d}^l \mathbf{R}_{k,d}^l$ we have

$$\begin{aligned} \|\widehat{\mathbf{H}}_{k,d}^l \widehat{\mathbf{R}}_{k,d} - \mathbf{H}_{k,d}^l \mathbf{R}_{k,d}\| &= \|\widehat{\mathbf{H}}_{k,d}^l \widehat{\mathbf{R}}_{k,d} - \widehat{\mathbf{H}}_{k,d}^l \mathbf{R}_{k,d}^l + \widehat{\mathbf{H}}_{k,d}^l \mathbf{R}_{k,d}^l - \mathbf{H}_{k,d}^l \mathbf{R}_{k,d}\| \\ &\leq \|\widehat{\mathbf{H}}_{k,d}^l\| \|\widehat{\mathbf{R}}_{k,d} - \mathbf{R}_{k,d}^l\| + \|\widehat{\mathbf{H}}_{k,d}^l - \mathbf{H}_{k,d}^l\| \|\mathbf{R}_{k,d}\| \\ &\leq r_{k,d}\varepsilon_{k,d} + C'_{k,d}\Delta_{k,d}\epsilon_{k,d}r_{k,d} \end{aligned} \quad (\text{E.40})$$

where we use the stability result of the lower SCF $\mathbf{H}_{k,d}^l$ in (E.35). By substituting (E.40) into (E.39), we have

$$\phi_{k,d}^l \leq \hat{r}_{k,d} \|\hat{\mathbf{x}}_{k-1}^{l-1} - \mathbf{x}_{k-1}^{l-1}\| + (r_{k,d}\varepsilon_{k,d} + C'_{k,d}\Delta_{k,d}\epsilon_{k,d}r_{k,d}) \|\mathbf{x}_{k-1}^{l-1}\|. \quad (\text{E.41})$$

By following the same procedure [cf. (E.39) and (E.40)], we obtain

$$\phi_{k,u}^l \leq \hat{r}_{k,u} \|\hat{\mathbf{x}}_{k+1}^{l-1} - \mathbf{x}_{k+1}^{l-1}\| + (r_{k,u}\varepsilon_{k,u} + C'_{k,u}\Delta_{k,u}\epsilon_{k,u}r_{k,u}) \|\mathbf{x}_{k+1}^{l-1}\|. \quad (\text{E.42})$$

3. Bound of $\|\hat{\mathbf{x}}_k^l - \mathbf{x}_k^l\|$. Using the notations $t_k, t_{k,d}$ and $t_{k,u}$ in Theorem 6.7, we then have a set of recursions, for $k = [K]$

$$\begin{aligned} \|\hat{\mathbf{x}}_k^l - \mathbf{x}_k^l\| &\leq C_\sigma(\hat{r}_{k,d} \|\hat{\mathbf{x}}_{k-1}^{l-1} - \mathbf{x}_{k-1}^{l-1}\| + t_{k,d} \|\mathbf{x}_{k-1}^{l-1}\| + \|\hat{\mathbf{x}}_k^{l-1} - \mathbf{x}_k^{l-1}\| + t_k \|\mathbf{x}_k^{l-1}\| \\ &\quad + \hat{r}_{k,u} \|\hat{\mathbf{x}}_{k+1}^{l-1} - \mathbf{x}_{k+1}^{l-1}\| + t_{k,u} \|\mathbf{x}_{k+1}^{l-1}\|). \end{aligned} \quad (\text{E.43})$$

Define vector \mathbf{b}^l as $[\mathbf{b}^l]_k = \|\hat{\mathbf{x}}_k^l - \mathbf{x}_k^l\|$ with $\mathbf{b}^0 = \mathbf{0}$. Let $\boldsymbol{\beta}^l$ collect the energy of all outputs at layer l , with $[\boldsymbol{\beta}^l]_k := \|\mathbf{x}_k^{l-1}\|$. We can express the Euclidean distances of all k -simplicial signal outputs for $k = [K]$, as

$$\mathbf{b}^l \preceq C_\sigma \widehat{\mathbf{Z}} \mathbf{b}^{l-1} + C_\sigma \mathbf{T} \boldsymbol{\beta}^{l-1} \quad (\text{E.44})$$

where \preceq indicates elementwise smaller than or equal, and we have

$$\mathbf{T} = \begin{bmatrix} t_0 & t_{0,u} & & & & \\ t_{1,d} & t_1 & t_{1,u} & & & \\ & \ddots & \ddots & \ddots & & \\ & & t_{K-1,d} & t_{K-1} & t_{K-1,u} & \\ & & & t_{K,d} & t_K & \end{bmatrix} \quad \text{and} \quad \widehat{\mathbf{Z}} = \begin{bmatrix} 1 & \hat{r}_{0,u} & & & & \\ \hat{r}_{1,d} & 1 & \hat{r}_{1,u} & & & \\ & \ddots & \ddots & \ddots & & \\ & & \hat{r}_{K-1,d} & 1 & \hat{r}_{K-1,u} & \\ & & & \hat{r}_{K,d} & 1 & \end{bmatrix}. \quad (\text{E.45})$$

We are now interested in building a recursion for (E.44) for all layers l . We start with term \mathbf{x}_k^l . Based on its expression in (E.2), we bound it as

$$\begin{aligned} \|\mathbf{x}_k^l\| &\leq C_\sigma(\|\mathbf{H}_{k,d}^l\| \|\mathbf{R}_{k,d}\| \|\mathbf{x}_{k-1}^{l-1}\| + \|\mathbf{H}_k^l\| \|\mathbf{x}_k^{l-1}\| + \|\mathbf{H}_{k,u}^l\| \|\mathbf{R}_{k,u}\| \|\mathbf{x}_{k+1}^{l-1}\|) \\ &\leq C_\sigma(r_{k,d} \|\mathbf{x}_{k-1}^{l-1}\| + \|\mathbf{x}_k^{l-1}\| + r_{k,u} \|\mathbf{x}_{k+1}^{l-1}\|), \end{aligned} \quad (\text{E.46})$$

which holds for $k = [K]$. Thus, it can be expressed in the vector form as $\beta^l \preceq C_\sigma \mathbf{Z} \beta^{l-1}$, with

$$\mathbf{Z} = \begin{bmatrix} 1 & r_{0,u} & & & & \\ r_{1,d} & 1 & r_{1,u} & & & \\ & \ddots & \ddots & \ddots & & \\ & & r_{K-1,d} & 1 & r_{K-1,u} & \\ & & & r_{K,d} & 1 & \end{bmatrix}. \quad (\text{E.47})$$

Similarly, we have $\beta^{l-1} \preceq C_\sigma \mathbf{Z} \beta^{l-2}$, leading to $\beta^l \preceq C_\sigma^l \mathbf{Z}^l \beta^0$ with $\beta^0 = \beta$ [cf. [assumption 6.5](#)]. We can then express the bound [\(E.44\)](#) as

$$\mathbf{b}^l \preceq C_\sigma \widehat{\mathbf{Z}} \mathbf{b}^{l-1} + C_\sigma^l \mathbf{T} \mathbf{Z}^{l-1} \beta. \quad (\text{E.48})$$

Thus, we have

$$\mathbf{b}^0 = \mathbf{0}, \mathbf{b}^1 \preceq C_\sigma \mathbf{T} \beta, \mathbf{b}^2 \preceq C_\sigma^2 (\widehat{\mathbf{Z}} \mathbf{T} \beta + \mathbf{T} \mathbf{Z} \beta), \mathbf{b}^3 \preceq C_\sigma^3 (\widehat{\mathbf{Z}}^2 \mathbf{T} \beta + \widehat{\mathbf{Z}} \mathbf{T} \mathbf{Z} \beta + \mathbf{T} \mathbf{Z}^2 \beta), \mathbf{b}^4 \preceq \dots, \quad (\text{E.49})$$

which, inductively, leads to

$$\mathbf{b}^l \preceq C_\sigma^l \sum_{i=1}^l \widehat{\mathbf{Z}}^{i-1} \mathbf{T} \mathbf{Z}^{l-i} \beta. \quad (\text{E.50})$$

By setting $l = L$, we obtain the bound $\mathbf{b}^L \preceq \mathbf{d} = C_\sigma^L \sum_{i=1}^L \widehat{\mathbf{Z}}^{i-1} \mathbf{T} \mathbf{Z}^{L-i} \beta$ in [Theorem 6.7](#). \square

E.4. Discussions on Stability of SCCNNs in [Theorem 6.7](#)

From the bound \mathbf{d} , we see how factors \mathbf{T} and $\mathbf{Z}, \widehat{\mathbf{Z}}$ affect the stability of an SCCNN, which further reflects the factors of k -simplices and other simplices. For $L = 1$, we have $\mathbf{d} = C_\sigma \mathbf{T} \beta$, and $d_k = C_\sigma (t_{k,d} \beta_{k-1} + t_k \beta_k + t_{k+1} \beta_{k+1})$. That is, the stability d_k of k -simplicial output depends on k -simplicial input energy β_k via constant t_k and $k \pm 1$ -simplicial input energies via constants $t_{k,d}$ and $t_{k,u}$. The common factors $\Delta_{k,d}, \epsilon_{k,d}$ in $t_{k,d}$ and t_k measure the perturbations on lower simplicial adjacency. Specifically, $\Delta_{k,d}$ is a degree of topology misalignment between $\mathbf{L}_{k,d}$ and $\widehat{\mathbf{L}}_{k,d}$, and $\epsilon_{k,d}$ is a measure of the perturbation magnitude. The factor $C_{k,d}$ is the integral Lipschitz property of the SCFs operating in the gradient frequencies. The factor $r_{k,d}$ in $t_{k,d}$ measures the degree of projections $\mathbf{R}_{k,d}$ from $(k-1)$ -simplices to k -simplices. Discussions can be made on other factors in $t_{k,u}$ and t_k likewise. Thus, the stability of k -simplicial output is dependent on perturbations on k -simplicial adjacencies, integral Lipschitz properties of k -SCFs, and projection degrees from $(k \pm 1)$ - to k -simplices, given fixed inputs after a one-layer SCCNN.

For $L = 2$, we have $\mathbf{d} = C_\sigma (\widehat{\mathbf{Z}} \mathbf{T} \beta + \mathbf{T} \mathbf{Z} \beta)$. In an SC order $K = 2$, we can find the entries of $\mathbf{T} \mathbf{Z} \beta$ as

$$\mathbf{T} \mathbf{Z} \beta = \begin{bmatrix} t_0(\beta_0 + r_{0,u} \beta_1) + t_{0,u}(r_{1,d} \beta_0 + \beta_1 + r_{1,u} \beta_2) \\ t_{1,d}(p_0 + r_{0,u} \beta_1) + t_1(r_{1,d} \beta_0 + \beta_1 + r_{1,u} \beta_2) + t_{1,u}(r_{2,d} \beta_1 + \beta_2) \\ t_{2,d}(r_{1,d} \beta_0 + \beta_1 + r_{1,u} \beta_2) + t_2(r_{2,d} \beta_1 + \beta_2) \end{bmatrix} \quad (\text{E.51})$$

from which, we see that the stability of node output depends also on the triangle input energy β_2 , which is scaled by the projection degree $r_{1,u}$ from triangles to edges, then by $t_{0,u}$. Moreover, for the other term $\widehat{\mathbf{Z}} \mathbf{T} \beta$, we have its entries as

$$\widehat{\mathbf{Z}} \mathbf{T} \beta = \begin{bmatrix} (t_0 \beta_0 + t_{0,u} \beta_1) + \hat{r}_{0,u}(t_{1,d} \beta_0 + t_1 \beta_1 + t_{1,u} \beta_2) \\ \hat{r}_{1,d}(t_0 \beta_0 + t_{0,u} \beta_1) + (t_{1,d} \beta_0 + t_1 \beta_1 + t_{1,u} \beta_2) + \hat{r}_{1,u}(t_{2,d} \beta_1 + t_2 \beta_2) \\ \hat{r}_{2,d}(t_{1,d} \beta_0 + t_1 \beta_1 + t_{1,u} \beta_2) + (t_{2,d} \beta_1 + t_2 \beta_2) \end{bmatrix}. \quad (\text{E.52})$$

We see that the dependence of node output stability on β_2 is also mediated through the factors $t_{1,d}, t_1$ and $t_{1,u}$, which describe instead perturbations on edge adjacencies, integral Lipschitz properties of edge-SCFs and projection degrees from nodes and triangles to edges. In turn, these induce instability of node outputs through projection perturbations from edges to nodes. Thus, the stability d_k is in general dependent on perturbations, integral Lipschitz properties of SCFs and projections in the k -simplicial space (constants $t_{k,d}, t_k$ and $t_{k,u}$), as well as those in the $(k \pm 1)$ -simplicial spaces through projection perturbations $\hat{r}_{k,d}$ and $\hat{r}_{k,u}$.

When $L = 3$, we have $\mathbf{d} = C_\sigma^3 (\widehat{\mathbf{Z}}^2 \mathbf{T} \beta + \widehat{\mathbf{Z}} \mathbf{T} \mathbf{Z} \beta + \mathbf{T} \mathbf{Z}^2 \beta)$. We would observe that factors of perturbations on triangle adjacencies and properties of triangle SCFs, measured by $t_{2,d}$ and t_2 , will further appear in the stability d_0 of node output, controlled by the degrees $\hat{r}_{1,u}$ and $\hat{r}_{0,u}$ of upper perturbations on edge and node.

As the SCCNN becomes deeper, for k -simplicial output, the dependence of its stability on perturbations, properties of SCFs and projections in k -simplicial space remains, and the dependence on those factors in simplicial spaces of different orders will extend, up to the whole SC. Specifically, d_k has a dependence on factors in (up to) $(k \pm l)$ -simplicial space when $L = l + 1$. This mutual stability dependence of different simplicial outputs is the result of the extended inter-simplicial locality of SCCNNs.

Remark E.4. The stability analysis of SCCNNs adapts to other NNs on SCs. For the NNs in Yang et al. (2022a), matrices \mathbf{T} , \mathbf{Z} and $\widehat{\mathbf{Z}}$ will contain only the diagonal entries. We can focus on the stability bound $[d]_k$ of k -simplicial output, given by $[d]_k \leq C_\sigma^L L t_k [\beta]_k$ with $t_k = C_{k,d} \Delta_{k,d} \epsilon_{k,d} + C_{k,u} \Delta_{k,u} \epsilon_{k,u}$. Since this method focuses only on simplices of the same order, it is unaffected by the perturbations from simplices of other orders. The same holds true for the NNs in Ebli et al. (2020) but with $t_k = C_k \Delta_k \epsilon_k$ where we have a relative perturbation model on \mathbf{L}_k with a perturbation $\|\mathbf{E}_k\| \leq \epsilon$ and Δ_k measures the eigenvector misalignment between \mathbf{L}_k and \mathbf{E}_k . Setting $k = 0$, we then obtain the stability bound for GNNs in Defferrard et al. (2016); Gama et al. (2020a). For the simplicial NNs performing one-step simplicial shifting, e.g., Bunch et al. (2020), a stability bound can be obtained based on the procedure in Appendix E.3.2 which will be related to the degree of the simplicial shiftings, measured by spectral radii of Hodge Laplacians. This is another limitation of one-step shifting as the filters have only a linear shape affecting their selectivity Corollary 5.4, compared to higher-order convolutions in SCCNNs and Ebli et al. (2020); Yang et al. (2022a).

F. Experiments

In this section, we provide more details about the two experiments.¹ All of the experiments were run on a single NVIDIA A40 GPU with 48 GB of memory using CUDA 11.5.

F.1. Simplex Prediction

Link prediction on graphs is to predict whether two nodes in a network are likely to form a link. Methods based on GNNs have shown better performance compared to the classical heuristic and latent feature based approaches (Kipf & Welling, 2016; Zhang & Chen, 2018). In higher-order network models, there is a growing need for the task of higher-order link prediction. This task is relevant in, e.g., predicting new groups of friends in social networks, inferring new relationships between genes and diseases, or recommending online thread participation for a group of users (Benson et al., 2018). Here we consider the task of simplex prediction: *given all the $(k - 1)$ -simplices in a set of $k + 1$ nodes, to predict if this set will be closed to form a k -simplex.* We can view this set of $k + 1$ nodes as an open k -simplex. For example, in 2-simplex (triangle) prediction, we predict if an open triangle $t = [i, j, k]$ will form a 2-simplex (a closed triangle), given its three edges $[i, j]$, $[j, k]$ and $[i, k]$ present in the SC. Although Benson et al. (2018) extended traditional methods for link prediction to SCs for a similar task, there is limited research on learning-based approaches, especially in SCs. Therefore, we aim to address 2- and 3-simplex predictions based on SCCNNs in this experiment.

F.1.1. METHOD

We propose the following method for simplex prediction, which is generalized from link prediction based on GNNs by Zhang & Chen (2018): For k -simplex prediction, we use an SCCNN in an SC of order k to first learn the features of lower-order simplices up to order $k - 1$. Then, we concatenate these embedded lower-order simplicial features and input them to a multilayer perceptron (MLP) which predicts if a k -simplex is positive (closed, shall be included in the SC) or negative (open, not included in the SC).

Specifically, in 2-simplex prediction, consider an SC of order two, which is built based on nodes, edges and (existing positive) triangles. Given the initial inputs on nodes \mathbf{x}_0 and on edges \mathbf{x}_1 and zero inputs on triangles $\mathbf{x}_2 = \mathbf{0}$ since we assume no prior knowledge on triangles, for an open triangle $t = [i, j, k]$, an SCCNN is used to learn features on nodes and edges (denoted by \mathbf{y}). Then, we input the concatenation of the features on three nodes or three edges to an MLP, i.e., $\text{MLP}_{\text{node}}([\mathbf{y}_0]_i \parallel [\mathbf{y}_0]_j \parallel [\mathbf{y}_0]_k)$ or $\text{MLP}_{\text{edge}}([\mathbf{y}]_{[i,j]} \parallel [\mathbf{y}]_{[j,k]} \parallel [\mathbf{y}]_{[i,k]})$, to predict if triangle t is positive or negative. An MLP taking both node and edge features is possible, but we keep it on one simplex level for complexity purposes. Similarly, we consider an SCCNN in an SC of order three for 3-simplex prediction, which is followed by an MLP operating on either nodes, edges or triangles.

¹Code available at https://github.com/cookbook-ms/Learning_on_SCs.

F.1.2. DATA PREPROCESSING

We consider the data from the Semantic Scholar Open Research Corpus (Ammar et al., 2018) to construct a coauthorship complex where nodes are authors and collaborations between k -author are represented by $(k - 1)$ -simplices. Following the preprocessing in (Ebli et al., 2020), we obtain 352 nodes, 1472 edges, 3285 triangles, 5019 tetrahedrons (3-simplices) and a number of other higher-order simplices. The node signal \mathbf{x}_0 , edge flow \mathbf{x}_1 and triangle flow \mathbf{x}_2 are the numbers of citations of single author papers and the collaborations of two and three authors, respectively.

For the 2-simplex prediction, we use the collaboration impact (the number of citations) to split the total set of triangles into the positive set $\mathcal{T}_P = \{t | [\mathbf{x}_2]_t > 7\}$ containing 1482 closed triangles and the negative set $\mathcal{T}_N = \{t | [\mathbf{x}_2]_t \leq 7\}$ containing 1803 open triangles such that we have balanced positive and negative samples. We further split the 80% of the positive triangle set for training, 10% for validation and 10% for testing; likewise for the negative triangle set. Note that in the construction of the SC, i.e., the incidence matrix \mathbf{B}_2 , Hodge Laplacians $\mathbf{L}_{1,u}$ and $\mathbf{L}_{2,d}$, we ought to remove negative triangles in the training set and all triangles in the test set. That is, for 2-simplex prediction, we only make use of the training set of the positive triangles since the negative ones are not in the SC.

Similarly, we prepare the dataset for 3-simplex (tetrahedron) prediction, amounting to the tetradic collaboration prediction. We obtain balanced positive and negative tetrahedron sets based on the citation signal \mathbf{x}_3 . In the construction of \mathbf{B}_3 , $\mathbf{L}_{2,u}$ and $\mathbf{L}_{3,d}$, we again only use the tetrahedrons in the positive training set.

F.1.3. MODELS

For comparison, we first use heuristic methods proposed in Benson et al. (2018) as baselines to determine if a triangle $t = [i, j, k]$ is closed, namely,

- 1) Harmonic mean: $s_t = 3 / ([\mathbf{x}_1]_{[i,j]}^{-1} + [\mathbf{x}_1]_{[j,k]}^{-1} + [\mathbf{x}_1]_{[i,k]}^{-1})$,
- 2) Geometric mean: $s_t = \lim_{p \rightarrow 0} ([[\mathbf{x}_1]_{[i,j]}^p + [\mathbf{x}_1]_{[j,k]}^p + [\mathbf{x}_1]_{[i,k]}^p])^{1/p}$, and
- 3) Arithmetic mean: $s_t = ([\mathbf{x}_1]_{[i,j]} + [\mathbf{x}_1]_{[j,k]} + [\mathbf{x}_1]_{[i,k]}) / 3$,

which compute the triangle weight based on its three faces. Similarly, we generalized these mean methods to compute the weight of a 3-simplex $[i, j, k, m]$ based on the four triangle faces in 3-simplex prediction.

We also consider different learning methods. Specifically,

- 1) Simplicial 2-Complex NN (“Bunch”) [cf. (B.8)] by Bunch et al. (2020) (we also generalized this model to 3-dimension for 3-simplex prediction), which provides a baseline for SCCNNs to see the effect of using the higher-order convolutions.
- 2) Convolutional filters on SC (“CF-SC”) by Isufi & Yang (2022), which is a linear version of SCCNN and has a limited extended simplicial locality. The comparison to it reveals the effect of the extended simplicial locality.
- 3) Principled SNN (“PSNN”) by Roddenberry et al. (2021), which performs a one-step simplicial shifting, providing as a baseline to observe the benefit of higher-order convolutions and inter-simplicial couplings;
- 4) SNN by Ebli et al. (2020), which performs higher-order convolutions but without separating the lower and upper adjacencies. We can see the benefit of allowing different processing in the gradient and curl spaces by comparing to it.
- 5) Simplicial Convolutional NN (“SCNN”) [cf. (B.7)] by Yang et al. (2021), which does not include information from adjacent simplices. The comparison to it shows the effect of inter-simplicial couplings.
- 6) SCF on edges by Yang et al. (2022b), which is a linear version of SCNN.
- 7) GNN [cf. (B.6)] by Defferrard et al. (2016) and Gama et al. (2020a), which performs a higher-order graph convolution without using the SC model. The comparison to it is necessary to observe the benefit of SC models in simplex prediction.
- 8) Linear graph filters on nodes (“GF”) by Sandryhaila & Moura (2013), which is a linear version of GNNs;
- 9) MLP: $\mathbf{Y}_k = \sigma(\mathbf{X}_k \mathbf{W}_k)$, providing as a baseline for the effect of using inductive models.

For MLP, Bunch, CF-SC and our SCCNN, we consider the outputs in the node and edge spaces, respectively, for 2-simplex prediction, which are denoted by a suffix “-Node” or “-Edge”. For 3-simplex prediction, the output in the triangle space can be used as well, denoted by a suffix “-Tri.”, where we also build SCNNs in both edge and triangle spaces.

F.1.4. EXPERIMENTAL SETUP AND HYPERPARAMETERS

2-Simplex Prediction. We consider normalized Hodge Laplacians and incidence matrices. Specifically, we use the symmetric version of the normalized random walk Hodge Laplacians in the edge space, proposed by [Schaub et al. \(2020\)](#), given by $\mathbf{L}_1^s = \mathbf{M}_{11}^{-1/2} \mathbf{L}_1 \mathbf{M}_{11}^{1/2}$ where

$$\mathbf{L}_{1,d} = \mathbf{M}_{11} \mathbf{B}_1^\top \mathbf{M}_{01}^{-1} \mathbf{B}_1, \quad \mathbf{L}_{1,u} = \mathbf{B}_2 \mathbf{M}_{21} \mathbf{B}_2^\top \mathbf{M}_{11}^{-1} \quad (\text{F.1})$$

with $\mathbf{M}_{11} = \max(\text{diag}(|\mathbf{B}_2| \mathbf{1}), \mathbf{I})$, $\mathbf{M}_{01} = 2 \text{diag}(|\mathbf{B}_1| \mathbf{M}_{11} \mathbf{1})$ and $\mathbf{M}_{21} = 1/3 \mathbf{I}$. In the node space, we use the symmetric random walk graph Laplacian, given by $\mathbf{L}_0^s = \mathbf{M}_{00}^{-1/2} \mathbf{L}_0 \mathbf{M}_{00}^{1/2}$, where we have

$$\mathbf{L}_0 = \mathbf{B}_1 \mathbf{M}_{10} \mathbf{B}_1^\top \mathbf{M}_{00}^{-1} \quad (\text{F.2})$$

with $\mathbf{M}_{00} = \max(\text{diag}(|\mathbf{B}_1| \mathbf{1}), \mathbf{I})$ and $\mathbf{M}_{10} = \mathbf{I}$. In the triangle space, we have

$$\mathbf{L}_{2,d} = \mathbf{M}_{22} \mathbf{B}_2^\top \mathbf{M}_{12}^{-1} \mathbf{B}_2 \quad (\text{F.3})$$

with $\mathbf{M}_{12} = \text{diag}(|\mathbf{B}_2| \mathbf{1})$ and $\mathbf{M}_{22} = \mathbf{I}$, and the symmetric version is $\mathbf{L}_{2,d}^s = \mathbf{M}_{22}^{-1/2} \mathbf{L}_{2,d} \mathbf{M}_{22}^{1/2}$. In the projection steps, we have $\mathbf{R}_{0,u} = \mathbf{M}_{01}^{-1} \mathbf{B}_1$, $\mathbf{R}_{1,d} = \mathbf{M}_{11} \mathbf{B}_1^\top \mathbf{M}_{01}^{-1}$, $\mathbf{R}_{1,u} = \mathbf{B}_2 \mathbf{M}_{21}$, and $\mathbf{R}_{2,d} = \mathbf{M}_{22} \mathbf{B}_2^\top \mathbf{M}_{12}^{-1}$. The above normalizations also respect the definitions in [Bunch et al. \(2020\)](#).

3-Simplex Prediction. Keeping the same for $k = 0, 1$, for $k = 2$, we have

$$\mathbf{L}_{2,d} = \mathbf{M}_{22} \mathbf{B}_2^\top \mathbf{M}_{12}^{-1} \mathbf{B}_2, \quad \mathbf{L}_{2,u} = \mathbf{B}_3 \mathbf{M}_{32} \mathbf{B}_3^\top \mathbf{M}_{22}^{-1} \quad (\text{F.4})$$

with $\mathbf{M}_{22} = \max(\text{diag}(|\mathbf{B}_3| \mathbf{1}), \mathbf{I})$, $\mathbf{M}_{12} = 3 \text{diag}(|\mathbf{B}_2| \mathbf{M}_{22} \mathbf{1})$ and $\mathbf{M}_{32} = 1/4 \mathbf{I}$. This definition respects the way of constructing random walk Laplacians on simplices ([Schaub et al., 2020](#)), also used by [Chen et al. \(2022a\)](#). In the 3-simplex space, we have

$$\mathbf{L}_{3,d} = \mathbf{M}_{33} \mathbf{B}_3^\top \mathbf{M}_{23}^{-1} \mathbf{B}_3 \quad (\text{F.5})$$

with $\mathbf{M}_{33} = \mathbf{I}$ and $\mathbf{M}_{23} = \text{diag}(|\mathbf{B}_3| \mathbf{1})$. For the projection matrices, we have $\mathbf{R}_{1,u} = \mathbf{M}_{12}^{-1} \mathbf{B}_2$, $\mathbf{R}_{2,d} = \mathbf{M}_{22} \mathbf{B}_2^\top \mathbf{M}_{12}^{-1}$, $\mathbf{R}_{2,u} = \mathbf{B}_3 \mathbf{M}_{32}$ and $\mathbf{R}_{3,d} = \mathbf{M}_{33} \mathbf{B}_3^\top \mathbf{M}_{23}^{-1}$.

Hyperparameters. The hyperparameters are set as:

- 1) the number of layers: $L \in \{1, 2, 3, 4, 5\}$;
- 2) the number of intermediate and output features to be the same as $F \in \{16, 32\}$;
- 3) the convolution orders for SCCNNs are set to be the same, i.e., $T'_d = T_d = T_u = T_u = T \in \{1, 2, 3, 4, 5\}$. We do so to avoid the exponential growth of the parameter search space. For GFs ([Sandryhaila & Moura, 2014](#)), GNNs ([Defferrard et al., 2016](#)) and SNNs ([Ebli et al., 2020](#)), we set the convolution orders to be $T \in \{1, 2, 3, 4, 5\}$ while for SCNNs ([Yang et al., 2022a](#)) and SCFs ([Yang et al., 2022b](#)), we allow the lower and upper convolutions to have different orders with $T_d, T_u \in \{1, 2, 3, 4, 5\}$;
- 4) the nonlinearity in the feature learning phase: LeakyReLU with a negative slope 0.01;
- 5) the MLP in the prediction phase: two layers with a sigmoid nonlinearity. For 2-simplex prediction, the number of the input features for the node features is $3F$, and for the edge features is $3F$. For 3-simplex prediction, the number of the input features for the node features is $4F$, for the edge features is $6F$ and for the triangle features is $4F$ since a 3-simplex has four nodes, six edges and four triangles. The number of the intermediate features is the same as the input features, and that of the output features is one;
- 6) the binary cross entropy loss and the adam optimizer with a learning rate of 0.001 are used; the number of the epochs is 1000 where an early stopping is used. We compute the AUC to compare the performance and run the same experiments for ten times with random data splitting.

F.1.5. RESULTS

In [Table F.1](#), we report the best results of each method with the corresponding hyperparameters. Different hyperparameters can lead to similar results, but we report the ones with the *least* complexity. We make the following observations:

Table F.1. 2- (Left) and 3-Simplex (Right) prediction AUC (%) results, where the *first* and *second* best are highlighted in *red* and *blue*.

METHODS	AUC	PARAMETERS	METHODS	AUC	PARAMETERS
HARM. MEAN	62.8±2.7	—	HARM. MEAN	63.6±1.6	—
ARITH. MEAN	60.8±3.2	—	ARITH. MEAN	62.2±1.4	—
GEOM. MEAN	61.7±3.1	—	GEOM. MEAN	63.1±1.4	—
MLP-NODE	68.5±1.6	$L = 1, F = 32$	MLP-NODE	68.9±1.8	$L = 1, F = 32$
MLP-EDGE	65.5±4.5	$L = 4, F = 16$	MLP-TRI.	69.0±2.2	$L = 3, F = 32$
GF	78.7±1.2	$L = 2, F = 32, T = 2$	GF	83.9±2.3	$L = 1, F = 32, T = 2$
SCF	92.6±1.8	$L = 1, F = 32, T_d = 1, T_u = 5$	SCF-EDGE	77.6±3.8	$L = 5, F = 32, T_d = 0, T_u = 4$
CF-SC-NODE	96.9±0.8	$L = 5, F = 32, T = 4$	SCF-TRI.	94.9±1.0	$L = 2, F = 32, T_d = T_u = 3$
CF-SC-EDGE	93.2±1.6	$L = 2, F = 32, T = 4$	CF-SC-NODE	95.8±1.0	$L = 3, F = 32, T = 2$
GNN	93.9±1.0	$L = 5, F = 32, T = 2$	CF-SC-EDGE	97.9±0.7	$L = 5, F = 32, T = 3$
SNN	92.0±1.8	$L = 5, F = 32, T = 5$	CF-SC-TRI.	96.7±0.5	$L = 2, F = 32, T = 5$
PSNN	95.6±1.3	$L = 5, F = 32$	GNN	96.6±0.5	$L = 5, F = 32, T = 5$
SCNN	96.5±1.5	$L = 5, F = 32, T_d = 5, T_u = 2$	SNN	95.1±1.2	$L = 5, F = 32, T = 5$
BUNCH-NODE	98.0±0.5	$L = 4, F = 32$	PSNN	98.1±0.5	$L = 5, F = 32$
BUNCH-EDGE	94.6±1.2	$L = 4, F = 16$	SCNN-EDGE	98.3±0.4	$L = 4, F = 32, T_d = T_u = 3$
SCCNN-NODE	98.4±0.5	$L = 2, F = 32, T = 2$	SCNN-TRI.	98.3±0.4	$L = 5, F = 32, T_d = 2, T_u = 1$
SCCNN-EDGE	95.9±1.0	$L = 5, F = 32, T = 3$	BUNCH-EDGE	98.5±0.5	$L = 4, F = 16$
			BUNCH-TRI.	96.6±1.0	$L = 2, F = 32$
			SCCNN-NODE	99.4±0.3	$L = 3, F = 32, T = 3$
			SCCNN-EDGE	99.0±1.0	$L = 5, F = 32, T = 5$
			SCCNN-TRI.	97.4±0.9	$L = 4, F = 32, T = 4$

- 1) methods on graphs and SCs perform much better than heuristic methods and MLPs, because of the inductive bias proposed by the graph and SC models;
- 2) both NNs and filtering methods on SCs perform better than their counterparts on graphs in general, which validates the SC model in simplex predictions, showing the importance of higher-order structures;
- 3) jointly performing the simplicial convolution based on L_k limits the expressive power as shown in Section 5 and Figure F.1 from the spectral perspective, which can be seen from that SCNN performs better than SNN;
- 4) higher-order simplicial convolutions improve the performance. In 2-simplex prediction, SCNN is better than PSNN or Bunch-Edge which only performs a simplicial shifting. Moreover, using either node or edge features of SCCNN gives better results than the counterpart of Bunch, which also requires a deeper NN, inducing stronger mutual dependence between the stability of different simplicial outputs as studied in Section 6. In 3-simplex prediction, the same observations can be made;
- 5) taking into account the information from simplices of different orders further improves the performance, which corroborates our architecture.

F.2. Frequency Response

To further see the effects of using higher-order convolutions and differentiating the two adjacencies, we illustrate the frequency responses of SCFs \mathbf{H}_1 , $\mathbf{H}_{1,d}$ and $\mathbf{H}_{1,u}$ at first layer for several feature indices in Figure F.1. First, we see that the SCF \mathbf{H}_1 has different gradient and curl frequency responses, which allows separate processing in the gradient and curl frequencies. This is the result of differentiating the lower and upper adjacencies by using different parameter spaces, in contrast to Ebli et al. (2020). Second, we see that using higher-order convolution enables a more versatile relation rather than linear or simple scaling, which increases the expressive power of SCCNNs. As a counterexample, Bunch et al. (2020) and Roddenberry et al. (2021) perform a one-step simplicial shifting by L_1 , the frequency response of which is simply a straight line in terms of the simplicial frequencies. Also, merely summing the projected information leads to a simple scaling. This limited expressive power of Bunch requires more layers to have a comparable performance than SCCNN-Node.

F.2.1. ABLATION STUDY

We perform an ablation study to observe the roles of different components in SCCNNs.

Limited Input. We study the influence of limited input data for model SCCNN-Node of order two. Specifically, we consider

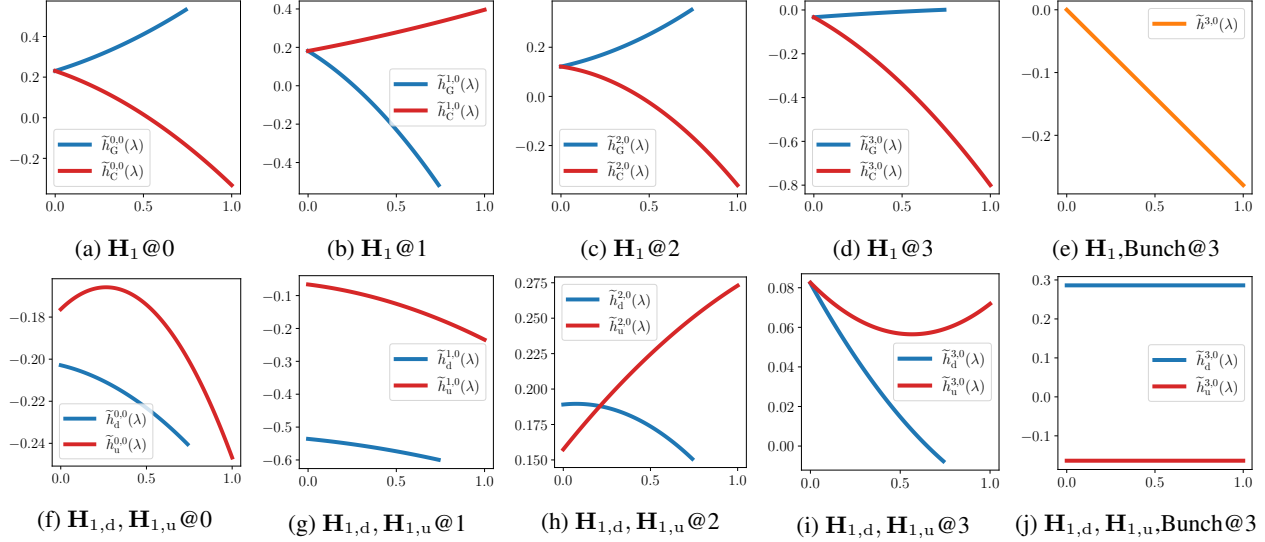


Figure F.1. The frequency responses of three SCFs of SCCNN-Node with $L = 2, T = 2, F = 32$ at first layer for different output-input feature pairs (f_1, f_0) with $f_1 = 0, 1, 2, 3, 4$ and $f_0 = 0$. (Top Row) (a-d): SCFs $\mathbf{H}_1 @ f_1$ where gradient and curl frequency responses are in blue and red; and (e): $\mathbf{H}_1 = \mathbf{L}_1$ for Bunch (in orange since it has one frequency response for all frequencies). (Bottom Row) (f-i): lower and upper SCFs $\mathbf{H}_{1,d}$ and $\mathbf{H}_{1,u} @ f_i$ in blue and red, respectively; and (j): $\mathbf{H}_{1,d} = \mathbf{H}_{1,u} = \mathbf{I}$ for Bunch.

a missing rate of $\{10\%, 40\%, 70\%, 100\%\}$ for either node input or edge input. From Table F.2, we see that the prediction performance does not deteriorate at a cost of the model complexity (higher convolution orders) when a certain part of the input missing except with full zeros as input. This ability of learning from limited data shows the robustness of SCCNNs.

Table F.2. 2-Simplex Prediction results of SCCNN-Node with missing input data.

MISSING RATE	AUC	PARAMETERS
NODE-0.1, EDGE-0	98.4 ± 0.5	$L = 2, F = 32, T = 2$
NODE-0.4, EDGE-0	98.6 ± 0.5	$L = 2, F = 32, T = 5$
NODE-0.7, EDGE-0	98.6 ± 0.5	$L = 2, F = 32, T = 3$
NODE-1.0, EDGE-0	98.2 ± 0.5	$L = 2, F = 32, T = 4$
NODE-0, EDGE-0.1	98.4 ± 0.4	$L = 2, F = 32, T = 1$
NODE-0, EDGE-0.4	98.5 ± 0.6	$L = 2, F = 32, T = 4$
NODE-0, EDGE-0.7	98.6 ± 0.3	$L = 2, F = 32, T = 3$
NODE-0, EDGE-1.0	98.1 ± 0.4	$L = 2, F = 32, T = 3$
NODE-0.1, EDGE-0.1	98.6 ± 0.4	$L = 2, F = 32, T = 1$
NODE-0.4, EDGE-0.4	98.6 ± 0.7	$L = 2, F = 32, T = 4$
NODE-0.7, EDGE-0.7	98.3 ± 0.5	$L = 2, F = 32, T = 4$
NODE-1.0, EDGE-1.0	50.0 ± 0.0	—

SC Order K . We then investigate the influence of the SC order K . Table F.3 reports the 2-simplex prediction results for $K = \{1, 2\}$ and the 3-simplex prediction results for $K = \{1, 2, 3\}$. We observe that for k -simplex prediction, it does not necessarily guarantee a better prediction with a higher-order SC, which further indicates that a positive simplex could be well encoded by both its faces and other lower-order subsets. For example, in 2-simplex prediction, SC of order one gives better results than SC of order two (similar for Bunch), showing that in this coauthorship complex, triadic collaborations are better encoded by features on nodes than pairwise collaborations. In 3-simplex prediction, SCs of different orders give similar results, showing that tetradic collaborations can be encoded by nodes, as well as by pairwise and triadic collaborations.

Missing Components in SCCNNs. With a focus on 2-simplex prediction with SCCNN-Node of order one, to avoid overcrowded settings, we study how each component of an SCCNN influences the prediction. We consider the following settings without: 1) “Edge-to-Node”, where the projection $\mathbf{x}_{0,u}$ from edge to node is not included, equivalent to GNN; 2) “Node-to-Node”, where for node output, we have $\mathbf{x}_0^l = \sigma(\mathbf{H}_{0,u}^l \mathbf{R}_{1,u} \mathbf{x}_1^{l-1})$; 3) “Node-to-Edge”, where the projection $\mathbf{x}_{1,d}$

Table F.3. Prediction results of SCCNNs with lower order K .

METHOD	2-SIMPLEX	PARAMETERS	METHOD	3-SIMPLEX	PARAMETERS
SCCNN-NODE	98.7±0.5	$K = 1, L = 2, F = 32, T = 2$	SCCNN-NODE	99.3±0.3	$K = 1, L = 2, F = 32, T = 1$
BUNCH-NODE	98.3±0.4	$K = 1, L = 4, F = 32$	SCCNN-NODE	99.3±0.2	$K = 2, L = 2, F = 32, T = 5$
SCCNN-NODE	98.4±0.5	$K = 2, L = 2, F = 32, T = 2$	SCCNN-NODE	99.4±0.3	$K = 3, L = 3, F = 32, T = 3$
BUNCH-NODE	98.0±0.4	$K = 2, L = 4, F = 32$	SCCNN-EDGE	98.9±0.5	$K = 1, L = 3, F = 32, T = 5$
SCCNN-EDGE	97.9±0.9	$K = 1, L = 3, F = 32, T = 5$	SCCNN-EDGE	99.2±0.4	$K = 2, L = 5, F = 32, T = 5$
BUNCH-EDGE	97.3±1.1	$K = 1, L = 4, F = 32$	SCCNN-EDGE	99.0±1.0	$K = 3, L = 5, F = 32, T = 5$
SCCNN-EDGE	95.9±1.0	$K = 2, L = 5, F = 32, T = 3$	SCCNN-TRI.	97.9±0.7	$K = 2, L = 4, F = 32, T = 4$
BUNCH-EDGE	94.6±1.2	$K = 2, L = 4, F = 32$	SCCNN-TRI.	97.4±0.9	$K = 3, L = 4, F = 32, T = 4$

from node to edge is not included, i.e., we have $\mathbf{x}_1^l = \sigma(\mathbf{H}_1^l \mathbf{x}_1^{l-1})$; and 4) “Edge-to-Edge”, where for edge output, we have $\mathbf{x}_1^l = \sigma(\mathbf{H}_{1,d}^l \mathbf{R}_{1,d} \mathbf{x}_0^{l-1})$.

Table F.4. (Left): 2-Simplex prediction results with SCCNN-Node without certain components. (Right): Running time in ms per epoch.

MISSING COMPONENT	2-SIMPLEX	PARAMETERS
—	98.7±0.5	$K = 1, L = 2, F = 32, T = 2$
EDGE-TO-NODE	93.9±0.8	$K = 1, L = 5, F = 32, T = 2$
NODE-TO-NODE	98.7±0.4	$K = 1, L = 4, F = 32, T = 2$
EDGE-TO-EDGE	98.5±1.0	$K = 1, L = 3, F = 32, T = 3$
NODE-TO-EDGE	98.8±0.3	$K = 1, L = 4, F = 32, T = 3$

From the results in Table F.4 (Left), we see that “No Edge-to-Node”, i.e., GNN, gives much worse results as it leverages no information on edges with limited expressive power. For cases with other components missing, a similar performance can be achieved, however, at a cost of the model complexity, with either a higher convolution order or a larger number of layers L , while the latter in turn degrades the stability of the SCCNNs, as discussed in Section 6. As studied by Bodnar et al. (2021b, Thm. 6), SCCNNs with certain inter-simplicial couplings pruned/missing can be powerful as well, but it comes with a cost of complexity which might degrade the model stability if more number layers are required.

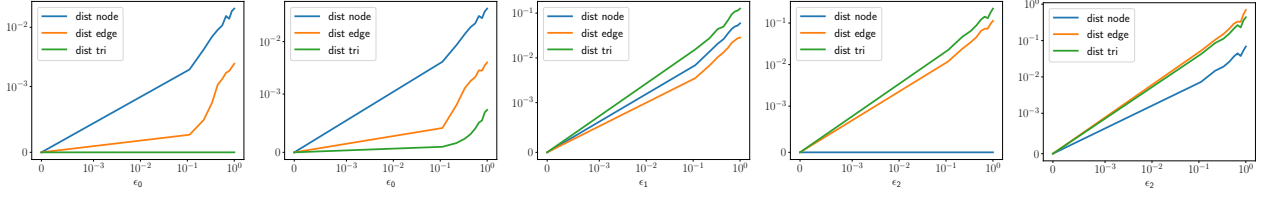
F.2.2. STABILITY ANALYSIS

We then perform a stability analysis of SCCNNs. We artificially add perturbations to the normalization matrices, which resemble the weights of simplices. Specifically, normalization matrices \mathbf{M}_{00} and \mathbf{M}_{01} resemble the node weights, matrices \mathbf{M}_{10} , \mathbf{M}_{11} and \mathbf{M}_{12} the edge weights, and \mathbf{M}_{21} and \mathbf{M}_{22} the triangle weights.

We consider small perturbations \mathbf{E}_0 on node weights which is a diagonal matrix following that $\|\mathbf{E}_0\| \leq \epsilon_0/2$. We generate its diagonal entries from a uniform distribution $[-\epsilon_0/2, \epsilon_0/2]$ with $\epsilon_0 \in [0, 1]$, which represents a one degree of deviation of the node weights from the true ones. Normalization matrices \mathbf{M}_0 are accordingly deviated from the true ones, based which perturbed projection matrices and Hodge Laplacians are defined. Similarly, perturbations on edge weights and triangle weights are applied to study the stability.

With an SCCNN-Node for 2-simplex prediction, we measure the distance between the node outputs with and without perturbations, i.e., $\|\mathbf{x}_0^L - \hat{\mathbf{x}}_0^L\|/\|\mathbf{x}_0^L\|$; and likewise the distance between the edge outputs $\|\mathbf{x}_1^L - \hat{\mathbf{x}}_1^L\|/\|\mathbf{x}_1^L\|$ and the distance between triangle outputs $\|\mathbf{x}_2^L - \hat{\mathbf{x}}_2^L\|/\|\mathbf{x}_2^L\|$. We take as the baseline the setting $L = 2, F = 32, T = 2$ of the best result, studying the influence of the following three factors on the stability.

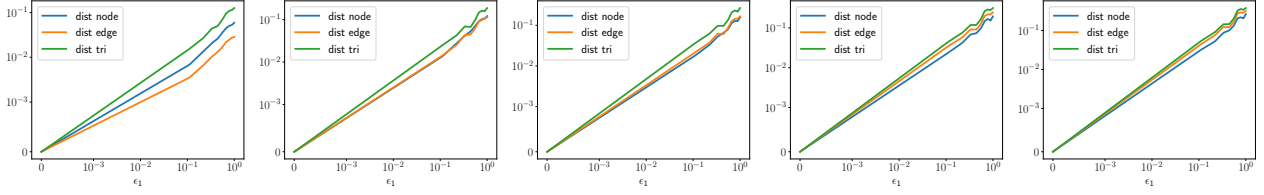
Stability Dependence. We first show the stability dependence between different simplices in Figure F.2. We see that under perturbation on node weights, triangle output is not influenced until the number of layers becomes two; likewise, node output is not influenced by perturbations on triangle weights with a one-layer SCCNN. Also, a one-layer SCCNN under perturbations on edge weights will cause outputs on nodes, edges, triangles perturbed. Lastly, we observe that the same degree of perturbations added to different simplices causes different degrees of instability, owing to the number N_k of k -simplices in the stability bound. Since $N_0 < N_1 < N_2$, the perturbations on node weights cause less instability than those on edge and triangle weights.



(a) Node pert. $\mathbf{E}_0, L = 1$ (b) Node pert. $\mathbf{E}_0, L = 2$ (c) Edge pert. $\mathbf{E}_1, L = 1$ (d) Tri. pert. $\mathbf{E}_2, L = 1$ (e) Tri. pert. $\mathbf{E}_2, L = 2$

Figure F.2. The stabilities of different simplicial outputs are dependent on each other.

Number of Layers. Figure F.3 shows that the stability of SCCNNs degrades as the number of layers increases as studied in Theorem 6.7.



(a) $\mathbf{E}_1, L = 1$

(b) $\mathbf{E}_1, L = 2$

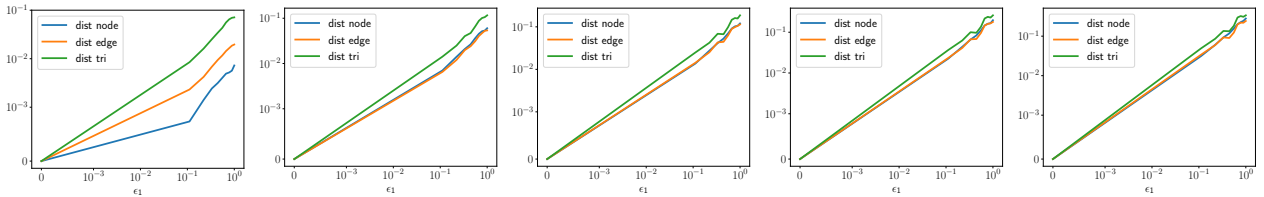
(c) $\mathbf{E}_1, L = 3$

(d) $\mathbf{E}_1, L = 4$

(e) $\mathbf{E}_1, L = 5$

Figure F.3. The stability of SCCNNs in terms of different numbers of layers. We consider perturbations on edge weights.

Convolution Order T . As the order of SCFs becomes larger, the SCFs become more selective at a cost of stability as shown in Figure E.1b. We see that the stability does not deteriorate when T becomes larger. This is owing to the information spillage of the nonlinearity in SCCNNs such that information at higher frequencies where the SCFs cannot be more selective is spread over the lower frequency where the SCFs can be made arbitrarily selective, as studied by Gama et al. (2019b).



(a) $\mathbf{E}_1, T = 0$

(b) $\mathbf{E}_1, T = 1$

(c) $\mathbf{E}_1, T = 2$

(d) $\mathbf{E}_1, T = 3$

(e) $\mathbf{E}_1, T = 4$

Figure F.4. The stability of SCCNNs in terms of the convolution orders. We consider perturbations on edge weights.

From this study, we see the advantage of using higher-order simplicial convolutions in the SCCNNs, which improves the expressive power of SCCNNs without sacrificing the stability much. In this case, it requires a small number of layers such that the stability is guaranteed.

F.3. Trajectory Prediction

Machine learning based methods are commonly used in trajectory prediction, e.g., CNN, RNN, and GNN (Nikhil & Tran Morris, 2018; Rudenko et al., 2020; Wu et al., 2017; Cordonnier & Loukas, 2019). While trajectories can be naturally viewed as edge flows (Ghosh et al., 2018; Schaub et al., 2020), PSNN by Roddenberry et al. (2021), as an instance of the SCCNN, was the first attempt to use the SC model. Here, we first formulate the trajectory prediction problem proposed by Roddenberry & Segarra (2019), then we evaluate the performance.

F.3.1. PROBLEM FORMULATION

A trajectory of length m can be modeled as a sequence of nodes $[v_0, v_1, \dots, v_{m-1}]$ in an SC. The task is to predict the next node v_m from the neighbors of v_{m-1} , $\mathcal{N}_{v_{m-1}}$. The algorithm in Roddenberry et al. (2021) first represents the trajectory

equivalently as a sequence of oriented edges $[[v_0, v_1], [v_1, v_2], \dots, [v_{m-2}, v_{m-1}]]$. Then, an edge flow \mathbf{x}_1 is defined, whose value on an edge e is $[\mathbf{x}_1]_e = 1$ if edge e is traversed by the trajectory in a forward direction, $[\mathbf{x}_1]_e = -1$ if edge e is traversed in a backward direction by the trajectory, and $[\mathbf{x}_1]_e = 0$, otherwise.

With the trajectory flow \mathbf{x}_1 as the input, together with zero inputs on the nodes and triangles, an SCCNN of order two is used to generate a representation \mathbf{x}_1^L of the trajectory, which is the output on edges. This is followed by a projection step $\mathbf{x}_{0,u}^L = \mathbf{B}_1 \mathbf{W} \mathbf{x}_1^L$, where the output is first passed through a linear transformation via \mathbf{W} , then projected into the node space via \mathbf{B}_1 . Lastly, a distribution over the candidate nodes $\mathcal{N}_{v_{m-1}}$ is computed via a softmax operation, $\mathbf{n}_j = \text{softmax}([\mathbf{x}_{0,u}^L]_j), j \in \mathcal{N}_{v_{m-1}}$. The best candidate is selected as $v_m = \text{argmax}_j \mathbf{n}_j$. We refer to Roddenberry & Segarra (2019, Alg. S-2) for more details.

Given that an SCCNN of order two generates outputs also on nodes, we can directly apply the node feature output \mathbf{x}_0^L to compute a distribution over the candidate nodes $\mathcal{N}_{v_{m-1}}$ without the projection step. We refer to this as SCCNN-Node, and the method of using the edge features with the projection step as SCCNN-Edge.

F.3.2. MODEL

In this experiment, we consider the following methods: 1) PSNN by Roddenberry et al. (2021); 2) SNN by Ebli et al. (2020); 3) SCNN by Yang et al. (2022a) where we consider different lower and upper convolution orders T_d, T_u ; and 4) S2CCNN (Bunch) by Bunch et al. (2020) where we consider both the node features and edge features, namely, Bunch-Node and Bunch-Edge, as SCCNN.

F.3.3. DATA AND EXPERIMENTAL SETUP

Synthetic Data. Following the procedure in Schaub et al. (2020), we generate 1000 trajectories as follows. First, we create an SC with two ‘‘holes’’ by uniformly drawing 400 random points in the unit square, and then a Delaunay triangulation is applied to obtain a mesh, followed by the removal of nodes and edges in two regions, as depicted in Appendix F.3.3. To generate a trajectory, we consider a starting point at random in the lower-left corner, and then connect it via a shortest path to a random point in the upper left, center, or lower-right region, which is connected to another random point in the upper-right corner via a shortest path.

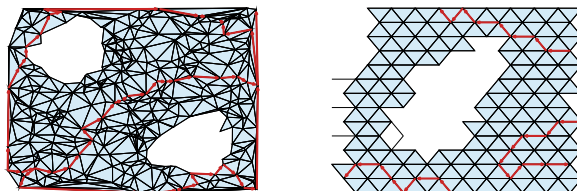


Figure F.5. Synthetic and real trajectories illustrations.

In this experiment, we consider the random walk Hodge Laplacians $\mathbf{L}_0, \mathbf{L}_{1,d}, \mathbf{L}_{1,u}$ and $\mathbf{L}_{2,d}$ defined in (F.2), (F.1) and (F.3). For Bunch method, we set the shifting matrices as the simplicial adjacency matrices defined in Bunch et al. (2020). We consider different NNs with three intermediate layers where each layer contains $F = 16$ intermediate features. The tanh nonlinearity is used such that the orientation equivariance holds. The final projection \mathbf{n} generates a node feature of dimension one. In the 1000-epoch training, we use the cross-entropy loss function between the output \mathbf{d} and the true candidate and we consider an adam optimizer with a learning rate of 0.001 and a batch size 100. To avoid overfitting, we apply a weight decay of $5 \cdot 10^{-6}$ and an early stopping.

As done in Roddenberry et al. (2021), besides the standard trajectory prediction task, we also perform a reverse task where the training set remains the same but the direction of the trajectories in the test set is reversed and a generalization task where the training set contains trajectories running along the upper left region and the test set contains trajectories around the other region. We evaluate the correct prediction ratio by averaging the performance over 10 different data generations.

Real Data. We also consider the Global Drifter Program dataset,² localized around Madagascar. It consists of ocean drifters whose coordinates are logged every 12 hours. The ocean is meshed with hexagons, as shown in Appendix F.3.3, and we consider the trajectories of drifters based on their presence in the hexagonal meshes following the procedure in Schaub et al. (2020). An SC can then be created by treating each mesh as a node, connecting adjacent meshes via an edge and filling the triangles, where the ‘‘hole’’ is yielded by the island. Following the process in Roddenberry et al. (2021), it results in 200 trajectories and we use 180 of them for training. In the training, a batch size of 10 is used and no weight decay is used. The

²Data available at <http://www.aoml.noaa.gov/envids/gld/>.

rest experiment setup remains the same as the synthetic case.

F.3.4. RESULTS

We report the prediction accuracy of different tasks for both datasets in Table F.5. We first investigate the effects of applying higher-order SCFs in the simplicial convolution and accounting for the lower and upper contributions. From the standard accuracy for both datasets, we observe that increasing the convolution orders improves the prediction accuracy, e.g., SCNNs become better as the orders T_d, T_u increase and perform always better than PSNN, and SCCNNs better than Bunch. Also, differentiating the lower and upper convolutions does help improve the performance as SCNN of orders $T_d = T_u = 3$ performs better than SNN of $T = 3$.

However, accounting for the node and triangle contributions in the SCCNN does not help the prediction compared to the SCNNs, likewise for Bunch compared to PSNN. This is due to the zero node and triangle inputs because there are no available node and triangle features. Similarly, the prediction directly via the node output features is not accurate compared to projection from edge features.

Moreover, we also observe that the performance of SCCNNs that are trained with the same data does not deteriorate in the reverse task because the orientation equivariance ensures SCCNNs to be unaffected by the orientations of the simplicial data. Lastly, we see that, like other NNs on SCs, SCCNNs have good transferability to the unseen data.

Table F.5. Trajectory Prediction Accuracy. (Left): Synthetic trajectory in the standard, reverse and generalization tasks. (Right): Ocean drifter trajectories. For SCCNNs, we set the lower and upper convolution orders T_d, T_u to be the same as T .

METHODS	STANDARD	REVERSE	GENERALIZATION	PARAMETERS	STANDARD	PARAMETERS
PSNN	63.1±3.1	58.4±3.9	55.3±2.5	—	49.0±8.0	—
SCNN	65.6±3.4	56.6±6.0	56.1±3.6	$T_d = T_u = 2$	52.5±9.8	$T_d = T_u = 2$
SCNN	66.5±5.8	57.7±5.4	60.6±4.0	$T_d = T_u = 3$	52.5±7.2	$T_d = T_u = 3$
SCNN	67.3±2.3	56.9±4.8	59.4±4.2	$T_d = T_u = 4$	52.5±8.7	$T_d = T_u = 4$
SCNN	67.7±1.7	55.3±5.3	61.2±3.2	$T_d = T_u = 5$	53.0±7.8	$T_d = T_u = 5$
SNN	65.5±2.4	53.6±6.1	59.5±3.7	$T = 3$	52.5±6.0	$T = 3$
BUNCH-NODE	35.4±3.4	38.1±4.6	29.0±3.0	—	35.0±5.9	—
BUNCH-EDGE	62.3±4.0	59.6±6.1	53.9±3.1	—	46.0±6.2	—
SCCNN-NODE	46.8±7.3	44.5±8.2	31.9±5.0	$T = 1$	40.5±4.7	$T = 1$
SCCNN-EDGE	64.6±3.9	57.2±6.3	54.0±3.0	$T = 1$	52.5±7.2	$T = 1$
SCCNN-NODE	43.5±9.6	44.4±7.6	32.8±2.6	$T = 2$	45.5±4.7	$T = 2$
SCCNN-EDGE	65.2±4.1	58.9±4.1	56.8±2.4	$T = 2$	54.5±7.9	$T = 2$

F.3.5. INTEGRAL LIPSCHITZ PROPERTY

We investigate the effect of the integral Lipschitz property of the SCFs in a NN on SC. To do so, given an NN on SCs with an SCF \mathbf{H}_k for k -simplicial signals, we add the following integral Lipschitz regularizer to the loss function during training so to promote the integral Lipschitz property

$$r_{\text{IL}} = \|\lambda_{k,G} \tilde{h}'_{k,G}(\lambda_{k,G})\| + \|\lambda_{k,C} \tilde{h}'_{k,C}(\lambda_{k,C})\| = \left\| \sum_{t=0}^{T_d} t w_{k,d,t} \lambda_{k,G}^t \right\| + \left\| \sum_{t=0}^{T_u} t w_{k,u,t} \lambda_{k,C}^t \right\| \quad (\text{F.6})$$

for $\lambda_{k,G} \in \{\lambda_{k,G,i}\}_{i=1}^{N_{k,G}}$ and $\lambda_{k,C} \in \{\lambda_{k,C,i}\}_{i=1}^{N_{k,C}}$, which are the gradient and curl frequencies. To avoid computing the eigendecomposition of the Hodge Laplacian, we can approximate the true frequencies by sampling certain number of points in the frequency band $(0, \lambda_{k,G,m}]$ and $(0, \lambda_{k,C,m}]$ where the maximal gradient and curl frequencies can be computed by efficient algorithms, e.g., power iteration (Watkins, 2007; Sleijpen & Van der Vorst, 2000).

Here, to illustrate that the integral Lipschitz property of the SCFs helps the stability of NNs on SCs, we consider the effect of regularizer r_{IL} against perturbations in PSNNs and SCNNs in (B.7) with different T_d and T_u for the standard synthetic trajectory prediction. The regularization weight on r_{IL} is set as $5 \cdot 10^{-4}$ and the number of samples to approximate the frequencies is set such that the sampling interval is 0.01.

Figure F.6 shows the prediction accuracy and the relative distance between the edge outputs of the NNs trained with and without the integral Lipschitz regularizer in terms of different levels of perturbations. We see that the integral Lipschitz

regularizer helps the stability of the NNs, especially for large SCF orders, where the edge output is less influenced by the perturbations compared to without the regularizer. Meanwhile, SCNN with higher-order SCFs, e.g., $T_d = T_u = 5$, achieves better prediction than PSNN (with one-step simplicial shifting), while maintaining a good stability with its output not influenced by perturbations drastically.

We also measure the lower and upper integral Lipschitz constants of the trained NNs across different layers and features, given by $\max_{\lambda_{k,G}} |\lambda_{k,G} \tilde{h}_{k,G}(\lambda_{k,G})|$ and $\max_{\lambda_{k,C}} |\lambda_{k,C} \tilde{h}_{k,C}(\lambda_{k,C})|$, shown in Figure F.7. We see that the SCNN trained with r_{IL} indeed has smaller integral Lipschitz constants than the one trained without the regularizer, thus, a better stability, especially for NNs with higher-order SCFs.

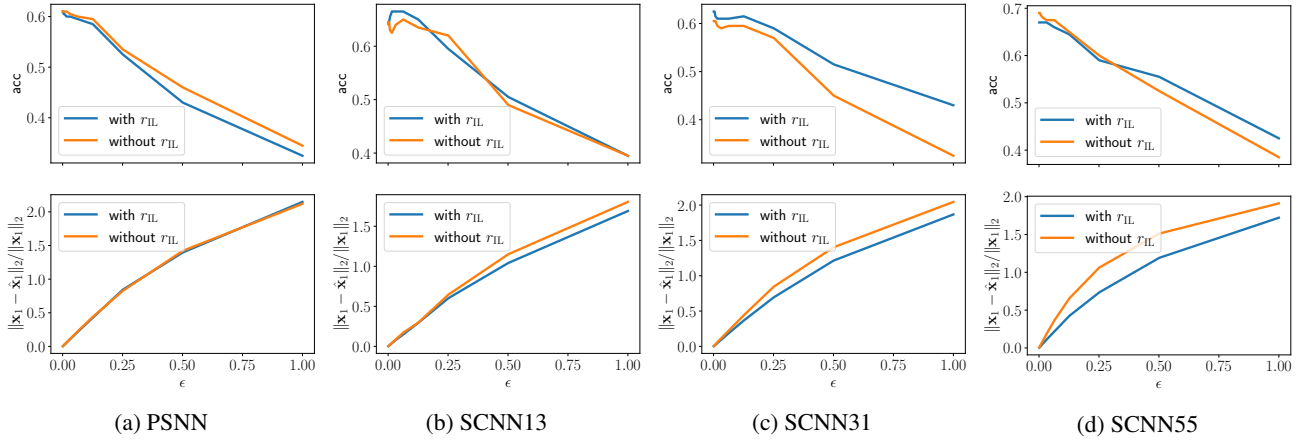


Figure F.6. Effect of the integral Lipschitz regularizer r_{IL} in the task of synthetic trajectory prediction against different levels ϵ of random perturbations on $\mathbf{L}_{1,d}$ and $\mathbf{L}_{1,u}$. We show the accuracy (Top row) and the relative distance between the edge output (Bottom row) for different NNs on SCs with and without r_{IL} . SCNN13 is the SCNN with $T_d = 1$ and $T_u = 3$.

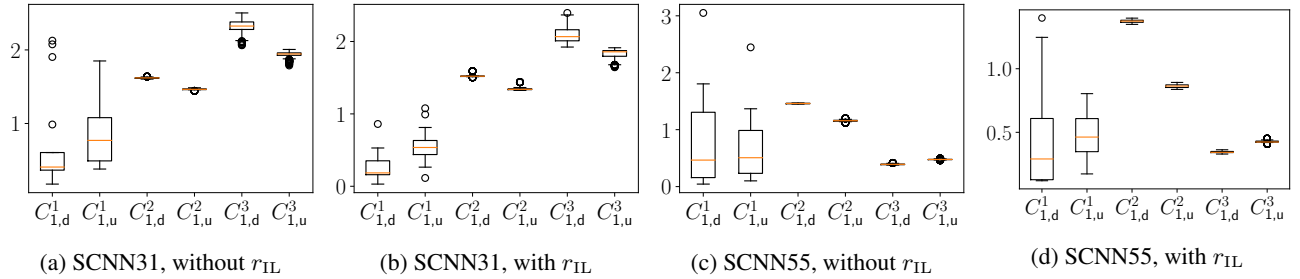


Figure F.7. The integral Lipschitz constants of SCFs at each layer of the trained SCNNs with and without the integral Lipschitz regularizer r_{IL} . We use symbols $C^l_{k,d}$ and $C^l_{k,u}$ to denote the lower and upper integral Lipschitz constants at layer l . Regularizer r_{IL} promotes the integral Lipschitz property, thus, the stability, especially for NNs with large SCF orders.